ACOUSTIC SIGNAL PROPAGATION CHARACTERIZATION OF CONDUIT NETWORKS

by

Muhammad Safeer Khan

A dissertation submitted to the faculty of
The University of North Carolina at Charlotte
in partial fulfillment of the requirements
for the degree of Doctor of Philosophy in
Electrical Engineering

Charlotte

2013

Approved by:

_____
Dr. Ivan Howitt

_____
Dr. Thomas Weldon

_____
Dr. Ryan Adams

_____
Dr. Peter Schmidt

_____
Dr. Harrison Campbell, Jr.

© 2013
Muhammad Safeer Khan
ALL RIGHTS RESERVED

ABSTRACT

MUHAMMAD SAFEER KHAN. Acoustic signal propagation characterization of conduit networks. (Under the direction of Dr. IVAN HOWITT.)

Analysis of acoustic signal propagation in conduit networks has been an important area of research in acoustics. One major aspect of analyzing conduit networks as acoustic channels is that a propagating signal suffers frequency dependent attenuation due to thermo-viscous boundary layer effects and the presence of impedance mismatches such as side branches. The signal attenuation due to side branches is strongly influenced by their numbers and dimensions such as diameter and length. Newly developed applications for condition based monitoring of underground conduit networks involve measurement of acoustic signal attenuation through tests in the field. In many cases the exact installation layout of the field measurement location may not be accessible or actual installation may differ from the documented layout. The lack of exact knowledge of numbers and lengths of side branches, therefore, introduces uncertainty in the measurements of attenuation and contributes to the random variable error between measured results and those predicted from theoretical models.

There are other random processes in and around conduit networks in the field that also affect the propagation of an acoustic signal. These random processes include but are not limited to the presence of strong temperature and humidity gradients within the conduits, blockages of variable sizes and types, effects of aging such as cracks, bends, sags and holes, ambient noise variations and presence of variable layer of water. It is reasonable to consider that the random processes contributing to the error in the measured attenuation are independent and arbitrarily distributed. The error, contributed by a large

number of independent sources of arbitrary probability distributions, is best described by an approximately normal probability distribution in accordance with the central limit theorem. Using an analytical approach to model the attenuating effect of each of the random variable sources can be very complex and may be intractable. A tractable approach is to develop an empirical model of the attenuation that has a stochastic component of a finite mean and variance to account for the random variable error akin to addition of a normally distributed random variable shadowing component in the path loss models of radio frequency (RF) wireless communication channels. This approach forms the crux of the present study.

To develop an empirical model, a large number of measurements in conduit networks were made in the field and in a laboratory test set up to measure the variability of attenuation with variation in four parameters. These parameters include distance of the receiver from the source, frequency, numbers and lengths of side branches. Variation in signal attenuation with distance at each transmitted frequency is predicted by using linear regression through the scatter plot of the measured data. Variations in signal attenuation due to change in frequency, number and lengths of side branches are measured in the field and laboratory tests by comparing the reference transmitted pressure with the received pressure at either the open end or at some distance away from the source along the conduit length. Residuals between measured and predicted sound pressure levels are computed and tested for normal probability distribution through a graphical method as well as a statistical goodness of fit test for quantifiable results. The findings indicate that an empirical model of signal attenuation, which includes a normally distributed random variable component to account for random variable errors in the attenuation

measurements, gives a more accurate prediction of received acoustic signal strength in a conduit compared to existing theoretical models.

ACKNOWLEDGEMENTS

I would like to profoundly thank my advisor Dr. Ivan Howitt for his guidance and support during the course of this research. My sincere thanks are due to other members of my advisory committee: Dr. Thomas Weldon, Dr. Ryan Adams, Dr. Peter Schmidt and Dr. Harrison Campbell, Jr. for their support and helpful comments during the course of this study. Thanks are also due to Charlotte Mecklenburg Utilities Department (CMUD) and InfoSense Inc. for their support during field and laboratory measurement campaigns.

I am also indebted to the Department of Electrical and Computer Engineering at UNC Charlotte for providing support during my Ph.D. program through Graduate Assistantship Support Plan. I also appreciate and acknowledge the financial support of my sponsors, National University of Science and Technology (NUST), Pakistan during early years of my program. Special thanks are also due to the International Student/Scholar Office (ISSO) team for their help during my Ph.D.

I wish to express my heartfelt gratitude to my parents for their constant support and motivation during hard times. Finally, my wife Nafisa provided companionship, listened to my troubles, and took care of our sons Zain and Azlan. Without the support of all of them this dissertation would not have been possible.

TABLE OF CONTENTS

LIST OF TABLES

LIST OF FIGURES

LIST OF SYMBOLS

$\boldsymbol{\Phi}$	Velocity Potential	k_{mn}	Wave number of a mode (*m*,*n*)
c	Speed of sound	c_p	Phase speed
t	Time	c_g	Group speed
z	Axial Space Vector	I_{mn}	Specific admittance parameter
r	Radial Space Vector	R_{mn}	Specific admittance parameter
φ	Circumferential Space Vector	A_{mn}	Square of k_{mn}
$\boldsymbol{R}$	General space vector	α_{mn}	Modal attenuation coefficient
ρ_0	Equilibrium density of fluid medium	ε_v	Viscosity parameter
p	Pressure	ε_t	Thermal conduction parameter
∇	Gradient Operator	α_{00}	Attenuation of plane wave mode
∇^2	Laplacian Operator	S	Cross-sectional area of a conduit
$\mathbf{v}$	Particle Velocity	U	Volume velocity
k	Wave number	L	Length of conduit
ω	Angular Frequency (rad/s)	Z_r	Radiation impedance
γ_{mn}	Roots of Bessel function derivative	Z_c	Characteristic impedance
j	$\sqrt{-1}$	Z_{in}	Input impedance
m	An integer	Z_c'	Complex characteristic impedance
n	An integer	R	Reflection coefficient
a	Radius of a conduit	δl	Length correction
f_{mn}	Cut-off frequency of a mode (*m*,*n*)	$J_m(x)$	Bessel function of the first kind of order *m*
f_n	Resonant frequency	μ'	Approximation parameter
f	Frequency	ν	Approximation parameter
$\Im$	Imaginary Part	$\Re$	Real part
C_2	Reflected wave pressure amplitude	P_r	Prandtl number

C_0	Source pressure	ΔT	Temperature deviation
R_r	Real part of complex Z_r	r_t	Thermal conduction parameter
X_r	Imaginary part of complex Z_r	r_v	Viscosity parameter
C_p	Specific heat at constant pressure	d_v	Viscous skin depth
C_v	Specific heat at constant volume	Γ	Complex propagation wave number
κ	Thermal conductivity	d_h	Heat conduction skin depth
γ	Ratio of specific heats	β	Phase constant
η	Coefficient of shear viscosity	ϵ_w	Wall loss parameter
C_w	Wall material specific heat	κ_w	Wall material thermal conductivity
ρ_w	Wall material mass density	P'	Pressure at side branch junction
C_1	Forward pressure amplitude	R_b	Side branch resistance
X_b	Side branch reactance	l	Side branch length
b	Side branch radius	Ω	Side branch pressure Loss
α	Attenuation coefficient	ζ	Viscosity and heat conduction loss parameter
S	Cross-sectional area	R_b	Side branch resistance
L_b	Side branch inductance	C_b	Side branch leakance
T	Temperature	$SPL, \overline{P}$	Sound Pressure Level
α_c	Combined attenuation coefficient	p_{ref}	Reference for pressure level
ψ	Normal random variable	$\mathcal{F}$	Function of
P_R	Pressure at the receiver	R_{reg}	Coefficient of regression
μ	Mean Value	σ^2	Variance
Ω_T	Pressure Transmission Loss	T_π	Power transmission coefficient
Z_{eq}	Equivalent Impedance	K_e	Empirical Correction Factor
Z_L	Load Impedance	σ	Standard Deviation
AD	Anderson-Darling Test Statistic	F_0	Assumed Normal Distribution

$Z_{(i)}$	Sample Value	M	Maximum sample size

CHAPTER 1: INTRODUCTION

1.1 Background

Sound propagation in conduits has historically been an important subject for researchers in acoustics. The historic research effort was primarily driven by applications of acoustic propagation in conduits for the design of musical instruments, noise suppression in heating ventilation and air-conditioning (HVAC) systems, design of mufflers in automobiles, acoustic delay lines and modeling of the human vocal tract. Resultantly, there is a profusion of literature describing theoretical principles governing the propagation of acoustic signals in conduit environments (Long 1947; McSkimin 1948; Beranek, Reynolds et al. 1953; Dyer 1958; Schroeder 1967; Wyerman 1976; Keefe 1982; Munjal 1987; Okamoto, Boden et al. 1994; Kang and Jung 2001).

In contrast to propagation in free space, the sound propagation in conduits is peculiar since the propagating signal is subjected to a wave guiding effect through confinement of its energy within the guide walls akin to propagation of radio frequencies in waveguides. There are two principal effects of this confinement of acoustic energy (Kinsler, Frey et al. 2000). First, it limits the modal content of the acoustic energy that may propagate at any particular frequency enabling a one dimensional approach to model the signal propagation. This occurs at low frequencies where the signal wavelength is sufficiently large compared to the radius of the conduit and acoustic energy transfer

between source and the receiver is through the fundamental plane wave only. As the signal wavelength becomes small compared to the radius of the conduit, the propagation is best described using modal analysis. The second effect of confinement of acoustic energy is the reduction in its geometric attenuation compared to the propagation in a free field. Acoustic signals are, therefore, well suited for applications requiring evaluation of acoustic signal attenuation in narrow conduits (Fishburne and Howitt 2010; Howitt 2012).

1.2 Research Problem Formulation

In contrast to the theory of ideal rigid walled conduit with lossless propagation, practical conduits attenuate the acoustic signal not only due to the boundary layer effects of viscosity and heat conduction but also due to various other sources. One important source of signal attenuation in conduit networks is the presence of numerous impedance mismatches such as side branches, cracks, holes, bulges and sags etc. The existing theoretical approaches can be used to model the acoustic signal attenuation in a conduit due to side branches with known parameters (such as open or closed end condition, radii, lengths, numbers and locations etc.). Recent developments in condition based monitoring systems for underground conduits in the field (e.g. sewer pipes) are based on classifying the state of a conduit section through measurement of acoustic signal attenuation (Howitt 2012). Condition classification based on attenuation measurement is complicated because most of the underground conduit infrastructure is almost a century old (USEPA 2012). Consequently, the exact installation layout of the conduit and its side branches at the measurement location may not be accessible or actual installation may differ from the documented layout. The lack of exact knowledge of conduit layout, therefore, introduces

uncertainty in the measurements of attenuation and contributes to the random variable error between measured results and those predicted from theoretical models. The presence of random processes in and around the conduit also affects the propagating signal and further complicates the evaluation of signal attenuation in the conduit by introduction of a random variable error in the measured attenuation. Examples of such random processes include unknown or inaccurately known lengths and number of side branches, temperature and humidity gradients, blockages of variable sizes, types and locations, effects of conduit aging, effects of reflections from the open end, the ambient noise source variations and anomalies in the measurement setup.

In order to model the effect of random processes on signal attenuation in the conduit, it is reasonable to consider that each of the random process belongs to an arbitrary distribution. It is also realistic to consider that the random processes do not convey any information about each other and as a result knowledge of one random process does not change the probability distribution of another. This makes them independent of each other in a statistical sense. Considering the random processes to be independent and arbitrarily distributed enables use of the central limit theorem under its weak convergence condition (Henke 2007). This implies that the mean of the error due to independent and arbitrarily distributed sources belongs to an approximately normal probability distribution.

The above stated stochastic based approach can be applied to model acoustic attenuation in a conduit network in the presence of random variable error sources in a manner similar to the modeling of the multipath shadowing effect in radio frequency (RF) wireless communication channels (Andersen, Rappaport et al. 1995). As in the case

of wireless communication channels a normally distributed random variable with finite mean and variance can be added to the analytically evaluated attenuation coefficient of a conduit network to more accurately predict the total attenuation of the received signal. Analysis of signal attenuation in a conduit network as a function of change in distance from the source, frequency and side branch impedance including the effect of other random variable processes forms the main theme of the present study.

In light of the above discussion, the main research questions answered in this study are:

1) What modeling approaches are available to analytically model the attenuation of an acoustic signal in a straight conduit with no impedance mismatches and a conduit network comprising T-joints with numerous side branches of different lengths?
2) How can an empirical model be developed to characterize the acoustic propagation in conduits using the deterministic evaluation through existing analytical expressions?
3) What is the variation in attenuation of a propagating signal in a conduit section or a network as a function of the change in distance of receiver from the source, frequency, number and lengths of side branches?
4) How can the empirical measurements be analyzed to include the effect of random variable error in the measured attenuation caused by numerous random processes in and around a conduit network?

5) How to statistically analyze the error between the measured and theoretically evaluated attenuation to validate that it is a normally distributed random variable of finite mean and known variance?
6) What is the validated form of the empirical model that includes the effects of random variable error in the total attenuation of the acoustic signal?

The present study uniquely contributes to the state of the art in modeling acoustic propagation in conduit networks by laying out a stochastic based approach to model the inaccuracy in the measurement of attenuation in conduit networks caused by lack of information of random processes. The proposed approach lays out a method to use the empirical data to determine a correction factor for the propagation model. The empirical correction factor significantly improves the agreement between the measured and model predicted attenuation of a conduit network with variation in number and length of side branches. The developed model also reduces the complexity of analysis compared to the existing analytical approaches of solving acoustic signal propagation in conduit networks. It also enables characterization of the nature of probability distribution of the residuals that would otherwise be intractable to analyze. The modeling of acoustic propagation in conduits using this approach is generic and can be applied to any network of conduits enabling its use in a variety of applications requiring evaluation of acoustic attenuation.

1.3 Assumptions

In order to answer the research questions highlighted above, a large amount of empirical data has been collected through extensive measurements in conduit networks already laid out in the field and those in a laboratory setting. In order to use that measured

data for analyzing the probability distribution of random variable error, various assumptions are made that govern the present study:

1) The conduits are primarily made of polyvinyl chloride (PVC) material. They are circular in cross section and are considered infinitely rigid as the acoustic impedance of the conduit walls is over three orders of magnitude higher than that of the propagating medium (Density of air is about 1.22 Kg/m^3 whereas that of PVC is about 1380 Kg/m^3). One end of the conduit is open and the acoustic source is placed at the other end. To apply an appropriate length correction due to the effects of reflections from open end, conduits are considered as rigid walled and flanged.
2) Plane wave propagation is assumed as the primary source of energy transfer. As the conduits measured in this study especially during field tests are very long (typical lengths are about 30.0 m) and the receiving microphone is placed approximately at the centerline of the conduit as far as is practicable, the effects of higher order modes are assumed to be insignificant.
3) The receiving transducer during measurements for data collection is assumed to be in the acoustic far field.
4) The effect of reflections from the open end of the conduit is assumed to be considerably reduced by the extension of the conduit beyond the measurement point (about 12 wavelengths at 1.0 kHz) during laboratory measurements. The receiving microphone is placed at the

center of the conduit a significant distance away from the open end. An empirical correction factor that equals the difference between the measured and theoretically evaluated attenuation of a straight conduit is introduced in the proposed model to further reduce the effect of reflections from open end. The inclusion of the empirical correction factor significantly improves the accuracy of the prediction. The analysis of exact effects of reflections from the open end of the conduit in a manhole as observed during the field measurements is analytically complex and therefore merits a separate study. During field tests, several measurements were conducted that involved consecutive pipe segments spanning multiple manholes. The manhole transmission loss is not being analyzed in this study. It is assumed that the manhole transmission loss manifest itself as part of the random variable error in the signal attenuation.

5) The fluid column in the conduits is assumed to be air. Variations in the properties of air due to temperature and relative humidity conditions encountered during measurements for this study are assumed to be insignificant, in that they do not affect the outcome of the analytical evaluation of attenuation coefficient. The density, coefficient of shear viscosity, the ratio of specific heats at constant volume and pressure and the thermal conductivity parameters of air are therefore treated as constants of the medium.

Having presented the assumptions made for the present study, next section presents the outline of the dissertation.

1.4 Outline

Following the introduction of Chapter 1, Chapter 2 presents an overview of historical research on acoustic signal propagation in conduits. Chapter 3 includes the theoretical foundations on acoustic propagation in straight conduits with no side branches. Chapter 4 covers the modeling of attenuation in conduit networks such as those with side branch. In Chapter 5, the proposed model is developed and the approach for using the empirical data to validate the proposed model is presented. Chapter 6 gives the description of the test set up of the field and laboratory measurements. Chapter 7 presents the analysis of the results obtained through comparison between the predicted and measured data. It also includes the deductions made from the data analysis. Chapter 8 concludes the dissertation and presents recommendations for future work to further refine the empirical model.

CHAPTER 2: LITERATURE REVIEW

2.1 Review of Research on Straight Acoustic Conduits

The subject of acoustic propagation in cylindrical conduits has a long history. Stokes was the first to investigate the nature of the acoustic field by studying the internal friction of moving fluids (Stokes 1845). He investigated the absorption of acoustic energy in the gaseous medium inside the conduit due to viscosity. However, because he considered free propagation and not the forced propagation, he found the temporal absorption coefficient and not the spatial one. He worked with Claude-Louis Navier to present the Navier-Stokes equations that form the basis of most of the work on acoustics. The solution of these equations resulted in a lossy wave equation which describes exponential decay of pressure with distance for plane wave propagation. Following Stoke's work, Helmholtz published his monumental work analyzing the physiological basis of sensations of tone for developing his theory of music (Helmholtz 1885). He invented the Helmholtz resonator to identify various frequencies of pure sine wave components of complex multi-tonal sounds. Kirchhoff published a benchmark work on absorption in a thermo-viscous gaseous medium (Kirchhoff 1883). He studied the effects of viscosity and heat conduction on acoustic propagation through rigid cylindrical conduits. Subsequent work was focused on understanding relationship between oscillatory pressure and volume velocity of fluid within a cylindrical conduit and finding accurate approximations to Kirchhoff's exact results. Rayleigh was the first to obtain

useful approximations to Kirchhoff's transcendental solution for the case of narrow tubes with an acoustic boundary layer larger than the radius of the conduit (Rayleigh 1896).

Subsequent to Kirchhoff's derivation, only analytical approximations of his complete solution were used to estimate the propagation coefficients. Brown extended these approximations to frequencies where the acoustic boundary layer is on the order of or smaller than the radius of the conduit (Brown 1962). Shields *et al*. were the first to numerically solve the original Kirchhoff's transcendental formulation (Shields, Lee et al. 1965). Tijdeman determined that the attenuation inside tubes depended on four non-dimensional parameters (Tijdeman 1975). These parameters included shear wavenumber (Stokes number), the reduced frequency, square root of Prandtl number and the ratio of specific heats of the fluid medium. Daniels was the first to evaluate the characteristic impedance and propagation constant for a cylindrical conduit in terms of Bessel's function using electrical network theory (Daniels 1950). Benade extended the work of Daniels by using an electrical transmission line analogy to express the characteristic impedance, phase velocity and attenuation coefficient in exact and limiting forms for the case of large and small diameter conduits (Benade 1968). Keefe presented approximate expressions for characteristic impedance and transmission wavenumber for a gaseous fluid enclosed in a rigid conduit (Keefe 1984). He also modeled the tone holes in woodwind musical instruments using T-circuit sections comprising a series and shunt impedance arms for each tone hole whose values varied depending upon whether the tone hole was open or closed (Keefe 1982) (Nederveen, Jansen et al. 1998).

Another important aspect of research on acoustic propagation in conduits involved analyzing the reflections from an open end of the conduit. An approximate end correction value of 0.6 times the radius was found by Lord Rayleigh (Rayleigh 1896) . His results were experimentally modified by Blaikley (Blaikley 1879), Boehm (Boehm 1910), Anderson and Ostensen (Andersen 1928) and Bait (Bait 1937). Levine and Schwinger proposed a rigorous and explicit solution to the problem of radiation of sound from the open end of an un-flanged conduit assuming plane wave propagation for various ranges of the product of wavenumber and the conduit radius (Levine and Schwinger 1948). Their analysis was further refined in (Morse and Feshbach 1953) and (Noble 1988). Zorumski studied the case of flanged ducts and proposed generalized expressions for radiation impedance and reflection coefficient that were applicable for higher order modes (Zorumski 1973).

In many practical situations acoustic propagation parameters for conduits such as input impedance, normal reflection, attenuation and transmission coefficients and transmission loss cannot be determined analytically due to complex geometry of the conduit or the presence of mean flow. In such cases, experimental techniques were used to determine the propagation parameters of the conduits. A standing wave ratio (SWR) technique involving a traversing microphone was used to measure the standing wave pattern inside the conduit from which the required propagation parameters were deduced (ANSI/ASTM 1977). As this technique required operation at single frequency and a travelling microphone, it was time intensive and the minima of acoustic pressure could not be accurately located. Subsequently, methods for measuring reflection coefficient in conduits using the correlation function and the cross spectral density were reported in

(Ross and Seybert 1977; Seybert and Ross 1977; Johnston and Schmidt 1978; Seybert and Soenarko 1980). Chung and Blaser proposed a much simpler two microphone transfer function method to measure normal incident acoustic properties (Chung and Blaser 1980; Chung and Blaser 1980; Chung and Blaser 1980). Their method involved decomposing the incident and reflected components of the acoustic wave in the conduit from the simple transfer function relation between acoustic pressures at the two microphone locations (Hull 1992). Boden and Abom analyzed the errors on the two-microphone method for measuring acoustic properties in a conduit (Boden and Abom 1986). Chu presented modification to the two-microphone technique by proposing that by using a periodic pseudorandom sequence as the noise signal it was possible to measure the acoustic properties in conduits with a single microphone (Chu 1986; Chu 1986).

2.2 Review of Research on Acoustic Conduit Networks

In addition to the above highlighted work, there has been considerable effort to study networks of acoustic elements comprising straight conduits with side branches for acoustic filtering applications. Stewart, in a series of papers, proposed that acoustic filters could be modeled using lumped parameters as an analog of an electrical filter comprising a combination of electrical circuit elements (Stewart 1922; Stewart 1925; Stewart 1926). He presented an analytical expression for attenuation and phase coefficients to analyze the influence of a side branch upon acoustic transmission through a conduit (Stewart 1924) (Stewart 1925). He also laid out a method for direct and absolute measurement of acoustic impedance of a side branch (Stewart 1926). Mason was instrumental in conducting rigorous mathematical analysis of propagation characteristics of conduit networks as acoustic filters (Mason 1927; Mason 1928; Mason 1930). The results of

Mason and Stewart were compared by Lindsay (Lindsay 1929) and further simplified by Irons (Irons 1931). The research conducted to support this dissertation builds upon Stewart's approach to analyze the effect of side branches on sound propagation in a conduit.

More recently, the acoustic filters have been studied in the context of noise reduction in modern buildings with centralized air conditioning systems. The research effort by Chen looked at the use of Helmholtz resonators to improve the acoustic transmission loss of a conduit (Chen, Chen et al. 1998). Enescu et al. looked at low frequency filtering characteristics of side branches by considering an acoustical tube with multiple side branches (Enescu 1999). Tang looked at the sound transmission characteristics of the T junction formed by a side branch and an infinitely long duct using a finite element based modeling approach (Tang 2004).

The most recent work on analyzing acoustic signal propagation in conduit networks has been undertaken by the Pennine Water Group based at The Universities of Bradford and Sheffield in the UK. They approached the problem of characterizing in-pipe acoustic propagation in the presence of impedance mismatches through the use of mode matching technique in acoustic reflectometry (Horoshenkov 2003; Yin and Horoshenkov 2005; Tolstoy, Horoshenkov et al. 2009). They also proposed an acoustic method for condition classification of live sewer networks using pattern recognition approach based on the "K-nearest neighbor classifier" method (Feng, Horoshenkov et al. 2012).

Having taken a look at the background work on acoustic propagation in conduit networks, the relevant theory to model acoustic propagation in conduit networks is presented in the next chapter.

CHAPTER 3: ACOUSTIC PROPAGATION IN CONDUITS

3.1 Wave Propagation in Conduit Air Column

The sound propagation in an infinitely long cylindrical conduit with radius *a*, as shown in Fig. 1, is governed by a linearized wave equation. This equation expressed in terms of velocity potential ($\boldsymbol{\Phi}$) in cylindrical coordinates is given in (Dyer 1958) as:

$$\nabla^2\boldsymbol{\Phi} = \frac{1}{c^2}\frac{\partial^2\boldsymbol{\Phi}}{\partial t^2}, \qquad \text{where } \nabla^2 = \frac{1}{r}\frac{\partial}{\partial r}\left(r\frac{\partial}{\partial r}\right) + \frac{1}{r^2}\frac{\partial^2}{\partial \varphi^2} + \frac{\partial^2}{\partial z^2}. \tag{1}$$

In (1), $\boldsymbol{\Phi}(\boldsymbol{R}, t)$ is the velocity potential, *c* is the speed of sound and *t* is the time coordinate. $\boldsymbol{R}$ is a general space vector, which in the case of a cylindrical conduit is described by axial, radial and circumferential dimensions (*z*, *r*, φ). The sound source is assumed to be located at $z = 0$. The sound pressure (*p*) and the sound particle velocity **v**

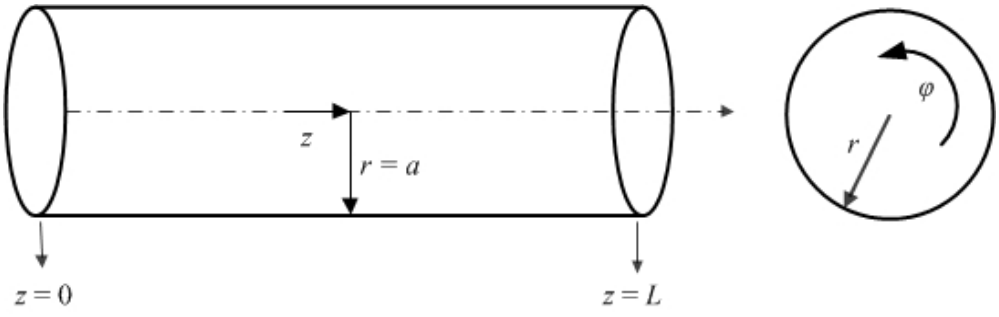

Figure 1: Cylindrical Conduit.

are related to the velocity potential by the following expressions where ρ_0 is the density of the fluid medium in the conduit:

$$p = \rho_0 \frac{\partial \mathbf{\Phi}}{\partial t};\ \mathbf{v} = -\nabla \mathbf{\Phi}\,. \tag{2}$$

In order to analyze the sound propagation in conduits, the solutions of (1) that obey the appropriate boundary conditions are desired. The general forms of the solutions to the wave equation are found by applying the method of separation of variables. In the case of a rigid walled, infinitely long circular conduit, and assuming a harmonic time dependence of velocity potential (single frequency, pure tone) with complex exponential representation ($e^{j\omega t}$), in (1) the operator $\frac{\partial}{\partial t}$ is replaced by $j\omega$ and $\frac{\partial^2}{\partial t^2}$ is replaced by $-\omega^2$. The wave equation in (1) then becomes the Helmholtz equation given by (Dyer 1958):

$$\begin{gathered} \nabla^2 \mathbf{\Phi} + \left(\frac{\omega}{c}\right)^2 \mathbf{\Phi} = 0\,, \\ \nabla^2 \mathbf{\Phi} + (k)^2 \mathbf{\Phi} = 0\,, \end{gathered} \tag{3}$$

where, $k = \frac{\omega}{c}$ is the wave number. The general solution of (3) found using the method of separation of variables for waves propagating away from the source in $+z$ direction is a sum of all modes of oscillation given as:

$$\begin{aligned} \mathbf{\Phi}(\mathbf{R}, \omega) = \sum_{m=0}^{\infty} \sum_{n=1}^{\infty} & J_m(\gamma_{mn} r)\,[C_{mn}(\omega) \cos m\varphi) \\ & + D_{mn}(\omega) \sin m\varphi)] e^{jk_{mn} z}\,, \end{aligned} \tag{4}$$

where

$$k_{mn} = \sqrt{(k^2 - \gamma_{mn}^2)}\,, \tag{5}$$

and for a hard walled conduit, γ_{mn} is the nth root of the Bessel function of the first kind derivative J'_m such that:

$$J'_m(\gamma_{mn}a) = 0. \quad \forall\, m,n = 0,1,2,3,\ldots \tag{6}$$

The coefficients C_{mn} and D_{mn} in (4) are determined from the properties of the source and its match to the conduit. That determination is out of the scope of the present study and details can be found in (Dyer 1958).

Analysis of wave propagation in circular conduits indicates that there are two possible conditions of the waves (Morse and Ingard 1968). First, when the wavelength is large compared to the radius of the conduit, only the direct wave propagates. It corresponds to the (0, 0) mode (plane wave) among an infinite number of modes (*m*,*n*). This plane wave mode is not affected by reflections off of the conduit walls and therefore has the lowest attenuation of any wave mode. The plane wave is non-dispersive as its phase speed is independent of the frequency of transmission and equals the speed of sound. The acoustic pressure disturbances in the plane wave do not suffer any change in their shapes because of their constant phases. Second, when the wavelength is small compared to the radius of the conduit, the wave propagation is best described using a multi-modal approach comprising a plane wave and an infinite number of other modes. The multi-modal wave can propagate in one of two possible ways. It can reflect more or less normally from the walls and focus into the center of the conduit. This corresponds to the modes with small *m* and large *n*. These modes suffer approximately double the attenuation due to reflections from the walls compared to the plane wave mode (Morse and Ingard 1968). Alternatively, for modes with large *m* and small *n*, the waves can move in a spiral path roughly parallel to the conduit walls with a multitude of radial nodes. These spiral modes cannot avoid reflections from the walls. Their energies are concentrated near the wall and have very small amplitudes close to the axis of the

conduit. These spiral-tangential modes, with energies clinging to the conduit walls, suffer quick absorption due to the boundary layer at the walls (Morse and Ingard 1968). Therefore, these modes do not persist outside the acoustic near field.

From (5) the conditions for propagation of modes in circular conduits can be determined. It can be observed that the plane wave mode always propagates as the modal wavenumber $k_{mn} = k$. When the frequency is high enough to satisfy the condition ($k_{mn} > 0$), the higher order modes also propagate. At those modal frequencies for which the propagation condition is not satisfied i.e. ($k_{mn} < 0$), the wave number (k_{mn}) becomes purely imaginary and the modes attenuate axially at an exponential rate. The axially decaying modes are called the evanescent modes and the frequency at which this occurs is called the cut-off frequency. For a propagation mode (*mn*), the cut-off frequency and the mode wave number are related. The mathematical expressions for the two as given in (Kinsler, Frey et al. 2000) are:

$$f_{mn} = \frac{c}{2a}\left(\frac{\gamma_{mn}}{\pi}\right), \qquad k_{mn} = k\left[1 - \left(\frac{f_{mn}}{f}\right)^2\right]^{\frac{1}{2}}. \tag{7}$$

Values of zeros of the Bessel function of the first kind derivative (γ_{mn}) and cut-off frequencies (f_{mn}) for first ten modes of 0.1 m diameter conduits are given in Table 1. The speed of sound (c) in the conduit is taken as 343 m/s.

The phase speed (c_p) of an acoustic mode is the speed at which a surface of constant phase appears to propagate along the z-axis of the conduit. The phase speed is dependent on the cut-off frequency of the mode and is greater than speed of sound in a conduit. Therefore, in case of modal propagation, the acoustic wave inside the conduit

Table 1: First ten values of γ_{mn} and f_{mn} .

Mode (m,n)	1,1	2,1	0,2	3,1	4,1	1,2	5,1	2,2	0,3	3,2
γ_{mn}	1.84	3.05	3.83	4.20	5.32	5.33	6.41	6.71	7.02	8.02
f_{mn}(kHz)	1.97	3.25	4.08	4.48	5.67	5.68	6.84	7.16	7.48	8.55

travels axially with continual reflections off of the walls. Thus, the group speed (c_g) at which the wave energy moves in the z-direction is the fraction of the speed of sound along the conduit axis z. In case of a plane wave, the phase and group speeds are roughly equal to the speed of sound for the fluid in the conduit (for air, at 20 Celsius it is 343 m/s). The expressions for phase speed and group speed of a particular mode can be observed from (5) and are given by:

$$c_p = \frac{\omega}{k_{mn}} = c\left[1 - \left(\frac{f_{mn}}{f}\right)^2\right]^{-0.5}; \; c_g = c\sqrt{\left[1 - \left(\frac{f_{mn}}{f}\right)^2\right]}. \qquad (8)$$

The phase and group speeds are plotted for the plane wave and first three modes in a 0.1 m diameter conduit and are given in Figs. 2 and 3.

As stated briefly earlier, the major cause of attenuation of the higher order modes in conduits is the thermo-viscous losses due to the boundary layer at the conduit walls. This aspect has been addressed in detail by Beatty (Beatty Jr 1950) and Yin and Horoshenkov (Yin and Horoshenkov 2005). Bruneaua et al. have presented an analytical solution that describes the attenuation coefficient of higher order modes in the circular conduits due to non-zero wall admittance of the walls (Bruneaua, Bruneaua et al. 1987).

They considered rigid walled conduits with dimensions of the same order of magnitude or greater than the acoustic wavelength.

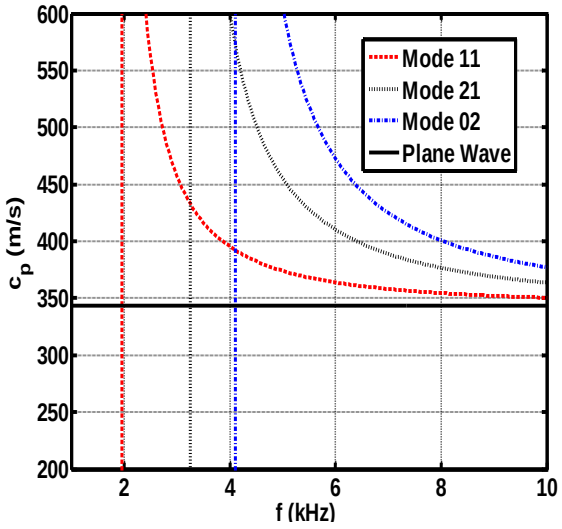

Figure 2. Phase speed as function of frequency.

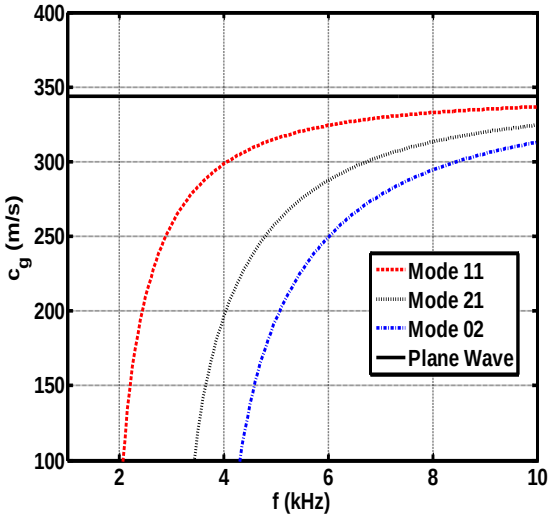

Figure 3. Group speed as a function of frequency.

The transverse dimensions of the duct are assumed to be greater than the boundary layer thickness, but small enough so that wall losses are preponderant. The attenuation coefficient is then described in terms of the boundary specific admittance for the *(m,n)* mode and is given as the imaginary part of the complex axial wave number k_{mn}. The modal attenuation coefficient is evaluated by:

$$\alpha_{mn} = \pm \frac{1}{\sqrt{2}} \left[-(A_{mn} + I_{mn}) + \sqrt{(A_{mn} + I_{mn})^2 + R_{mn}^2} \right]^2. \tag{9}$$

The values of I_{mn} , R_{mn} and A_{mn} can be found in (Bruneaua, Bruneaua et al. 1987). For the plane wave mode, the modal attenuation coefficient in terms of wall admittance parameters ε_v (viscosity parameter) and ε_t (thermal conduction parameter) is given in (Bruneaua, Bruneaua et al. 1987) as:

$$\alpha_{00} = \pm \frac{\Re\,(\varepsilon_v + \varepsilon_t)}{a}. \qquad (10)$$

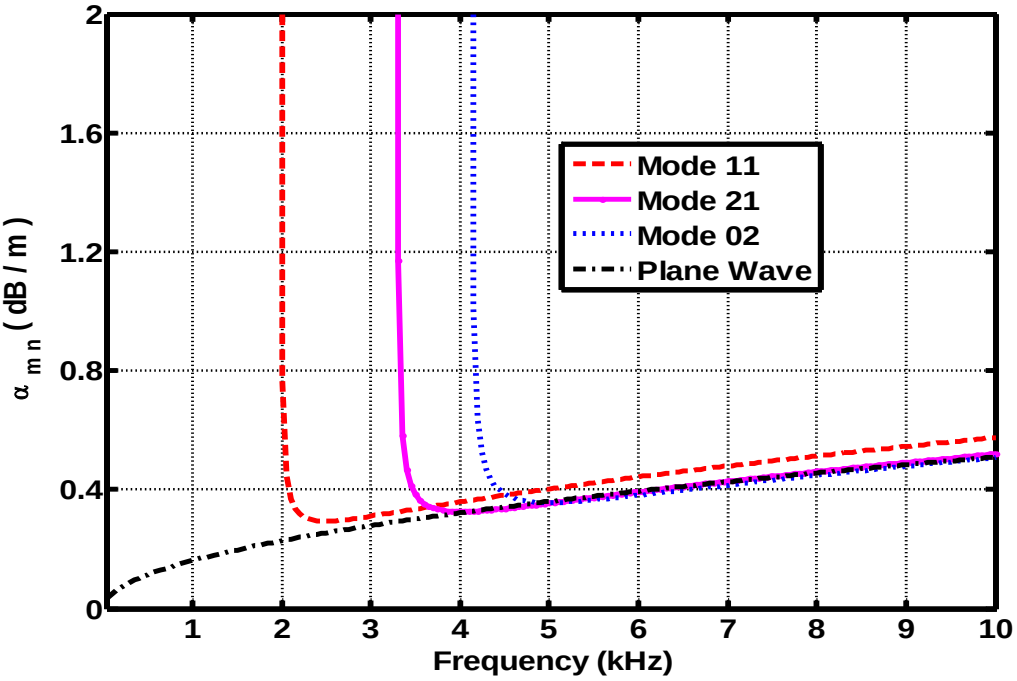

Figure 4. Attenuation coefficient vs. frequency for plane wave and first three higher order modes.

The plot of attenuation coefficients of plane wave and first three higher order modes for a circular rigid walled conduit of 0.1 m diameter computed from (9) and (10) are given in Fig. 4.

Two other important points regarding propagation of modes in hard walled circular conduits need to be highlighted here. In a study by McSkimin, the Helmholtz wave equation for a circular conduit has been solved using the method of separation of variables (McSkimin 1948). Based on his experiments of sound propagation through a circular conduit delay line, it was established that, at a receiving microphone, the contribution of higher order modes is very small except when it is in a very close proximity to the source (at $\approx z < \lambda$). In close proximity to the source, variations in the

signal pressure due to higher order modes become pronounced as the microphone is moved over a radial distance of $r = a$, i.e. from the centerline of the conduit to the wall. When close to the source, the prediction of acoustic pressure at the receiver by summing the pressure contained in all modes as highlighted by (4) gives results only slightly greater (about 1.6 dB) than those given by just considering the fundamental plane wave mode. Therefore, when measuring the acoustic signal away from the source, it is sufficient to consider the pressure contribution from the plane wave mode only. The accuracy of the pressure measurements can be enhanced by placing the receiving microphone as close to the centerline of the conduit as is possible. A similar conclusion is also presented by Dyer in her study on analyzing the measurement of noise in ventilation ducts (Dyer 1958). Dyer's study also establishes that the modes of propagation in the circular conduits are statistically independent to the extent that the cross correlation of different modes is zero. Therefore, for the purposes of this study, measuring the pressure in the principal plane wave mode is considered sufficient to predict pressure at the receiving microphone away from the source within a frequency range of 50 Hz to 10.0 kHz for a 0.2 m and 0.1 m diameter circular rigid walled conduits. Further analysis in this study is limited to considering the plane wave only, as the source of maximum pressure transfer to the receiving microphone away from the source. The next section presents analysis of plane wave propagation in cylindrical conduits.

3.2 Plane Waves in Cylindrical Conduits

As described in (Kinsler, Frey et al. 2000) under the assumption that only the plane waves are propagating in an infinitely long rigid lossless cylindrical conduit, (1)

reduces to a linear, one dimensional, homogenous, constant coefficient partial differential equation given as:

$$\frac{\partial^2 p}{\partial z^2} = \frac{1}{c^2}\frac{\partial^2 p}{\partial t^2}. \tag{11}$$

The general solution of (11) for a plane wave travelling in +z direction with sinusoidal time dependence and having initial amplitude C_0 is given by:

$$P(z,t) = C_0 e^{j(\omega t - kz)}. \tag{12}$$

In order to determine the volume velocity and the characteristic acoustic impedance of the conduit, use is made of Newton's second law for one-dimensional plane waves in a conduit given by:

$$\frac{\partial p}{\partial z} = -\frac{\rho_0}{S}\frac{\partial U}{\partial t}, \tag{13}$$

where S is the circular cross-sectional area of the conduit and equals πa^2. The volume velocity (U) and the characteristic acoustic impedance (Z_c) of the conduit are given by the following relationships:

$$\begin{aligned} U(z,t) &= \frac{S}{\rho_0 c} P(z,t) \\ Z_c &= \frac{P(z,t)}{U(z,t)} = \frac{\rho_0 c}{S}. \end{aligned} \tag{14}$$

Practical conduits are not infinite in length as is the assumption for (11) from which the above relationships are derived. In cases where a plane wave travelling in a +z direction through a finite length conduit encounters a discontinuity such as an open end, part of the wave is reflected back which travels in a -z direction. Therefore, for a finite length conduit, wave equation in (11) has a general solution that represents superposition

of a wave propagating away from the source and a reflected wave. That solution has the form:

$$P(z,t) = \left[C_1 e^{j(\omega t - kz)} + C_2 e^{j(\omega t + kz)}\right], \quad (15)$$

where C_1 and C_2 are the pressure amplitudes of the wave propagating away from the source and reflected waves. Similarly the volume velocity can be calculated from (15) and (14) as:

$$U(z,t) = \left(\frac{1}{Z_c}\right)\left[C_1 e^{j(\omega t - kz)} - C_2 e^{j(\omega t + kz)}\right]. \quad (16)$$

For a cylindrical conduit of length L terminated at $z=L$ by load impedance (Z_L), the ratio of complex amplitudes C_2/C_1 is termed as the complex pressure reflection coefficient (R) and is given by:

$$R = \frac{C_2}{C_1} = e^{2jkL}\left[\frac{Z_L - Z_c}{Z_L + Z_c}\right]. \quad (17)$$

For an infinite cylindrical conduit, the load impedance (Z_L) equals the characteristic impedance Z_c and hence there is no reflection. For a finite length rigid conduit, however, R depends on the termination condition of the conduit. When a conduit is open at one end, the load impedance becomes equal to the radiation impedance and therefore part of the acoustic energy is reflected back into the conduit. The effect of these reflections has been analyzed in detail for flanged and unflanged conduits. For a conduit flanged at an open end, the reflections have been addressed in detail in (Rayleigh 1896), (Olson 1947) and (Fletcher and Rossing 1998). For unflanged conduits, when the thickness of the conduit is small compared to the acoustic wavelength, the effect of reflections due to the open end has been analyzed in (Levine and Schwinger 1948). This aspect is addressed in detail in section 3.5.

The input impedance (Z_{in}) of the air column in a conduit is defined as the ratio of pressure and volume velocity at the input end (z=0). Assuming lossless propagation over the length of air column in the conduit, it is given by (Munjal 1987):

$$Z_{in} = \frac{P(0,t)}{U(0,t)} = Z_c \left[\frac{C_1 + C_2}{C_1 - C_2}\right] = Z_c \left[\frac{Z_L \cos kL + jZ_c \sin kL}{jZ_L \sin kL + Z_c \cos kL}\right]. \quad (18)$$

The input impedance and the reflection coefficient (R) are related by the following expression:

$$R = \frac{Z_{in} - Z_c}{Z_{in} + Z_c};\ Z_{in} = Z_c \frac{1+R}{1-R} \quad (19)$$

The input impedance provides very useful information about the frequency response of the acoustic behavior of a conduit excited with a sinusoidal signal. It enables prediction of the response of the conduit such that the sharper and stronger peaks in the input impedance plots indicate frequencies that can be easily transmitted through the conduit. To demonstrate the usefulness of the expression in (18), the response of a conduit can now be determined for several ideal load impedance conditions. With a conduit rigidly closed at the terminal end, the load impedance is $Z_L = \infty$, and (18) reduces to:

$$Z_{in} = -jZ_c \cot kL. \quad (20)$$

The important feature of this expression is that it is entirely imaginary indicating that the acoustic energy does not leave the conduit. This is consistent with the physical situation where a rigidly closed end does not allow radiation out of the conduit. A plot of the magnitude of input impedance normalized by Z_c versus parameter kL is given in Fig. 5.

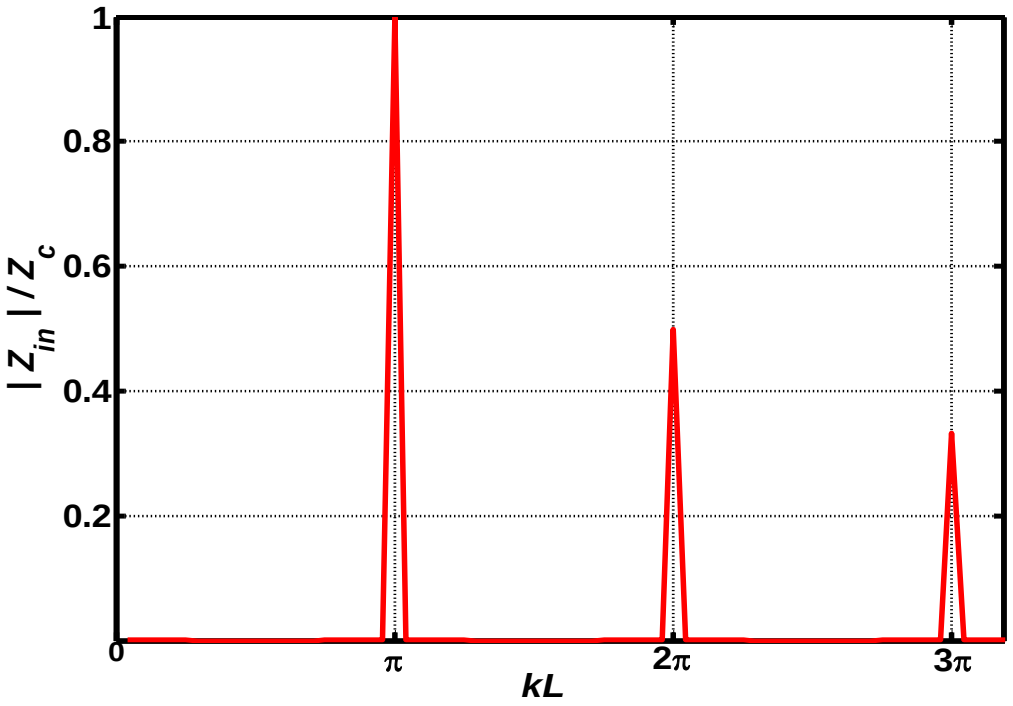

Figure 5: Normalized $|Z_{in}|$ vs. kL for $Z_L = \infty$.

Alternatively, when the conduit is ideally open at one end, it implies that Z_L is equal to zero. This situation is physically not realizable as a terminating medium with some finite Z_L always exists. This condition reduces (18) to:

$$Z_{in} = jZ_c \tan kL. \tag{21}$$

A plot of the magnitude of input impedance normalized by Z_c versus parameter kL for this case is given in Fig. 6. It can be observed that the impedance peaks in Fig. 5 occur at $kL = n\pi$. Substituting $k = 2\pi f/c$, the resonance peaks for a conduit closed at one end are found to be at:

$$f_n = \frac{nc}{2L} \tag{22}$$

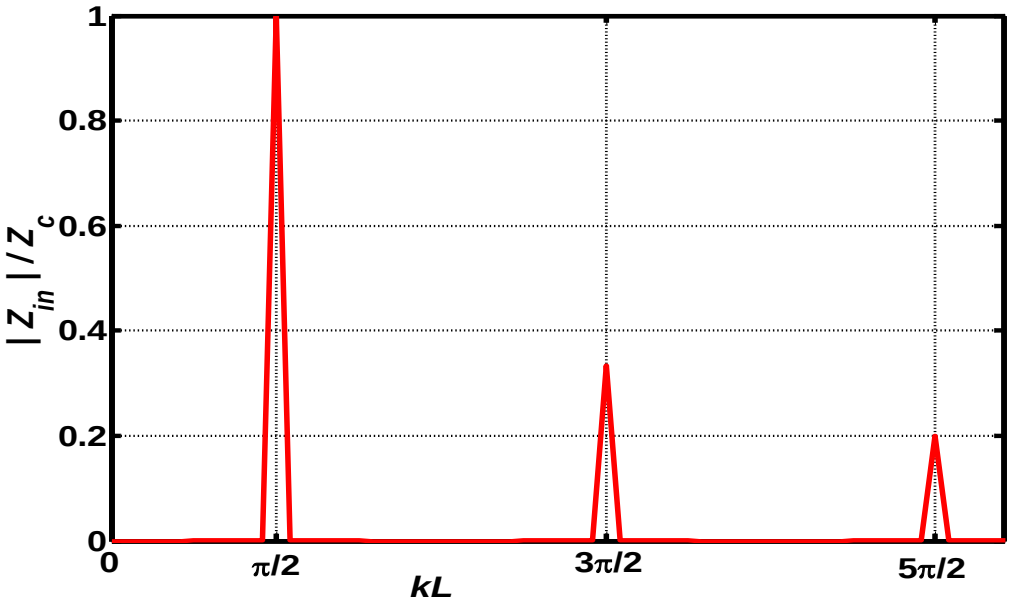

Figure 6: Normalized $|Z_{in}|$ vs. kL for $Z_L = 0$.

For the case in Fig. 6 of an open ended conduit, the resonances occur at $kL = n\pi/2$. Therefore the general expression for resonances is:

$$f_n = \frac{(2n-1)c}{4L} \tag{23}$$

Having analyzed the resonances in conduits with a closed and an open end, it is important to consider that the expression for input impedance of a conduit in (18), is of the same form as that for an electrical transmission line. The next section presents an approach in which the acoustic conduit is modeled using a two port analysis akin to electrical transmission lines.

3.3 Two Port Analyses of Plane Waves in a Conduit

There has been extensive work on analyzing acoustic wave propagation in conduits similar to electrical transmission line networks, using 'two port' analysis with transmission matrices (Keefe 1982; Okamoto, Boden et al. 1994). While analyzing acoustic conduit using this approach, it is considered that the pressure is analogous to the voltage and the volume velocity is analog of the current in electrical transmission line. The essence of the approach is to break the system being analyzed into discrete elements which can be modeled by using basic techniques in acoustics.

The analysis is accomplished by taking two state variables, acoustic pressure (*P*) and volume velocity (*U*) at the input and output sides of the conduit of length *L* shown in

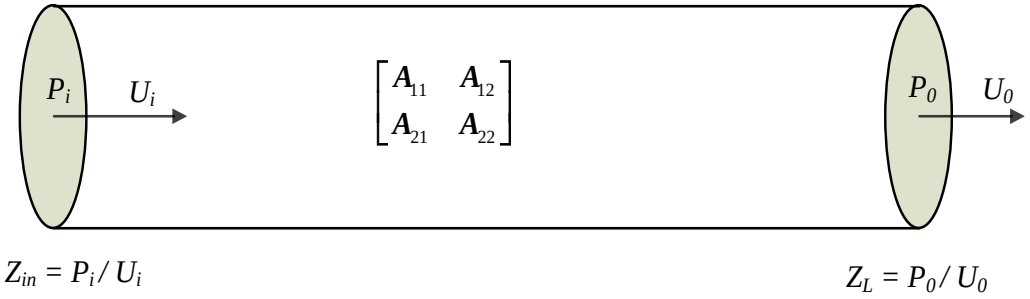

Figure 7: An acoustic conduit as a two port element.

Fig. 7 and establishing a relationship between them in terms of a 2×2 matrix as given in (Munjal 1987):

$$\begin{bmatrix} P_i \\ U_i \end{bmatrix} = \begin{bmatrix} A_{11} & A_{12} \\ A_{21} & A_{22} \end{bmatrix} \begin{bmatrix} P_0 \\ U_0 \end{bmatrix} \tag{24}$$

Where P_i, P_0, U_i and U_0 are the sound pressures and volume velocities at the input and output end of the conduit in Fig. 7. The four pole parameters of the transmission matrix (*T*) can be found by realizing that:

$$A_{11} = \left.\frac{P_i}{P_0}\right|_{U_0=0};\ A_{12} = \left.\frac{P_i}{U_0}\right|_{P_0=0};$$
$$A_{21} = \left.\frac{U_i}{P_0}\right|_{U_0=0};\ A_{22} = \left.\frac{U_i}{U_0}\right|_{P_0=0}. \quad (25)$$

The values of these four pole parameters can be derived using relationships given in (15) and (16). That derivation is given in (Munjal 1987) and is not reproduced here. Using that work, the transmission matrix parameters for the case of a lossless conduit can be given as:

$$A_{11} = \cos(kL);\ A_{12} = jZ_c \sin(kL);$$
$$A_{21} = \frac{j}{Z_c}\sin(kL);\ A_{22} = \cos(kL) \quad (26)$$

Using the above approach, a cylindrical conduit section can be represented by its transmission matrix. It also becomes apparent that description of conduit sections in terms of their four-pole transmission matrices is convenient because the output of one section is the input of the next section and therefore, the overall transmission matrix of a cascaded set of conduit sections can be found by multiplication of transmission matrices of each section in cascade. For a cascade of *n* cylindrical sections, the input end pressure and volume velocity can be found by:

$$\begin{bmatrix} P_i^1 \\ U_i^1 \end{bmatrix} = \begin{bmatrix} A_{11}^1 & A_{12}^1 \\ A_{21}^1 & A_{22}^1 \end{bmatrix} \begin{bmatrix} A_{11}^2 & A_{12}^2 \\ A_{21}^2 & A_{22}^2 \end{bmatrix} \dots \begin{bmatrix} A_{11}^n & A_{12}^n \\ A_{21}^n & A_{22}^n \end{bmatrix} \begin{bmatrix} P_0^n \\ U_0^n \end{bmatrix}$$
$$\begin{bmatrix} P_i \\ U_i \end{bmatrix} = \begin{bmatrix} T_{11} & T_{12} \\ T_{21} & T_{22} \end{bmatrix} \begin{bmatrix} P_0^n \\ U_0^n \end{bmatrix} \quad (27)$$

where

$$\begin{bmatrix} T_{11} & T_{12} \\ T_{21} & T_{22} \end{bmatrix} = \prod_{m=1}^{n} \begin{bmatrix} A_{11}^{m} & A_{12}^{m} \\ A_{21}^{m} & A_{22}^{m} \end{bmatrix} \tag{28}$$

By comparing (24) with (18) an expression can be found for the Z_{in} of a conduit section such that:

$$Z_{in} = \frac{A_{12} + A_{11}Z_L}{A_{22} + A_{21}Z_L} \tag{29}$$

The relationship in (29) can be applied to a system of cascaded conduits to find the overall Z_{in} of the cascade.

The above analysis of a conduit section and cascade of sections has assumed that the conduit is lossless. In practice, however, losses due to viscous drag and heat conduction in the boundary layer of a conduit cause deviations from ideal behavior. These losses due to viscous and thermal boundary layers in a conduit are addressed in the next section.

3.4 Effects of the Boundary Layer on Plane Waves in Conduits

In a constant cross section conduit, in addition to the losses at the boundary layer due to thermal conduction and viscosity, friction along the conduit walls also decelerates the moving fluid particles and reduces their kinetic energy. The transfer of thermal energy between the fluid medium and conduit walls violates the adiabatic character of sound waves thereby decreasing the potential energy of moving particles (Benade 1968). These energy losses occur within a thin boundary layer along the conduit walls. The parameter that governs the viscous losses at the boundary layer is known as viscous layer thickness or skin depth (d_v). The thermal layer thickness (d_h) controls the losses due to

heat conduction at the boundary walls. The expressions for frequency dependent viscous and thermal layer skin depths along with their approximations for air at standard conditions are given by (Kinsler, Frey et al. 2000) and (Benade 1968):

$$d_v = \sqrt{\frac{2\eta}{\omega\rho_0}} = 0.21 \times 10^{-2}\, f^{-0.5}\ \ (m)$$
$$d_h = \sqrt{\frac{2\kappa}{C_p\omega\rho_0}} = \ 0.25 \times 10^{-2}\, f^{-0.5}\ \ (m), \tag{30}$$

where f is frequency in Hz, ρ_0 is the density of the medium, η is the shear viscosity, κ is thermal conductivity and C_p is the specific heat of air at constant pressure. The losses due to friction at the boundary layer are characterized by a parameter r_v which is the ratio of conduit radius (a) to viscous boundary layer thickness (d_v):

$$r_v = a\ \times (\omega\rho_0/\eta)^{0.5}. \tag{31}$$

The losses due to thermal conduction are characterized by a parameter r_t which equals:

$$r_t = a\ \times \left(C_p\omega\rho_0/\kappa\right)^{0.5}. \tag{32}$$

Benade has provided the values of molecular constants and their combinations evaluated at a temperature of 26.85°C. He also stated the approximations to the values of r_v and r_t which are given as:

$$r_v = 632.8\ a\ f^{0.5}(1 - 0.0029\ \Delta T) \tag{33}$$

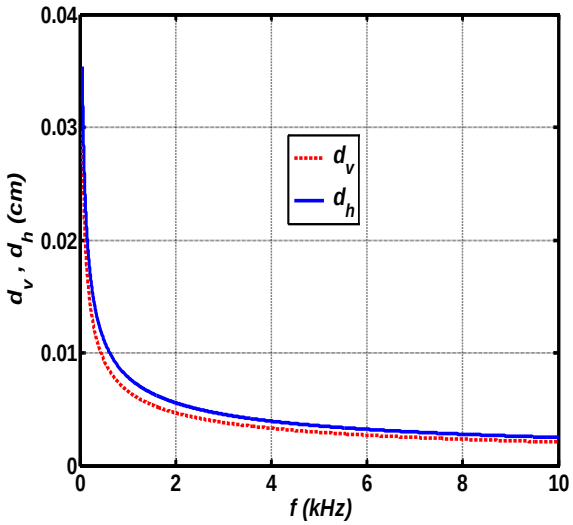

Figure 8: Viscous and thermal skin depths.

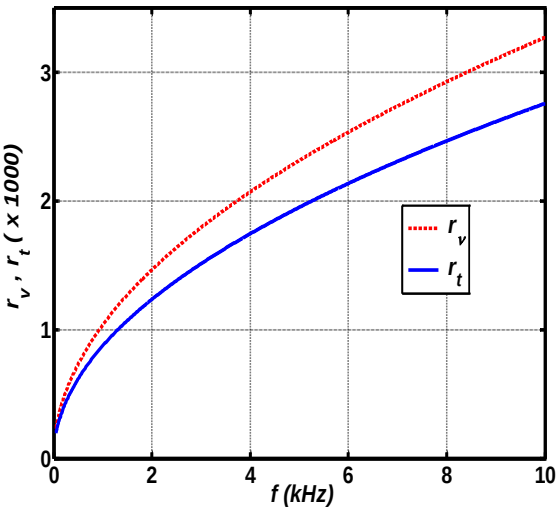

Figure 9: Dimensionless parameters r_v and r_t.

and

$$r_t = 532.2\ a\ f^{0.5}(1 - 0.0031\ \Delta T), \tag{34}$$

where ΔT is deviation of temperature in degree Celsius from 26.85°C.

The plots of d_v, d_h, r_v and r_t for a 0.1 m diameter conduit at 15°C computed using (30), (33) and (34) are given in Figs. 8 and 9. It is evident from the plots that at frequencies greater than 2.0 kHz the smaller viscous and thermal layer depths result in loss of energy in the acoustic wave due to surface friction and heat conduction at the conduit walls. The effect of losses discussed above is included in the wave equation for a plane wave given in (12) by rewriting the wave number (k) as a complex number, $\Gamma = \beta - j\alpha$, where β is the phase coefficient equal to ω/c_p and α is the attenuation coefficient per unit length. This change makes the wave equation in (12) applicable to the lossy conduits. The modified wave equation is then given as:

$$P(z,t) = C_0\ e^{-\alpha z}\ e^{j(\omega t - \beta z)} \tag{35}$$

The separation of complex wave number (Γ) into its real and imaginary parts shows in (35) that the pressure amplitude decays by e^{-1} in a distance α^{-1}meters. The reduction of pressure amplitude by e^{-1} corresponds to a power reduction of 8.686 dB,

therefore, the power attenuation in decibels per meter is given by $8.686 \times \alpha$. The pressure reduction due to thermo-viscous losses at the boundary layer also affects the phase speed of the plane wave. The expressions for phase speed and attenuation coefficient (α) for large r parameter values have been approximated by Keefe [Keefe – 1984] in terms of a dimensionless parameter r_v , γ the ratio (C_p/C_v) of specific heat at constant pressure (C_p) to specific heat at constant volume (C_v) and Prandtl number (P_r) given by $C_p\eta/\kappa$. At 26.85°C, the Prandtl number for air is 0.841 and γ has a value of 1.40. The expressions for phase speed (c_p) and attenuation coefficient (α) evaluated by Keefe are:

$$c_p^{-1} = \frac{1}{c}\left\{1 + \left(\frac{1}{r_v\sqrt{2}}\right)\left(1 + \frac{\gamma-1}{\sqrt{P_r}}\right) - \left(\frac{1}{r_v^3\sqrt{2}}\right)\left[\frac{7}{8} + \frac{\gamma-1}{\sqrt{P_r}} - \frac{1}{2}\left(\frac{\gamma-1}{P_r}\right) - \frac{1}{8}\left(\frac{\gamma-1}{(P_r)^{1.5}}\right) - \frac{1}{2}\left(\frac{\gamma-1}{\sqrt{P_r}}\right)^2 + \frac{1}{2}\left(\frac{\gamma-1}{(P_r)^{1.5}}\right)^2 + \frac{1}{2}\frac{(\gamma-1)^2}{(P_r)^{1.5}} + \frac{1}{2}\left(\frac{\gamma-1}{\sqrt{P_r}}\right)^3\right]\right\} \quad (36)$$

and

$$\alpha = \frac{\omega}{c}\left\{\left(\frac{1}{r_v\sqrt{2}}\right)\left(1 + \frac{\gamma-1}{\sqrt{P_r}}\right) + r_v^{-2}\left[1 + \frac{\gamma-1}{\sqrt{P_r}} - \frac{1}{2}\left(\frac{\gamma-1}{P_r}\right) - \frac{1}{2}\left(\frac{\gamma-1}{\sqrt{P_r}}\right)^2\right] + \left(\frac{1}{r_v^3\sqrt{2}}\right)\left[\frac{7}{8} + \frac{\gamma-1}{\sqrt{P_r}} - \frac{1}{2}\left(\frac{\gamma-1}{P_r}\right) - \frac{1}{8}\left(\frac{\gamma-1}{(P_r)^{1.5}}\right) - \frac{1}{2}\left(\frac{\gamma-1}{\sqrt{P_r}}\right)^2 + \frac{1}{2}\left(\frac{\gamma-1}{(P_r)^{1.5}}\right)^2 + \frac{1}{2}\frac{(\gamma-1)^2}{(P_r)^{1.5}} + \frac{1}{2}\left(\frac{\gamma-1}{\sqrt{P_r}}\right)^3\right]\right\} \quad (37)$$

For air at 26.85°C and $r_v > 2$, the phase speed and attenuation coefficient have been approximated as:

$$c_p^{-1} = \frac{1}{c}\left(1 + \frac{1.045}{r_v}\right) \tag{38}$$

and

$$\alpha = \frac{\omega}{c}\left(\frac{1.045}{r_v} + \frac{1.080}{r_v^2} + \frac{0.750}{r_v^3}\right). \tag{39}$$

Based on assuming an isothermal wall of the conduit, Keefe also approximated the value of the complex characteristic impedance of the conduit Z_c'. He presented a simplified expression for Z_c' of air at 26.85°C and $r_v > 2$, that can be used in engineering applications without significant loss of accuracy:

$$\begin{aligned} \Re(Z_c') &= Z_c\left(1 + \frac{0.369}{r_v}\right) \\ -\Im(Z_c') &= Z_c\left(\frac{0.369}{r_v} + \frac{1.149}{r_v^2} + \frac{0.303}{r_v^3}\right) \end{aligned} \tag{40}$$

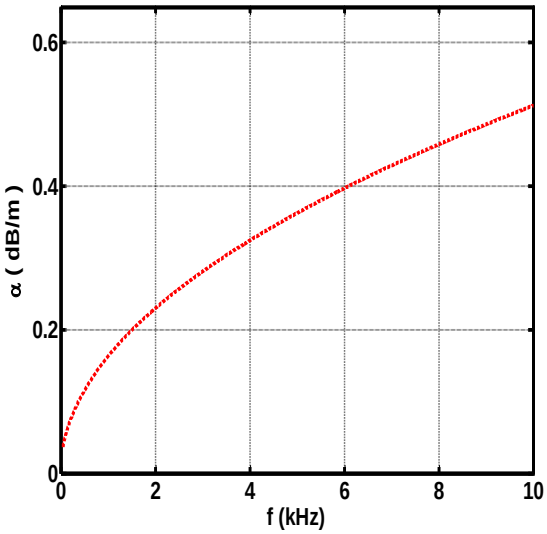

Figure 10: Attenuation coefficient (α) vs. frequency.

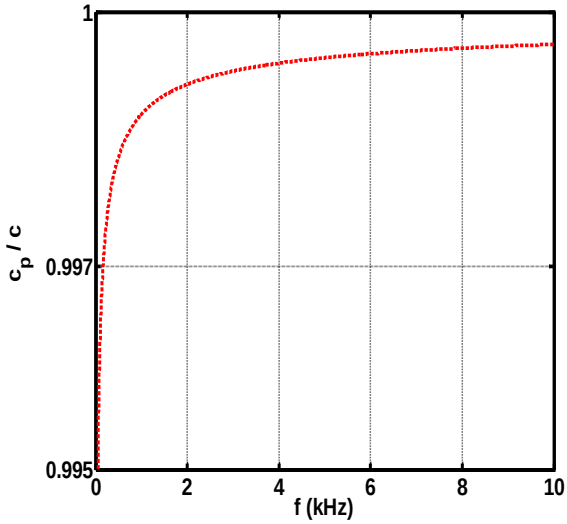

Figure 11: Phase speed (c_p) normalized to speed of sound (c) vs. frequency.

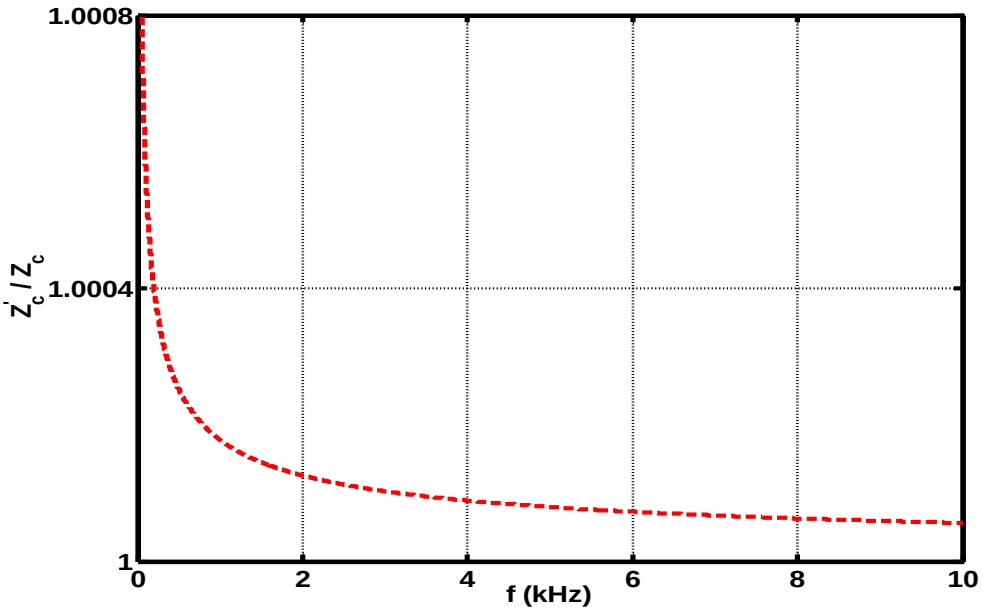

Figure 12: Ratio Z_c'/Z_c vs. frequency.

Figs. 10 and 11 show the attenuation coefficient for a 0.1 m diameter conduit and ratio of phase velocity to the speed of sound computed at 15°C. Fig. 12 shows the ratio Z_c'/Z_c for a 0.1 m diameter conduit. The density of air has been taken as 1.21 kg/m^3. It can be seen from the plots that the phase speed is almost equal to the speed of sound for a plane wave and Z_c' is also very close to Z_c. The attenuation coefficient increases due to wall friction and thermal conduction losses at the walls as the thickness of viscous and thermal boundary layers decreases.

It is also to be considered that these losses have been evaluated under the assumption that conduit walls remain isothermal during the oscillatory cycle. However, this ideal condition does not prevail in practical situations as localized heating of fluid transfers heat to the inner walls of conduit. As any conduit has a finite capacity to absorb heat, a local rise in temperature takes place at the conduit wall. This decreases the thermal gradients in the boundary layer of the fluid and the heat conduction losses are somewhat reduced compared to the ideal isothermal wall condition. Franken et al. have

analyzed the case of sound propagation in conduits with non-isothermal walls (Franken, Clement et al. 1981). Keefe has also analyzed this aspect and has shown that the effect of non-isothermal walls can be incorporated in (36) and (37) by substituting γ_e for γ such that:

$$\gamma_e = \frac{\gamma - 1}{1 + \epsilon_w} + 1. \tag{41}$$

The dimensionless parameter ϵ_w defines the oscillatory heat transfer at the solid-gas interface and is given by:

$$\epsilon_w = \left(\frac{C_p \kappa \rho_0}{\rho_w C_w \kappa_w}\right)^{\frac{1}{2}} \tag{42}$$

where ρ_w, C_w and κ_w are mass density, specific heat and thermal conductivity of the conduit wall material. Keefe has also concluded that in the case of air as the fluid medium in a PVC conduit, the parameter ϵ_w is on the order of 0.01 (Keefe 1984) and hence, its effect on attenuation coefficient in (37) is negligibly small. Therefore, for the purposes of this study effect of non-isothermal conduit walls is not considered any further.

The lossy conduit assumption with complex propagation wave number Γ and characteristic impedance Z_c', also results in modifications to the expressions of four pole parameters given in (26). The new set of the transmission matrix parameters is given in (Munjal 1987) (Shi 2009) by:

$$\begin{aligned} A_{11} &= \cos h(\Gamma L);\ A_{12} = jZ_c' \sinh(\Gamma L);\\ A_{21} &= \frac{j}{Z_c'} \sinh(\Gamma L)\ ;\ A_{22} = \cosh(\Gamma L). \end{aligned} \tag{43}$$

With the modified parameters, the value of frequency dependent input impedance can be computed for a lossy conduit using the expression in (29). However, for finding the input impedance, it is important to consider the reflections from the open end of a conduit and the effect of frequency dependent radiation impedance which acts as a load impedance. This aspect is analyzed in the next section.

3.5 Acoustic Radiation from Open Ends in Conduits

The discussion so far has been principally concerned with the propagation of sound waves within finite length conduits that are open at one end. For such cases the load impedance at the open end has been assumed to be given by the ideal, low-frequency approximation that is $Z_L = 0$. In order for the sound waves to be heard, however, it is necessary that they escape from the open end and propagate into the surrounding environment. The fact that acoustic waves can be heard originating from a cylindrical conduit with an open end indicates that the assumption of Z_L being equal to 0 is practically not valid. The surrounding atmosphere presents finite impedance, known as radiation impedance, to the acoustic energy coming out of the open end.

For the purpose of this analysis, consider that one end of the conduit at $z = L$ is open to free space and the other end has an acoustic source driving the sound energy into the conduit. Assuming a plane wave as the dominant mode of propagation within the conduit and neglecting the non-uniformity of volume velocity and pressure distribution across the open end, it can be assumed that the air at the open end acts like a piston, radiating sound out into the open as well as reflecting some back towards the driving source at the end z=0 (Kinsler, Frey et al. 2000). In the long wavelength limit ($ka \ll 1$), a strong standing wave builds up inside the conduit (Levine and Schwinger 1948).

However, as the driving frequency is increased more energy leaks out of the open end. Therefore, the load impedance at the open end, which is radiation impedance, can be defined as the ratio of mean pressure at $z = L$ to the mean axial velocity. This impedance is complex, its reactive part produces reflections back to the driving source and its resistive part represents energy being radiated out of the open end (Morse and Ingard 1968).

The conduits considered in present study have open ends with no flare (such as a horn) at the end of the fluid column that can transform the load impedance to match it with that of the source to achieve maximum radiation and reduce the reflections. It is therefore, necessary to determine the radiation characteristics of the open end. The derivation of complex radiation impedance terminated in a flanged or an un-flanged open end has been the subject of many researchers. The first results were obtained by considering a circular piston set in an infinite wall (Olson 1947; Morse and Ingard 1968). For the case of a conduit terminating in an infinite flange the approximation for radiation impedance was given by (Rayleigh 1896) as:

$$Z_r = R_r + jX_r$$

$$R_r = \frac{c}{\pi a^2}\left[\frac{(2ka)^2}{2.4} - \frac{(2ka)^4}{2^2.\ 4^2\ .6} + \frac{(2ka)^6}{2^2.\ 4^2\ .6^2.8} - \cdots\right] \tag{44}$$

$$X_r = \frac{c}{\pi a^2}\left[\frac{4}{\pi}\frac{(2ka)}{3} - \frac{(2ka)^3}{3^2.5} - \frac{(2ka)^5}{3^2.\ 5^2.7} + \frac{(ka)^7}{3^2.\ 5^2\ .7^2.9} - \cdots\right]$$

The radiation impedance Z_r is also related to the frequency dependent reflection coefficient R and the characteristic impedance of the conduit at the open end by the relationship given in (Munjal 1987):

$$Z_r = \frac{c}{\pi a^2}\left(\frac{1+R}{1-R}\right)$$
$$R = \left(\frac{Z_r + \frac{c}{\pi a^2}}{Z_r - \frac{c}{\pi a^2}}\right) \quad (45)$$

and the reflection coefficient at the open end is given by:

$$R = -|R|\, e^{2jkL}. \quad (46)$$

For the case of an unflanged conduit with an open end, Levine and Schwinger have found a rigorous and explicit solution to the problem of sound radiation assuming axial symmetry of the pressure excitation by solving an integral equation using Wiener-Hopf technique (Levine and Schwinger 1948). They determined that within the conduit the velocity potential was same as if the conduit was lengthened by a certain fraction of its radius as shown in Fig. 13. The conduit behaves as if it had a length of $L + \delta l$ with small purely real load impedance (R_r).

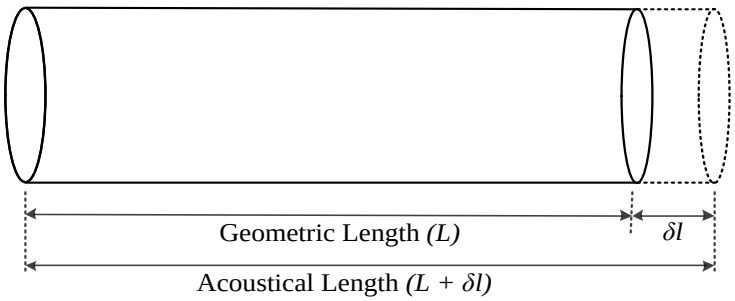

Figure 13: Geometric and acoustical length of a conduit.

The length correction is given by:

$$\delta l = \frac{1}{k}\tan^{-1}\frac{Z_r}{jZ_c'}. \quad (47)$$

The length correction, in case of lower frequencies, has been determined for a flanged conduit to be 0.85 times the radius and for an unflanged conduit 0.6133 times the radius of conduit. Due to the frequency dependence of the length correction, the resonance peaks inside the conduit get broader and less pronounced with the increase in frequency. This is apparent through comparison of input impedance plots for lossless and lossy conduit cases with radiation impedance of the open end as the load impedance.

As the determination of radiation impedance using the integral formulations of Raleigh and Levine and Schwinger are very complex, there have been many attempts at presenting approximations for computing the radiation impedance and reflection coefficient by putting some restrictions on the parameter *ka* (product of free space wave number and the conduit radius), for example in (Norris and Sheng 1989; Dalmont 2001). However, these approximations did not completely fulfill the conditions for a physically representative model e.g. the hermitian property of the reflection coefficient and causality of the impulse response of the reflection coefficient. This study uses the approximate formula for reflection coefficient based on accurate analytical or numerical fitting for an unflanged conduit given by Silva (Silva, Guillemain et al. 2009):

$$R(\omega) = -\left(1 - \frac{jka}{\mu'}\right)^{-(\nu+1)} \tag{48}$$

The values of parameter μ' and ν for flanged and unflanged cases are presented in Table. 2.

This model shows good agreement with that given by Levine and Schwinger for unflanged conduits in the low frequency limit (*ka* < 2) and by Zorumski for flanged conduits (Zorumski 1973). The plot of magnitude of *R* computed from (48) for a 0.1 m flanged and unflanged conduit corresponding to a frequency range between 50 Hz to 1.95

kHz ($0.046 < ka < 1.82$) is given in Fig. 14. Comparison between the computed reflection coefficient from (46) and (48) is given in Fig. 15.

It can be observed that both the approximations shown in Fig. 15 demonstrate good agreement for values below 1.42 kHz ($ka = 1.32$). At frequencies higher than this the deviation between the approximations increases. At those frequencies, approximation by Rayleigh gives more accurate results. The plot in Fig. 16 shows real and imaginary parts of the radiation impedance computed from (45) using the approximation given in (44). It indicates that for a 0.1 m diameter conduit, the imaginary part of the Z_r remains

Table 2: Values of parameters μ' and ν

Parameters	Unflanged conduit	Flanged Conduit
μ'	1.226	0.8216
ν	0.504	0.350

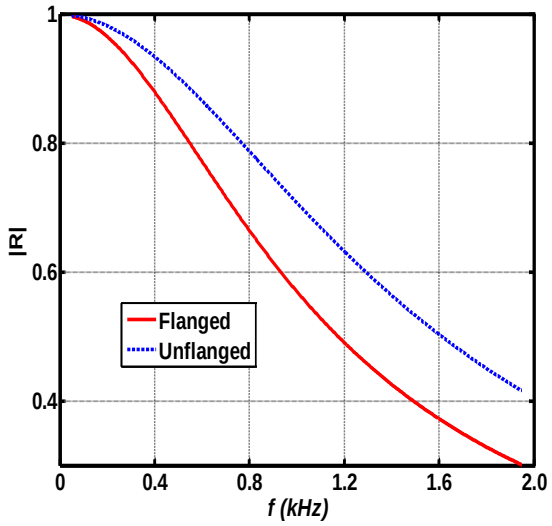

Figure 14: Reflection Coefficient magnitude computed for flanged and unflanged conduits using (48) and Table 2.

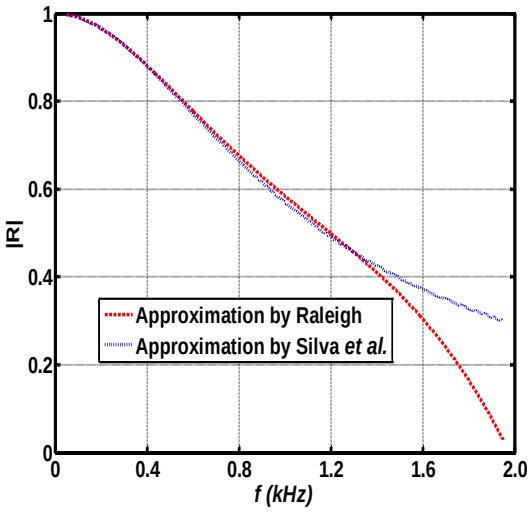

Figure 15: Comparison between $|R|$ from approximations in (46) and (48).

dominant at frequencies less than 1.3 kHz. For these frequencies the magnitude of the reflection dominates the magnification of the radiation from the open end. However beyond 1.3 kHz, the real part of Z_r becomes dominant which explains the greater radiation and lower reflection coefficient for frequencies higher than 1.3 kHz.

The evaluation of reflection coefficient and radiation impedance using (45) enables the determination of normal incidence acoustic absorption coefficient of sound

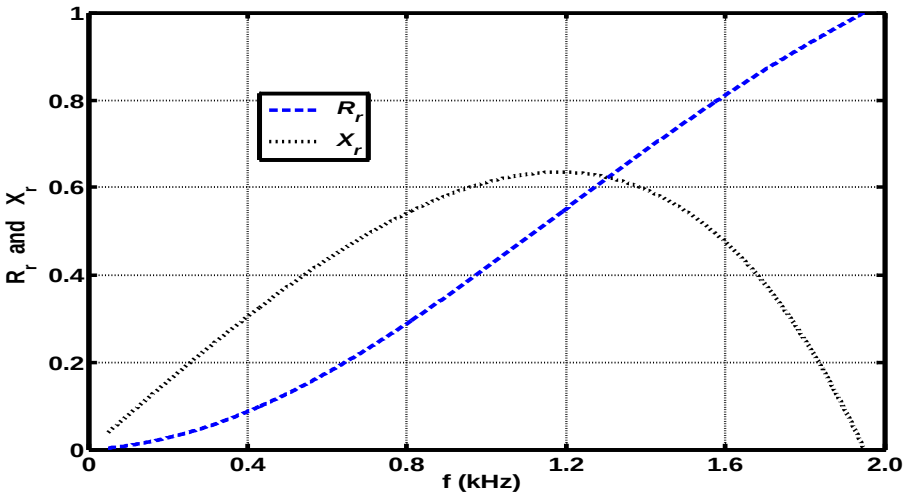

Figure 16: Normalized magnitudes of Z_r components vs. frequency.

absorbing materials as in (Chung and Blaser 1980) and (Wyerman 1976). In order to reduce the effect of reflections from an open end during the measurement of acoustic properties of conduit liner materials, two methods are generally used. In the first method a sound absorbing material is placed at the open end of the conduit so that the acoustic energy escaping from the open end of the conduit is absorbed and the effect of any reflections on the measurements is minimized. In the second method, the length of the conduit is increased so that the receiving microphone in the conduit can be placed away from the open end to minimize the effect of reflections akin to an infinitely long conduit that has no reflections. In the present study, the second approach is used and 17.56 m

long conduit is extended by about 12λ at 1.0 kHz from the location of the receiving microphone.

Using the expressions for radiation impedance, frequency dependent complex characteristic impedance and attenuation coefficient of the conduit as laid out in the previous discussion, the input impedance of a lossless and lossy conduit can be compared using (18). For lossless conduit, the characteristic impedance, Z_c, is determined from (14) and the load impedance is determined from the approximation for Z_r given in (44). For the lossy case, Z_c, is replaced with the complex frequency dependent characteristic impedance Z_c' given in (40). The input impedance in both cases for a 5 m long, 0.1 m diameter conduit is plotted in Fig. 17 within a frequency range of 200 Hz to 1200 Hz. The resonance peaks in both plots are visible. In case of lossy conduit, the peak magnitudes are in general less than those of the lossless conduit. Also, as the frequency is increased the peaks tend to shift in frequency in the case of lossy conduit due to higher open end length correction (0.85 a).

Having discussed the sound propagation in case of a straight conduit, it is important to also take a look at the effects of introducing junctions with side branches and how that affects the attenuation of acoustic signal in a conduit network. This is the subject of next chapter.

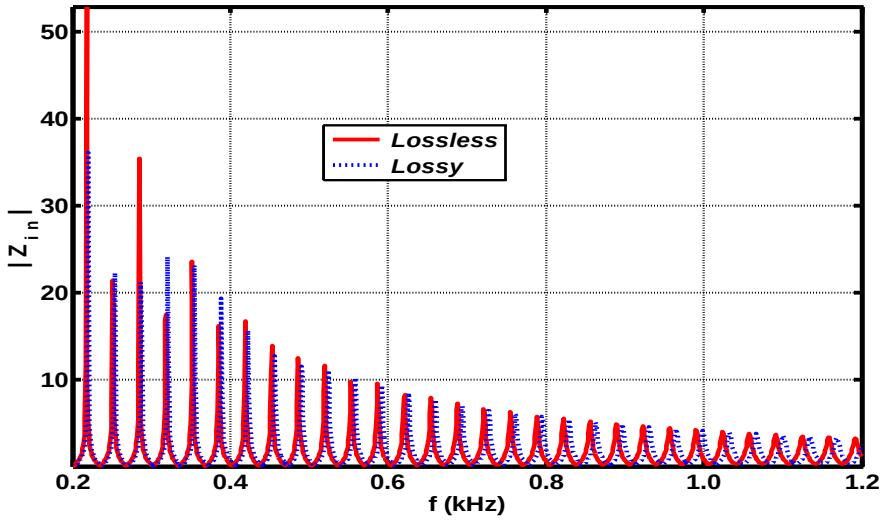

Figure 17: $|Z_{in}|$ vs. frequency for a 0.1 m diameter, 5 m long conduit.

CHAPTER 4: ACOUSTICS OF CONDUIT NETWORKS

4.1 Introduction

In many industrial and domestic applications conduits are used with multiple side branches that are connected to form a T-junction and thereby forming an acoustic network. When a sound wave is excited in the main conduit, it induces the sound waves in the connected side branches as well. The main principle governing this transport of sound energy into the side branches is that the energy incident upon a side branch must be conserved unless there are other sound attenuating mechanisms. The distribution of energy among the side branches depends upon the relative impedances of the junctions.

The combination of conduits connected in a network to produce the desired acoustic response has been studied in the context of design of acoustical filters. Following the development of electrical filters, Stewart was the first one to demonstrate that the combination of a straight conduit with a side branch can be used to control the transmission characteristics of the main conduit (Stewart 1925). Using lumped circuit analysis analogous to that for electrical filters, he showed that within the main conduit the transmission of frequencies that correspond to the resonant frequencies of the side branch would be adversely affected. In this study, the focus is on the approach mentioned by Stewart to model the signal attenuating effects of side branches.

4.2 Propagation Model of Conduit with One Side Branch

4.2.1 Stewart's Model

Stewart analyzed the influence of a side branch upon acoustic transmission through a conduit and developed an expression for the ratio between the transmitted acoustic energy with the branch present to that with the branch absent for the case of an acoustic filter (Stewart 1925). He assumed a plane wave propagating through a conduit of constant cross-sectional area with acoustic source at one end of the conduit. He also assumed that source pressure was not affected by the presence of side branch.

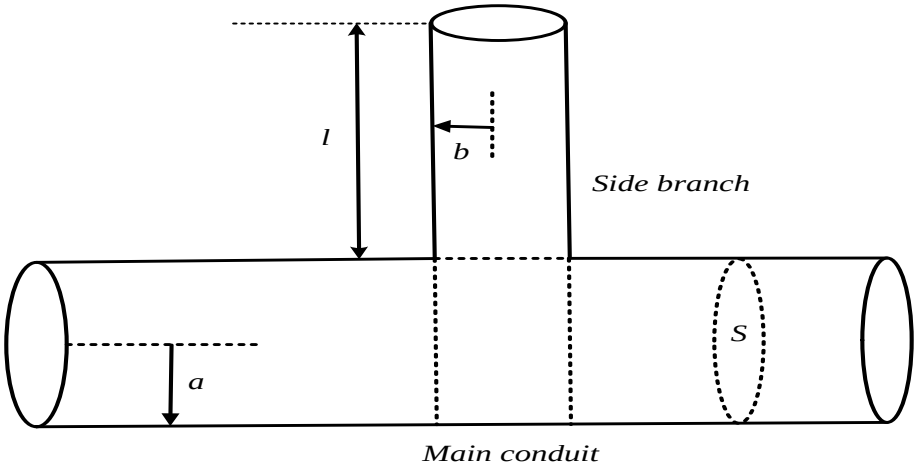

Figure 18: A conduit with one side branch.

A conduit with a radius a and cross sectional area S with one side branch having a radius b and cross-sectional area S_b is shown in Fig. 18. As an analog to electrical circuits, the sinusoidal source pressure is given as $P = P_0\, e^{j\omega t}$. At the junction point between the main conduit and the side branch the pressure is affected by the reflections from the side branch. At the junction point, therefore, the pressure in the main conduit is

given by $P' = P_0' e^{j\omega t}$. The altered pressure at the junction point P' is caused by two waves, one from the source and the other from the side branch. Stewart has also determined that the resulting pressure at the junction point due to the wave from the side branch is given by:

$$P' = P - \rho_0 c \frac{U}{2S}$$
$$U = \frac{P'}{Z_b} \tag{49}$$

Where *U* is the volume velocity in the side branch and Z_b is its complex input impedance given by $Z_b = R_b + j X_b$. The ratio P'/P is the pressure transmission coefficient (T_π) describing the fraction of transmitted signal propagating beyond the junction with side branch. From (49), it can be derived in terms of side branch impedance Z_b as follows:

$$\frac{P'}{Z_b} = U = \frac{P}{Z_b} - \rho_0 c \frac{U}{2SZ_b}$$
$$\frac{U}{P} = \frac{1}{\left(Z_b + \frac{\rho_0 c}{2S}\right)} \tag{50}$$
$$U = P \left(Z_b + \frac{\rho_0 c}{2S}\right)^{-1}$$

From (50), the pressure transmission coefficient is obtained by putting the value of the volume velocity *U* in (49), such that:

$$\frac{P'}{P} = T_\pi = 1 - \left(\frac{\rho_0 c}{2S}\right)\left(Z_b + \frac{\rho_0 c}{2S}\right)^{-1} \tag{51}$$

The pressure transmission coefficient is complex and frequency dependent as the impedance of side branch is complex and varies with frequency. From (51), the sound pressure transmission loss (Ω) due to the junction with side branch can be defined as:

$$\Omega = \frac{P}{P'} = \frac{1}{T_\pi} = \frac{Z_b + \frac{\rho_0 c}{2S}}{Z_b}$$
$$\Omega\,(\text{dB}) = 20 \times \log_{10}\left(\frac{1}{T_\pi}\right). \tag{52}$$

From (52), the transmission loss of the propagating signal due to the presence of side branch can be evaluated, provided that Z_b is evaluated from analytical expressions. To determine Z_b, Stewart's expressions for real and imaginary part of Z_b for an open ended side branch given in (Stewart 1926) are used. Stewart's expressions for R_b and X_b are reproduced below:

$$R_b = (\rho_0 k f) D^{-1}$$
$$X_b = \frac{\rho_0 \omega}{4b} + \left[\frac{\rho_0 \omega}{\pi b^2}.\sin kl\ \cos kl + \frac{\rho_0 \omega}{5.5b}(\cos^2 kl - \sin^2 kl)\right. \tag{53}$$
$$\left. - k\pi b^2 \rho_0 \omega \left(\frac{k^2}{4\pi^2} + \frac{1}{(5.5b)^2}\right).\sin kl \cos kl\ \right]$$
$$\times D^{-1}$$

where

$$D = k^2\pi^2 b^4 \left(\frac{k^2}{4\pi^2} + \frac{1}{(5.5b)^2}\right)\sin^2 kl + \cos^2 kl$$
$$- \frac{2k\pi b^2}{5.5b}\sin kl \cos kl, \tag{54}$$

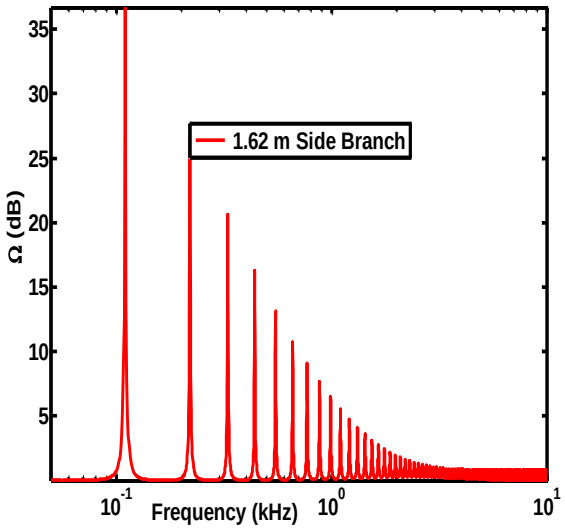

Figure 19: Transmission loss due to a 0.05 m diameter 1.62 m long side branch.

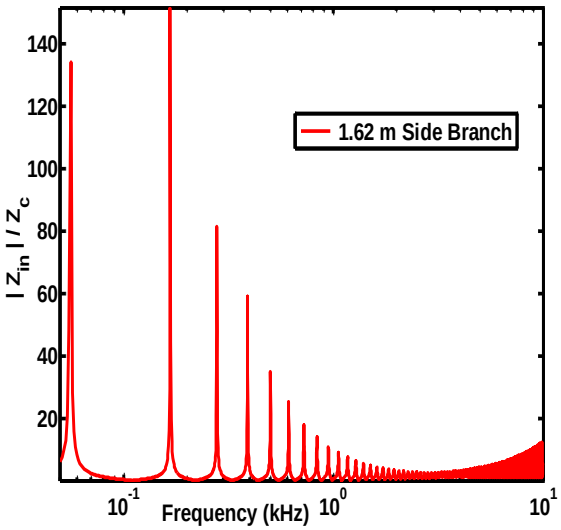

Figure 20: Input impedance of a 1.62 m long 0.05 m diameter side branch.

and b is the radius of the side branch and l is its length. Representative plot of the transmission loss over a logarithmic frequency range between 50 Hz to 10 kHz due to a 1.62 m, 0.05 m diameter side branch in a main conduit of 0.1 m diameter is given in Fig. 19. The normalized input impedance of the side branch obtained from Stewart's expressions in (53) and (54) is also plotted in Fig. 20.

It can be observed that the side branch impedance acts similar to parallel impedance in an electrical circuit. The maxima of transmission loss in the main conduit coincide with the minima of Z_b. When $Z_b = 0$, no power is transmitted past the junction as all of it is reflected back to the source. This condition is akin to a short in a parallel arm of an electrical circuit. When R_b is larger than 0 but is not infinite, some power is consumed in the side branch and part of it is transmitted past the junction. When either R_b or X_b is very large compared to Z_c, the characteristic impedance of the conduit, almost

all the incident power is transmitted past the side branch. In the limit, $R_b = X_b = \infty$, which corresponds to no side branch, the signal propagates with no transmission loss.

Stewart's model is general as it can be applied to an acoustic network with a number of side branches and is independent of the nature of the side branch. It has also been shown to agree very well with empirical data (Stewart 1926). However, it has two limitations that can make the predicted results using this model deviate from experimental measurements. First, this model does not take into account the losses due to reflections from the open end of the main conduit as it assumes an infinitely long conduit that terminates in its characteristic impedance with no reflections. The second limitation is that this model assumes no signal flow into the side branch. Although, it adequately models the effect of reflections at the junction point causing the transmission loss, however, it does not take into account the escape of acoustic energy due to the finite frequency dependent radiation impedance at the open end of the side branch. The simplicity of this model makes it a good choice for empirical modeling. The accuracy of the model, however, can be enhanced by including a correction term to take care of the losses in the main conduit due to reflections from the open end. This is explained in more detail in the development of the empirical model in the next chapter.

4.2.2 Mason's Model

Following Stewart's pioneering effort to model the effect of a side branch on the pressure transmission through a conduit, Mason extended Stewart's analysis and analyzed the filtering effects of recurrent side branches in a main conduit (Mason 1927). His analytical model is based on assuming a plane wave of sound propagating in a uniform duct to determine the propagation constant. The propagation constant is then

translated into attenuation and velocity characteristics by considering its real and imaginary parts. His approach is valid under the condition that:

$$\sqrt{\frac{\rho_0 \omega}{2\eta}} > \frac{2}{a} \tag{55}$$

For the frequencies of interest between 50 Hz to 10 kHz and air as a medium, this condition is satisfied for a 0.2 m and 0.1m diameter conduits. For a straight conduit with no side branches, the attenuation coefficient is given by:

$$\alpha = \Re\left[\sqrt{\frac{-\omega^2}{c^2} - \frac{-2\omega^2}{ac^2}\sqrt{\frac{\zeta}{2\omega\rho_0}} + j\frac{-2\omega^2}{ac^2}\sqrt{\frac{\zeta}{2\omega\rho_0}}}\right], \tag{56}$$

where ζ is parameter to take into account the losses due to viscosity and heat conduction. For a conduit with one side branch as shown in Fig. 21, the ordinary assumption is that the width of the junction is small compared to the wavelength. The side branch length correction is $0.785b$ at the junction end and $0.57b$ at the open end. So the total length of side branch becomes $l' = l + (0.785 + 0.57)b$. With this length correction, the attenuation coefficient of the structure in Fig. 21 is given by:

$$\alpha = \Re\left\{2j\Gamma L_s + cosh^{-1}\left(\frac{Z_c\, b^2}{2\, Z_b\, a^2}\sinh 2j\Gamma L_s\right)\right\} \tag{57}$$

where Γ is the complex propagation constant and L_s is half the length of one section of conduit with side branch. The side branch impedance Z_b is modeled using electrical circuit analogy with the circuit shown in Fig. 22. The expression for Z_b using the electrical circuit analogs becomes:

$$Z_b = \frac{(R_b + j\omega L_b)}{j\omega C_b\left(R_b + j\omega L_b + \frac{1}{j\omega C_b}\right)} \tag{58}$$

$$R_b = \frac{2}{\pi b}\sqrt{\frac{\zeta^2 \rho_0 \omega}{2}}\, l' \; ; \; L_b = \frac{\rho_0}{\pi b^2} l' \; ; \quad C_b = \frac{\pi b^2}{\rho_0 c^2}\, l'$$

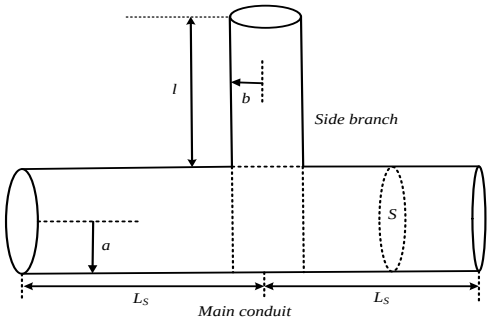

Figure 21: Main conduit with one side branch for Mason's Model

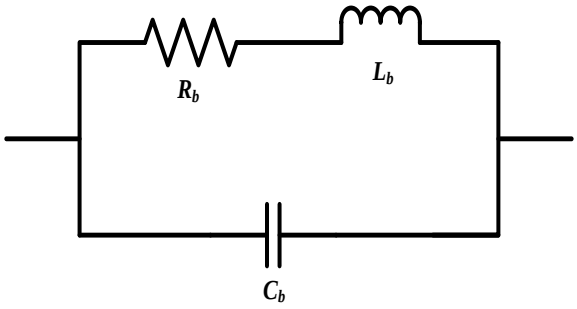

Figure 22: Electrical circuit equivalent of acoustic impedance in the conduit in Fig. 21.

The attenuation coefficient is computed using (56), (57) and (58) for a 0.1 m diameter, 6.24 m long conduit with a 0.05 m diameter 1.52 m long side branch at 3.12 m from the source. The attenuation coefficient for the same conduit dimensions with no side branch is also evaluated using (56). The computed attenuation coefficients for both cases are plotted in Fig. 23. It can be observed that the attenuation in a conduit increases with increase in frequency as is also the case with the results from Stewart's model. The theoretical works of Stewart and Mason stem from similar understanding of acoustic filters i.e. the effect of a side branch in a conduit can be best modeled by using an analytical approach akin to modeling electrical filters. Both the models have been compared using empirical data (Stewart and Sharp 1929). It has been concluded that the simplified theory of Stewart is superior and more easily applicable especially in determining the characteristic impedance of the side branch and including the effects of reflections from the joint between main conduit and side branch. One of the main requirements of Mason's theory is that the structure of a conduit with side branches is

symmetrical and side branches recur at equally spaced intervals. This is not the case with the conduits considered in this study as the side branch locations are mostly unknown random variables. Therefore, Mason's more detailed analysis is not readily applicable. For the purpose of this study, therefore, use is made of Stewart's simpler and more general approach rather than Mason's more specific theory.

Having discussed the acoustic propagation in conduit networks, the next chapter discusses the method used to model the propagation in conduit networks used in this study is presented.

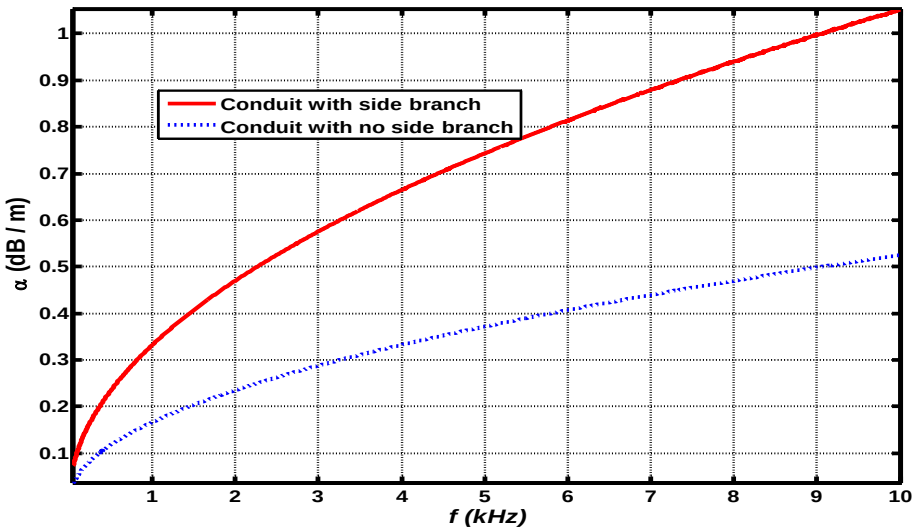

Figure 23: Attenuation coefficient vs. frequency using Mason's model.

CHAPTER 5: MODEL DEVELOPMENT AND APPROACH

5.1 Introduction

The theoretical behavior of conduit as an acoustic propagation channel has been described in the previous chapters. The analysis of signal attenuation in conduit networks indicates that it can be divided into two parts: one due to thermo-viscous losses in the main conduit and the other due to presence of side branch impedance mismatches. The attenuation due to the thermo-viscous losses depends upon the distance from the source, frequency, the radius of the conduit and the physical properties of the fluid medium (air) such as density, viscosity, thermal conductivity and specific heats at constant pressure and volume. The variation in speed of sound with change in humidity and temperature is given in Appendix A. The variation in thermodynamic properties of air with change in temperature is given in Appendix B. The effect of local variations in temperature on the fluid properties, when included in the analytical determination of attenuation coefficient does not appreciably change the results of computation. The effect on fluid properties due to change in relative humidity involves complex analysis of molecular interactions between water and the medium particles, and is beyond the scope of present study. Therefore, for analysis in this study, these parameters are treated as constants of the medium and variation in attenuation due to distance, frequency and conduit radius is analyzed using the analytical expressions. The attenuation due to the side branches depends upon the radius of the conduit and radii, number and length of side branches.

When considering the total attenuation of the signal in a conduit network, the attenuation due to both the parts needs to be considered.

In practical conduit networks, the measured signal attenuation deviates from the theoretical value due to the effects of processes that introduce a random variable error in the attenuation of the propagating signal. Therefore, there is a need to develop a model based on empirical data that can accurately characterize the attenuation in conduit environment such that:

$$\hat{\alpha} = \mathcal{F}(\{\hat{\alpha}\}_D, \{\hat{\alpha}\}_S), \tag{59}$$

where $\{\hat{\alpha}\}_D$ is the deterministic part and $\{\hat{\alpha}\}_S$ is the stochastic part. The deterministic part is dependent upon variations in parameters that can be modeled using existing analytical approaches. The development of deterministic model is presented in the next section.

The stochastic part is contributed by many sources in and around the conduit. Due to lack of information about the sources, their effect on acoustic signal attenuation in a conduit is intractable to analyze. This causes a random variable error between measured attenuation and that predicted from deterministic model. The stochastic based approach enables characterization of the probability distribution of the random variable error in accordance with Central Limit Theorem. The development of a stochastic based approach is presented in section 5.3.

5.2 Deterministic Model Development

5.2.1 Straight Conduit with no side branch

In case of a straight conduit with no side branch impedance mismatch, the received pressure at distance (z) from the source is given in (Blackstock 2000) as:

$$P_r(z) = P_0\, e^{-\alpha z}\, e^{j(\omega t - \beta z)}, \tag{60}$$

where P_r represents the received pressure at distance z from the source at frequency *f*, P_0 is the reference pressure measured at distance z_0 from the source such that $z > z_0$ and α is attenuation coefficient in nepers per meter (1 neper/m = 8.686 dB/m) and β is the phase constant. The sound pressure is normally measured with respect to a reference pressure in terms of Sound Pressure Level (SPL) in decibels [dB]. For brevity, SPL is denoted by $\bar{P}$ during further analysis in this study. From (60), $\bar{P}$ of the travelling wave at distance *z* is given by (Blackstock 2000):

$$\begin{gathered} \bar{P}_r\,(z) = 20\, log_{10}\left(\frac{P_0/\sqrt{2}}{p_{ref}}\right) + 20\, log_{10}(\, e^{-\alpha z}\,). \\ \bar{P}_r(z) = \bar{P}_0 - \alpha z. \end{gathered} \tag{61}$$

Where p_{ref} is 2×10^{-5} Pascals is the threshold of normal human hearing in air and α in the bottom equation of (61) is in dB/m (Blackstock 2000). The relationship in (61) suffices to determine the received SPL within a straight conduit with no side branches. The attenuation coefficient α is determined from (39). The reference pressure is obtained from the measurements.

5.2.2 Conduit with side branches

In case of a conduit with one side branch, the acoustic signal within the conduit suffers additional loss due to the presence of an impedance mismatch at the junction with the side branch. The additional transmission loss due to the junction point is evaluated using Stewart's analytical relationship given in (52). Therefore, the additional transmission loss due to any side branch (Ω) in dB is subtracted from (61). The received

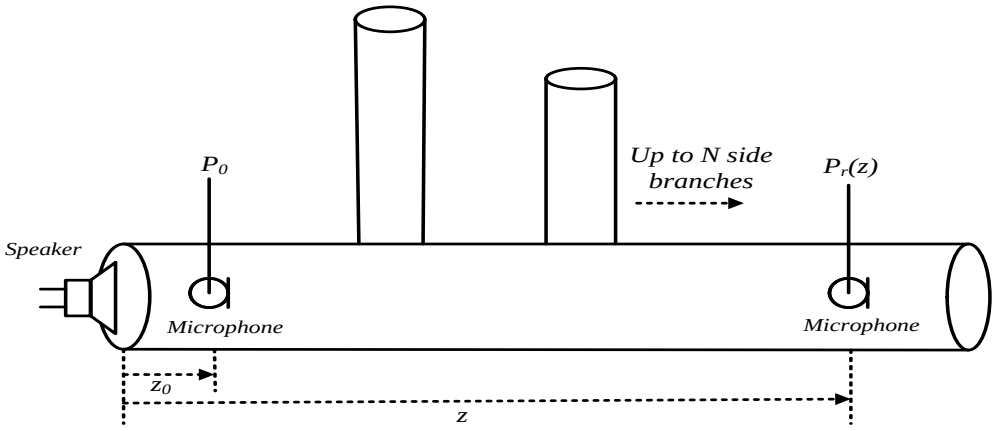

Figure 24: Conduit with multiple side branches.

pressure at distance z away from the source is then given by:

$$\bar{P}_r(z) = \bar{P}_0 - \alpha z - \Omega. \tag{62}$$

In the case of a conduit network involving up to N side branches as shown in Fig. 24, an additional source of loss in the propagating signal is presence of an impedance mismatch at the junction of each side branch with the main conduit. The total loss due to all side branches needs to be included in (62) to completely characterize the transmitted

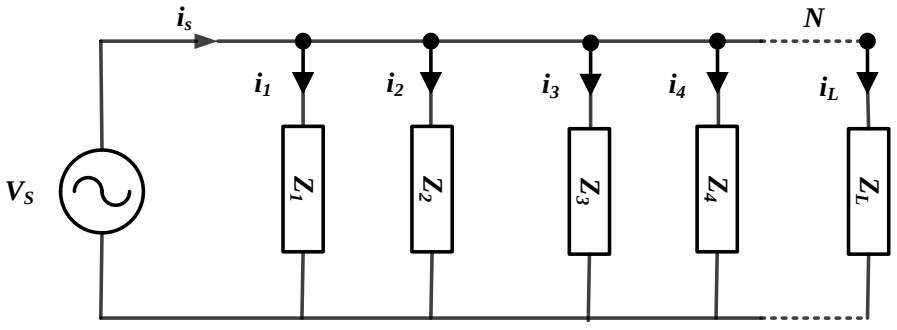

Figure 25: Electrical analog of a conduit with multiple side branches.

signal attenuation in the presence of multiple side branches. In order to analyze the total transmission loss due to multiple side branches, an electrical circuit based approach is followed which expresses the conduit with multiple side branches in terms of its electrical circuit equivalent as shown in Fig. 25.

Each side branch is represented by a parallel impedance (Z) in the circuit of Fig. 25. The current i_s is the analog of volume velocity in the conduit and V_s is the source voltage corresponding to the pressure source in a conduit. As the side branch impedances in parallel provide paths for the current to flow through, the equivalent impedance in the circuit is given by:

$$\frac{1}{Z_{eq}} = \frac{1}{Z_1} + \frac{1}{Z_2} + \frac{1}{Z_3} + \frac{1}{Z_4} \ldots . + \frac{1}{Z_N} \tag{63}$$

In case of an open ended conduit, the load impedance is the radiation impedance as discussed in Chapter 3. The goal here is to find the total loss of transmitted pressure in the conduit due to multiple parallel paths provided by side branch impedances. For a conduit with one side branch the pressure transmission loss is defined in (52). Our goal is to find the pressure transmitted past the multiple junctions with side branches i.e. pressure P'. Therefore, the individual impedance of each parallel path is lumped together into equivalent impedance given in (63) to find the transmitted pressure past the junctions with multiple side branches. The side branch impedance (Z_b) is then replaced with equivalent impedance of all parallel paths (Z_{eq}) such that the total transmission loss (Ω_T) is then given by:

$$\Omega_T = \frac{P}{P'} = \frac{\rho_0 c/2S + Z_{eq}}{Z_{eq}} \tag{64}$$

For the case of conduit network with multiple side branches, (62) is modified to include the total transmission loss computed in (64) and expressed in dB. The propagation model in (62), therefore, becomes:

$$\bar{P}_r(z) = \bar{P}_0 - \alpha z - \Omega_T. \quad (65)$$

5.2.3 Empirical Correction Factor

The theoretical propagation model for an open ended straight conduit with no side branches is given in (61). That model assumes an infinitely long conduit with no reflections from the open end. The practical conduits, however, are finite in length and the reflections from the open end are a major source of deviation from the results obtained by using the model in (61). In the case of a conduit with a side branch, the propagating signal in the main conduit suffers additional transmission loss due to the shunt impedance of the side branch. The propagation model for conduit with one or more side branches given in (62) and (65) also do not take into account the reflections from open end of the conduit. This increases deviation between the results obtained from theoretical models and the measured data. Therefore, there is a need to adjust the propagation models to take into account the effect of reflections at the open end to improve their accuracy. In order to achieve this, an empirical correction factor (K_e) is defined as the difference between the measured and theoretical transmission loss of a straight conduit open at one end with no side branch. The measured transmission loss is the difference of SPL between reference and output microphones. The empirical correction factor is then given by:

$$K_e(\mathrm{z}) = \bar{P}_0 - \bar{P}_r(z) - \alpha z \quad (66)$$

The correction factor accounts for the additional losses that a propagating signal suffers which are not accounted for by the theoretically evaluated loss given by the term αz in the propagation models. The use of correction factor significantly improves the accuracy of the predicted results from the models in (62) and (65) to analyze the variation in signal attenuation with change in the length and number of side branches.

The plots of empirical correction factors for 8.22 m and 17.56 m long conduits are given in Figs. 26 and 27 along with the measured transmission losses. It can be observed that the correction factor varies with the length of the conduit. This is due to the reason that the effect of standing waves on the propagating signal in the conduit varies with the length of the conduit. With the correction factor included, the propagation model in (65) takes its final form given as:

$$\bar{P}(z) = \bar{P}_0 - \alpha z - \Omega_T - K_e(z) \tag{67}$$

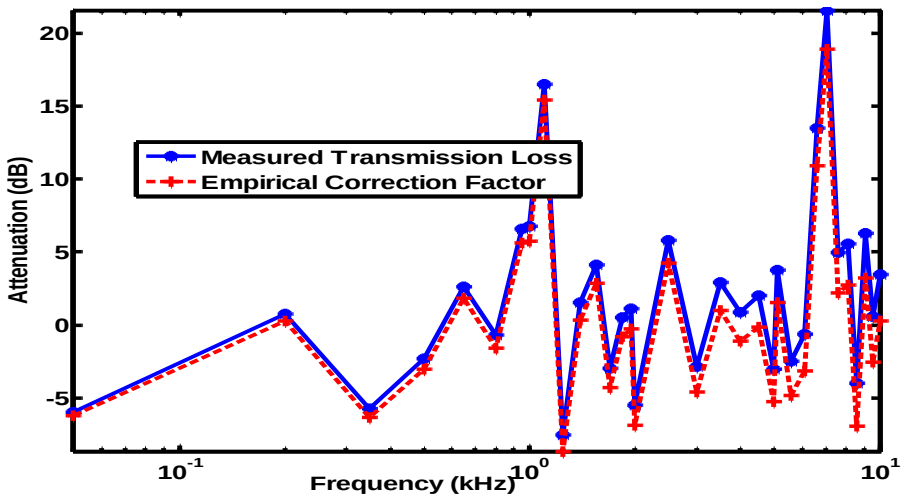

Figure 26: Empirical Correction Factor – 8.22 m long 0.1 m diameter straight conduit.

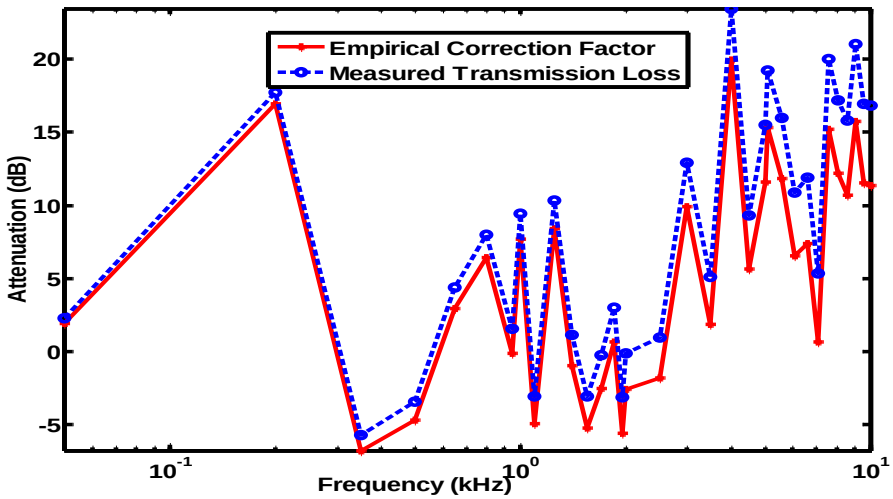

Figure 27: Empirical Correction Factor – 17.56 m long 0.1 m diameter straight conduit.

5.2.4 Model Evaluation

In order to evaluate (67), $\{\bar{P}_0, \alpha, \Omega_T\}$ need to be estimated. Deriving $\bar{P}_0$ analytically or numerically is in general complex and intractable unless under specific conditions (Dyer 1958). Therefore, $\bar{P}_0$ is obtained either through direct measurement or as y-intercept of linear regression through the scatter plot of $\bar{P}$ versus z. In the proposed approach, $\bar{P}_0$ is directly measured by placing a microphone at $z = z_0$ as shown in Fig. 24. Based on the dimensions of conduits considered in this study, the approximation for α given in (39) can be used for its evaluation as the parameter $r_v > 2$. Also, Ω_T can be analytically evaluated using (64) and corrected for the effect of reflections from open end of the conduit by subtracting the term K_e. The combined pressure attenuation (α_c) in a straight conduit with multiple side branches is then given by:

$$\{\alpha\}_D = \alpha_c = \frac{\omega}{c}\left(\frac{1.045}{r_v} + \frac{1.080}{r_v^2} + \frac{0.750}{r_v^3}\right) z + \Omega_T + K_e. \qquad (68)$$

The analysis of (68) reveals that loss of pressure signal depends upon following parameters:

1) Distance from the source (z).
2) Frequency of the signal (f).
3) Number of side branches (N).
4) Length of side branch (l).
5) Radius of the main conduit (a).
6) Radius of the side branch (b).

The expression for received pressure at distance z from the source, therefore, is given by:

$$\bar{P}(z, f, N, l, a, b) = \bar{P}_0 - \alpha_c(z, f, N, l, a, b), \tag{69}$$

where N represents the number of side branches and l represents their lengths and a and b are the radii of main conduit and the side branch. Based on extensive measurements in conduits of different lengths, at a set of frequencies with different numbers and lengths of side branches an empirical data set,

$$\left[\left\{z_j, f_k, N, l_n, \bar{P}\left(z_j, f_k, N, l_n, a, b\right)\right\}\right] \forall \begin{bmatrix} j = 1, \ldots J. \\ k = 1, \ldots K. \\ n = 1, \ldots N \end{bmatrix}, \tag{70}$$

is obtained which is used to estimate α_c. In (70), J represents the total number of distances at which the measured data was collected, K is the number of frequencies and N is the maximum number of side branches. The empirical model is given by:

$$\hat{\bar{P}}(z, f, N, l) = \bar{P}_0 - \widehat{\alpha_c}(z, f, N, l) \tag{71}$$

In further analysis (71), is used to predict the received pressure at distance z away from the source.

5.3 Stochastic Model

The data collection for the purposes of this study was based on a series of measurements made in conduits of variable lengths with variable number and length of side branches. This extensive data is used to predict the loss of pressure with distance in an approach similar to modeling attenuation of RF signals in conduits (Howitt, Khan et al. 2008). This is done by fitting a first order polynomial $\left(\hat{Y} = g - hz\right)$ regression line to the scatter plot of the measured data versus distance. The value of g is the *Y*-intercept and h is the slope of the line through the data. The slope represents the amount of change in $\hat{Y}$ when z increases by one unit. Therefore, the slope of the regression line through the scatter plot of measured SPL with distance from the source gives the predicted attenuation in dB/m. That predicted value is used to compute the model in (71). The difference between the measured SPL and that estimated from theory is defined as the residual and is given by (Henke 2007):

$$\varepsilon\,[dB] = [\bar{P}]_{Measured} - \left[\hat{\bar{P}}\right]_{Predicted} \tag{72}$$

The accuracy of measured attenuation in conduit networks is adversely affected by the lack of information of the factors that cause error between the measured and estimated attenuation results. Some of the factors that affect the audio signal and introduce error in the predicted attenuation of the acoustic signal are:

1) Unknown or inaccurately known number of side branches.
2) Unknown or inaccurately known lengths of side branches.

3) Presence of strong temperature and humidity gradients.
4) Blockages of variable sizes, types and locations e.g. root ingress, grease/waste build up or a moving rodent etc.
5) Deviation in the known properties of fluid medium.
6) Non-ideal installations that vary significantly from the available layout.
7) Effects of aging such as cracks, sags, bulges and holes etc.
8) Effect of reflections from a conduit end opening into a cavity with multiple paths for signal loss e.g. a manhole.
9) Inaccuracies of the measurement data recording.
10) Non-ideal placement of receiving sensor and the acoustic source.
11) Momentary ambient noise variations.

The error in the estimated attenuation caused by the above-stated factors can be best described using a stochastic based approach. In that each of the above-stated factors can be considered as a random process that is independent and arbitrarily distributed. The error in the estimated attenuation caused by lack of information of the independent and arbitrarily distributed random processes follows approximately normal distribution in accordance with the weak convergence condition of the Central Limit Theorem (Henke 2007).

The stochastic part of the attenuation coefficient is, therefore, represented by:

$$\{\hat{\alpha}\}_S = \psi(\mu, \sigma^2). \tag{73}$$

Where (ψ) is a normal random variable, with zero mean (μ) and finite variance σ^2. This stochastic part translates itself into pressure variations at the receiver and is used to

predict the received pressure at distance *z*. The deterministic analytical model given in (69), therefore, becomes:

$$\bar{P}(z, f, N, l, a, b) = \bar{P}_0 - \alpha_c(z, f, N, l, a, b) + \psi(\mu, \sigma^2). \quad (74)$$

The estimate of the total error in a data set containing *J* measurements of received pressure at distance *z* is then given by root mean square error (RMSE), such that:

$$\bar{\varepsilon} = \left\{ \frac{1}{J} \sum_{j=1}^{J} \left(\{\bar{P}\}_j - \left\{\hat{\bar{P}}\right\}_j \right)^2 \right\}^{½}. \quad (75)$$

The RMSE gives the standard deviation of residuals and is used as a metric to compare the estimated and the measured results. The adequacy of the proposed model when compared with the measured data is assessed based on the analysis of residuals obtained from (72). The residuals are checked for a normal distribution by using a normal probability plot which contains the plot of residuals on y-axis and the values from standard-normal distribution on x-axis. A straight line plot indicates that the residuals belong to a normal distribution.

In order to check the goodness of fit of the residuals to the normal probability distribution, hypothesis testing is done. If the results from normal probability plot of residuals hold the null hypothesis (H_0), it indicates that the data is normally distributed otherwise the alternate hypothesis (H_1) is true which indicates that the data does not belong to a normal distribution (Romano 2005). The Anderson Darling (AD) goodness of fit test is performed to check the normality of the residuals (Anderson 1954). If the AD test statistic is less than the critical value for the required confidence level, then the null hypothesis holds and the data belongs to the normal probability distribution otherwise the null hypothesis is rejected.

5.4 Model Validation with Empirical Data

In order to validate the model described in sections 5.2 and 5.3 with the empirical data, the variation in attenuation coefficient α_c has been observed with respect to following parameters:

1) Distance from the source (z).

2) Frequency of transmitted signal (f).

3) Number of side branches (N).

4) Length of side branch (l).

A discrete set of frequencies within a frequency range of 50 Hz to 10 kHz is used to measure the response of the conduits to an acoustic excitation. The lengths of the conduits ranged between 1.2 m to 221.1 m with a diameter of 0.1 m and 0.2 m. The side branch numbers ranged from 1 to 7 with a diameter of 0.1 m and 0.05 m. The side branch lengths varied between 0.1 m to 14.32 m.

5.4.1 Variation in Attenuation with Distance

The evaluation of variation in α_c with z is done in following steps:

1) A set of 28 frequencies between 50 Hz to 10 kHz are used to estimate the variation of attenuation coefficient with distance at each frequency.

2) A first order polynomial linear regression line is drawn through the scatter plot of measured SPL vs. frequency to predict the coefficients of the first order polynomial. The measured SPL is the response variable and the distance is the predictor variable. The slope of the linear regression line gives the attenuation in

dB/m for the particular frequency at which the measurements are made. This is $\widehat{\alpha_c}$, the predicted attenuation coefficient at each frequency.

3) The linear model is used to predict the SPL at each point along the distance vector. This gives the predicted SPL at each distance. The residuals are computed between the measured and estimated SPL through the linear regression model

4) As the critical assumption for using the linear regression model is that the residuals are normally distributed, therefore, the computed residuals are tested for normality. This is done by graphical methods by plotting the residuals along with the distance and observing their distribution around the zero mean line. A random distribution of the residuals around the zero mean indicates that the residuals are normally distributed.

5) The next step is to check the residuals for fitting to the normal distribution through a normal probability plot. A straight line plot indicates that the residuals are normally distributed. The graphical methods may have outliers and their effect on normality of residuals is ascertained by hypothesis testing using Andersen Darling (AD) goodness of fit tests.

6) The probability of AD test statistic is checked against the specified significance level (0.05). If the test statistical probability is greater than the significance level, then the null hypothesis holds and the data belongs to the normal probability distribution otherwise the null hypothesis is rejected.

7) With the normally distributed residuals, the use of a linear regression based model is validated. A comparison is then made between the attenuation

predicted through the linear model, the theoretical attenuation and the measured attenuation. The measured attenuation at each duct length is obtained by finding the difference between the reference pressure and the measured pressure at the receiver location. The measured attenuation coefficient in dB/m is obtained by dividing the difference of pressures by length (L) of the conduit i.e.:

$$\alpha_c[\frac{dB}{m}] = \left[\frac{\bar{P}_0 - \bar{P}}{L}\right] \tag{76}$$

where the reference pressure $\bar{P}_0$ is measured SPL at 1.21 m from the source for each measured frequency. This distance avoids the pressure variations at low frequencies in the near field of the acoustic source ($\approx 1.0\ m$) that arise because of evanescent modes.

8) A histogram of residuals from all measurements is plotted along with the probability density function (PDF) of the normal distribution. The mean and variance of the residuals from all tests are compared to the zero mean and finite variance of normal PDF. A normal probability plot of the residuals from all tests is also plotted to graphically observe their fitting to the normal distribution.

5.4.2 Variation in Attenuation with Frequency

Variation of α_c with frequency in each conduit section of a length L, is obtained by measuring $\bar{P}$ at each frequency. This gives the frequency response of the conduit to a pressure excitation. The attenuation is measured by finding the difference between the reference SPL and the measured received SPL. This gives the measured attenuation in the conduit and is converted into dB/m by dividing it with the distance between the microphones. The predicted SPL is then found by the following procedure:

1) The attenuation coefficient is computed from approximation in (39) under the assumption of a lossy conduit and with $r_v \gg 2$ for 0.1 m and 0.2 m diameter conduits considered in this study. The length of the conduit is adjusted assuming a flanged conduit with a length correction equal to 0.85 times the conduit radius.

2) The parameter r_v is computed from (31), taking the density of air, $\rho_0 = 1.21\ kg/m^3$ and the coefficient of shear viscosity $\eta = 1.78 \times 10^{-5}$P (1 Poise (P) = 0.1 $\frac{kg}{m\,s}$) for the frequencies between 50 Hz to 10.0 kHz and for conduit diameters of 0.1 m and 0.2 m.

3) The computed attenuation coefficient is in the units of nepers/m and is converted to dB/m. This value is the predicted attenuation coefficient.

4) The computed attenuation coefficient is used in (71) to predict the received SPL at distance *z* from the source. This predicted SPL is used to compute residuals by subtracting it from the measured SPL at the receiving microphone. The measured received SPL and the predicted received SPL are plotted to observe the predicted response of the conduit. The pressure received at the reference microphone in Fig. 24 is taken as reference pressure for use in (71).

5) The residuals between measured and predicted SPL are checked for fitting to the normal distribution through normal probability plot. The quantitative results of normality of residuals are ascertained through hypothesis testing using Andersen Darling goodness of fit test.

6) The measurement of attenuation in a straight conduit with no side branch is used to determine the correction term due to reflections and other losses from open ended conduit. The correction is used to analyze the variation of attenuation

with the change in number and length of side branches. The correction is determined in following steps.

7) The measured SPL at the receiving microphone is subtracted from the reference SPL. This gives the attenuation of a signal in a straight conduit. The effect of thermo-viscous losses which is part of the empirical model in (67) is removed by subtracting the loss term αz dB. The result is the empirical correction factor which is used to predict the transmission loss of the side branch in a conduit. This improves the accuracy of prediction from the theoretical model by taking into account the losses due to the open end of the main conduit.

5.4.3 Variation in Attenuation with Number of Side Branches

In this study, the variation of attenuation coefficients is analyzed by varying the number of side branches from one to seven. The following procedure is adopted:

1) Initially one side branch is introduced in the conduit section. The pressure at the reference microphone and the receiving microphone are measured. The difference between the pressure at the reference microphone and at the receiver microphone gives the attenuation in the signal. The pressure difference divided by the distance between measurement points gives the attenuation in dB/m. The result is the total measured attenuation of the signal due to side branch and the straight conduit.

2) The next step is to determine the theoretical transmission loss due to the side branch from (64) using the side branch impedance computed from (53). The theoretical transmission loss due to a side branch is corrected for the losses due to the standing wave in straight conduit. The three attenuations (measured,

theoretical and corrected) are plotted for each tested configuration of conduit with side branches.

3) The theoretically evaluated and corrected attenuations are used in (71) to predict the received SPL. The received SPL computed from (71) is plotted with that measured at the receiving microphone for each tested configuration of conduit with side branches.

4) The residuals between the measured and predicted SPL are computed and tested for normality initially using a graphical method of the normal probability plot. The quantitative testing for normality is performed using hypothesis testing with AD goodness of fit test.

5) The histogram of residuals from all the measurements of change in number of side branches is plotted along with the bell-shaped normal probability density function (PDF). The mean and variance of the residuals is compared to the mean and finite variance of the normal PDF.

6) A normal probability plot of the residuals from all tests is also plotted to graphically analyze the deviations from normality.

5.4.4 Variation in Attenuation with Length of Side Branches

The length of a side branch is an important parameter as any change of length alters the side branch input impedance and hence its resonances. The signal attenuation in the main conduit is strongly influenced by the resonances of the side branch. The approach to model the effect of changes in side branch length is similar to the procedure outlined above for change in the number of side branches and is outlined as follows:

1) The attenuation due to the introduction of side branch is measured as outlined for changing the number of side branches in section 5.4.3, step (1).

2) The theoretical input impedance and attenuation due to the side branch are obtained from (53) and (64). The theoretical attenuation is corrected for the loss due to the standing wave in the straight conduit. The three attenuations (measured, theoretically evaluated and corrected) are plotted for each tested configuration.

3) The theoretically evaluated and corrected attenuations are used in (71) to predict the received SPL. The received SPL computed from (71) is plotted with that measured at the receiving microphone for each tested configuration of conduit with side branches.

4) The residuals between the measured and predicted SPL are computed and tested for normality initially using a graphical method of the normal probability plot. The quantitative testing for normality is performed using hypothesis testing with AD goodness of fit test.

5) The histogram of residuals from all the measurements of change in length of side branches is plotted along with bell-shaped normal probability density function (PDF). The mean and variance of the residuals is compared to the mean and finite variance of the normal PDF.

6) A normal probability plot of the residuals from all tests is also plotted to graphically analyze the deviations from normality.

Having discussed the development of an empirical propagation model and the details of the modeling approach and validation, the next chapter presents the details of

experimental set up to obtain the measured data. Since the measurements are made in the field and in the laboratory settings, the details of both set ups are presented.

CHAPTER 6: MEASUREMENT SETUP

6.1 Field Measurements

In order to determine the propagation characteristics of long conduits to an acoustic excitation, a comprehensive measurement campaign was undertaken at selected sites in Charlotte, NC. This was accomplished with the support of the Charlotte Mecklenburg Utility Department (CMUD). The layout of one location where multiple tests were conducted to collect measurement data is shown in Fig. 28. The manholes are shown in solid red circles and distance between them is indicated in meters. The conduit material was PVC and the main conduits had a diameter of 0.2 m with 0.1 m diameter side branches. The goal of the measurement campaign was to estimate the attenuation coefficient in 0.2 m diameter conduits. The selected location enabled the determination of variation in attenuation coefficient over long conduit lengths, which is impractical in a laboratory setting. One limitation of testing the propagation of acoustic signals over long ranges was that some measurements spanned a number of manholes. This incurred greater attenuation due to the scattering, reflection and escape of acoustic signal through the manhole. However, the analysis of this loss is beyond the scope of present study.

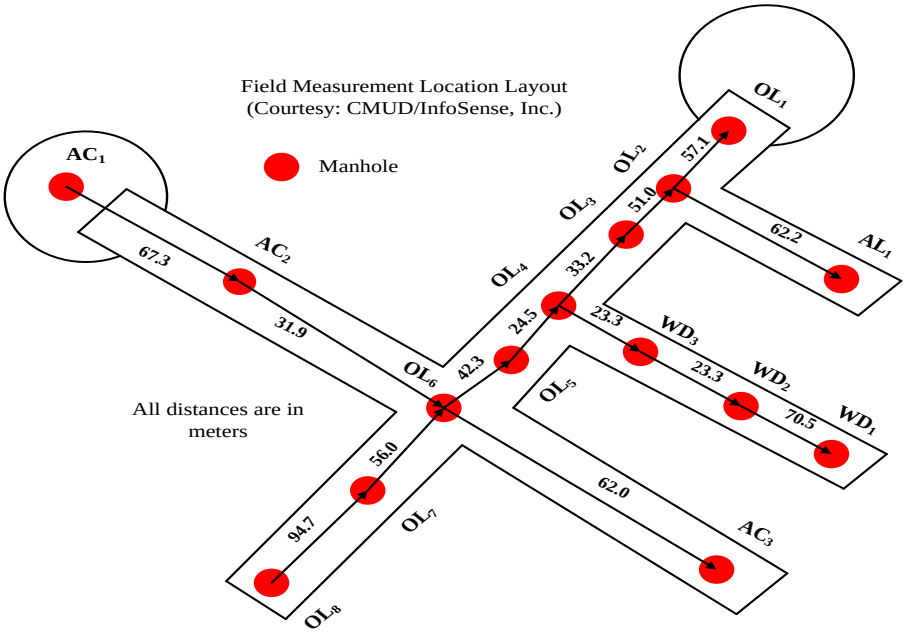

Figure 28: Field measurement location layout.

The pictures showing the measurement set up are included as Figs. 29 and 30. The test equipment comprised a 1/3 Octave band Phonic PAA3 audio spectrum analyzer, a

Figure 29: Audio spectrum analyzer and condenser microphone at receiving location.

Figure 30: Speaker in conduit at the source end.

condenser microphone, Alesis RA-150 audio amplifier and a 4-inch speaker. Two Dell notebooks were used as controllers at the transmitter and receiver locations. The PAA3 spectrum analyzer dynamic range was between 30 to 130 dB. It also had a USB interface for rapid data transfer to the controller for quick analysis. The condenser microphone was used to record the data using .wav file format. As far as practical, the speaker and microphone were placed 0.05 m to 0.1 m inside the open end of the conduit. In some instances the microphone was not able to reach the open end of the conduit due to tight dimensions of the manhole. In those situations, it was inserted into trough about 0.15 m to 0.3 m away from the open end of the conduit.

Table 3: Frequencies of transmitted tones during field tests.

Tone Number	Frequency (Hz)	Tone Number	Frequency (Hz)
1	50	13	800
2	63	14	1000
3	80	15	1250
4	100	16	1600
5	125	17	2000
6	160	18	2500
7	200	19	3150
8	250	20	4000
9	315	21	5000
10	400	22	6300
11	500	23	8000
12	630	24	10000

At each measurement location the ambient noise was recorded to adjust the measured sound pressure level. The test signal comprised 31 audio tones at 1/3 octave band frequencies. These frequencies lie between 20 Hz to 20 kHz. However, for the purpose of this study, 24 frequencies between 50 Hz to 10.0 kHz are selected for analysis. These frequencies are listed in Table 3. These are selected due to high attenuation at frequencies above 10.0 kHz. Each tone had duration of 5 seconds. The transmission of the test tone was preceded and succeeded by a 5 s long 1.0 kHz pilot tone. The data files containing test tones were recorded using a sampling rate of 96 kHz at 24 bits to be consistent with CD quality. The test tones were divided into 3 sets: 50 Hz -200 Hz, 250 Hz to 2.0 kHz and 2.0 kHz to 10.0 kHz. The temperature and humidity were recorded at each measurement location. Also, recorded were the approximate lengths and number of the side branches in each conduit section. The details of side branches between manhole pairs are given in Table 4.

6.2 Laboratory Measurements

In addition to testing 0.2 m diameter conduit networks at the field measurement location, a series of tests have also been conducted in a more controlled environment. The goal of the laboratory tests was to observe the variation in signal attenuation with frequency due to variation in number and length of side branches. The test set up for laboratory tests is shown in Fig. 31. It comprised a Data Acquisition (DAQ) system DT-9837A, an Alesis RA-150 audio amplifier, a DC Gold N7R 7-inch speaker and BSWA MP215 (1/2 inch free field) microphones. A Sony notebook was used to control the transmission of tones, data recording and preliminary analysis. The DAQ has four, 24-bit simultaneous channels with a 4 mA current source to support IEPE (Integrated Electronic

Piezoelectric) inputs. It can be set with a sampling rate of up to 52.73 kHz. The DAQ's interface with the controller is through a DAQ adapter for Matlab working with the Matlab's Data Acquisition Toolbox. The MP215 microphones have a sensitivity of 40 mv/Pa (BSWA 2013). The DC gold speaker has 80 W continuous power output with peaks of 300 W. A Scantek calibrator (model 407744) with an output of 94 dB at 1.0 kHz was used to calibrate the measurement set up. Three lengths of RG-50 (20 AWG) coaxial

Table 4: Manhole pairs with number and lengths of side branches

Manhole pairs	Number of side branches	Lengths of side branches (meters)
$AC_2 – AC_1$	7	l_1 = 7.9 ; l_2 = 6.1; l_3 = 8.1 ; l_4 = 8.0; l_5 = 6.6; l_6 = 9.4; l_7 = 14.3
$AC_3 – OL_6$	3	l_1 = 7.1 ; l_2 = 7.3; l_3 = 7.7
$OL_5 – OL_6$	4	l_1 = 7.4 ; l_2 = 9.0; l_3 = 10.0 ; l_4 = 7.4
$OL_4 – OL_5$	2	l_1 = 7.4 ; l_2 = 7.0
$OL_3 – OL_4$	2	l_1 = 7.7 ; l_2 = 5.5
$OL_2 – OL_3$	7	l_1 = 7.9 ; l_2 = 7.0; l_3 = 8.0 ; l_4 = 8.9; l_5 = 8.0; l_6 = 8.6; l_7 = 6.7
$OL_1 – OL_2$	1	l_1 = 5.28
$AL_1 – OL_2$	3	l_1 = 7.0 ; l_2 = 10.0; l_3 = 10.1
$WD_2 – WD_3$	2	l_1 = 8.9 ; l_2 = 7.7
$WD_1 – WD_2$	7	l_1 = 6 ; l_2 = 9.9; l_3 = 9.5 ; l_4 = 7.2; l_5 = 10.0; l_6 = 9.0; l_7 = 9.7

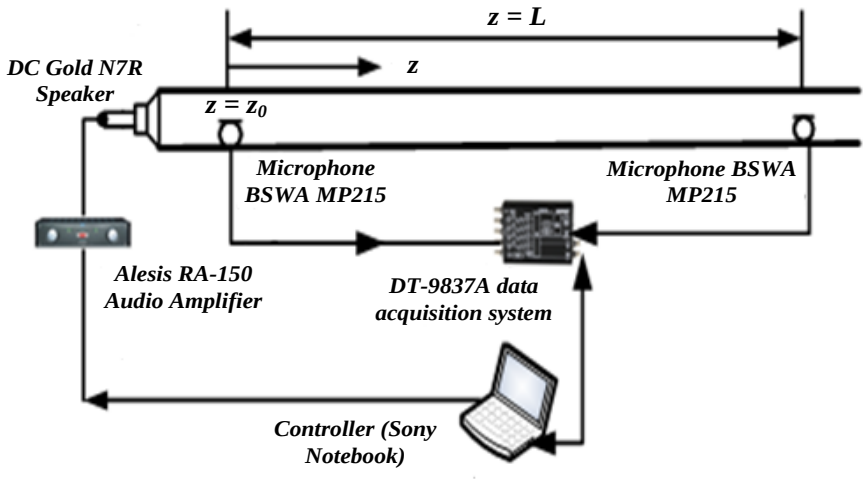

Figure 31: Laboratory test setup.

cable were used during the tests. The lengths of the cables were 8.0 m, 3.65 m and 0.91 m. The results of the calibration tests indicated that the cable losses are insignificant for the purpose of this study.

The test signal comprised three sets of discrete tones within a frequency range of 50 Hz – 10 kHz. Each tone within the set was 5 s long. The start of each set was preceded by a 5 s long pilot tone of 1.0 kHz. The tones were recorded at a sampling rate of 44100 samples per second. The first set of tonal frequencies comprised fifteen tones between 50 Hz to 1950 Hz. The second set comprised seven tones between 2.0 kHz to 5.0 kHz and the third set comprised eleven tones between 5.1 kHz to 10.0 kHz. The tonal frequencies are given in Table 5. The discrete tones were chosen as the test signal because the flexibility of setting the duration of each tone and reduced complexity of analyzing the conduit's response to each tonal excitation. The ambient noise was measured prior to the start of the tests. The outside air temperature and humidity readings were also recorded. During the tests, PVC Schedule 40 conduits of 0.1 m diameter were used. Each conduit

Table 5: Frequencies of transmitted tones during laboratory tests

Tone Number	Frequency (Hz)	Tone Number	Frequency (Hz)
1	50	17	3000
2	200	18	3500
3	350	19	4000
4	500	20	4500
5	650	21	5000
6	800	22	5100
7	950	23	5600
8	1100	24	6100
9	1250	25	6600
10	1400	26	7100
11	1550	27	7600
12	1700	28	8100
13	1850	29	8600
14	1950	30	9100
15	2000	31	9600
16	2500	32	10000

section was 1.62 m long. The sections were joined together with a 0.1 m diameter coupling. The side branches were installed through a 0.1 m to 0.05 m T coupling. The microphones were placed at the measurement positions with sensing heads at the centerline of the conduit through a 0.025 m adapter and a bushing. The initial trials were conducted on an 8.22 m long conduit. The reference microphone was placed at 0.76 m from the source to minimize the near field effect. The receiving microphone was placed

at 1.22 m from the open end of the conduit. This was done to reduce the effect of reflections from the open end.

The test setup involving a conduit with two side branches is shown in Fig. 32. Pictures of the conduit with the test set up are also given in Fig. 33 and 34. The tested configurations are given in Table 6.

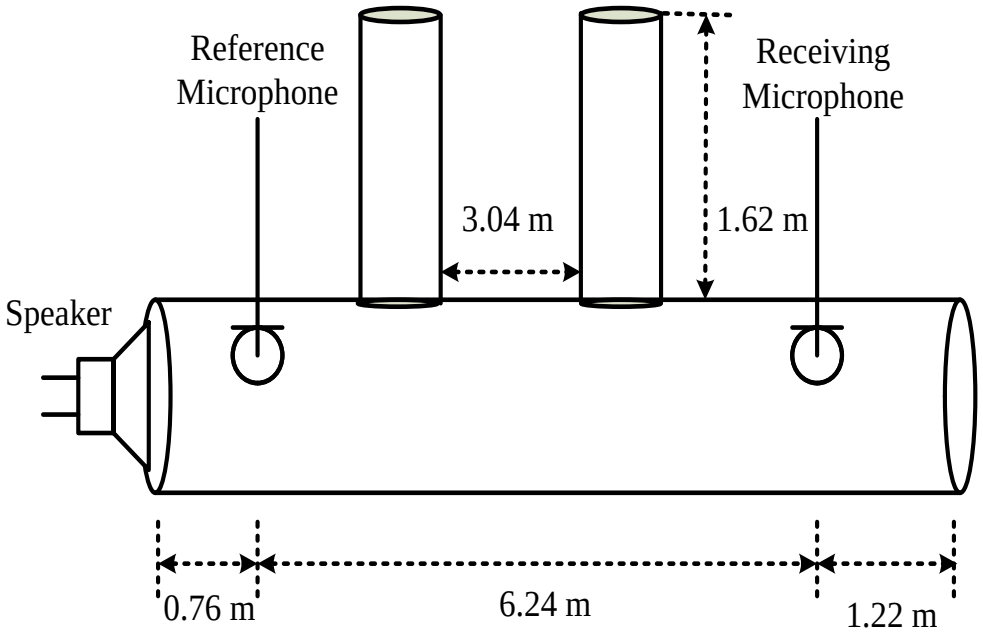

Figure 32: An 8.22 m long conduit with two side branches – initial test set up.

Figure 33: Conduit with one side branch.

Figure 34: Test set up.

A set of tests was also conducted to measure the attenuation versus frequency with change in the lengths and number of side branches. These tests comprised a longer

Table 6: Tested Configurations – 8.22 m long conduit.

Configuration Number	Description	Side branch location from receiving microphone (m)	Side branch lengths (m)
1.	Straight Conduit	-	-
2.	Conduit with one side branch	3.12	1.62 m
3.	Conduit with one side branch	1.62	1.62
4.	Conduit with one side branch	3.12	1.32
5.	Conduit with one side branch	3.12	1.02
6.	Conduit with one side branch	3.12	0.72
7.	Conduit with one side branch	3.12	0.42
8.	Conduit with two side branches	1.56 , 4.68	1.62
9.	Conduit with three side branches	1.52, 3.04 , 4.56	1.62

conduit (17.56 m from end to end) assembled by joining 1.62 m long PVC conduit sections through 0.1 m couplings. The number of tested side branches was increased from one to seven along the length of the conduit. The variation in attenuation vs. frequency was measured with the change in the length of the side branch in four 0.3 m steps between 0.12 m to 1.62 m. In order to reduce the near field effects, the reference microphone was placed at 2.38 m from the speaker and the receiving microphone was placed at 4.25 m from the open end to reduce the effects of reflections. The distance between two microphones was 10.93 m. The test setup for this case is shown in Fig. 35. The photographs of the test set up are given in Figs. 36 and 37. The ambient noise was recorded initially for 10 s and subsequently before each configuration change. The tested conduit configurations are given in Table 7.

The empirical data collected during the measurements was pre-processed before it was ready for analysis. The details of the pre-processing are given in the next section.

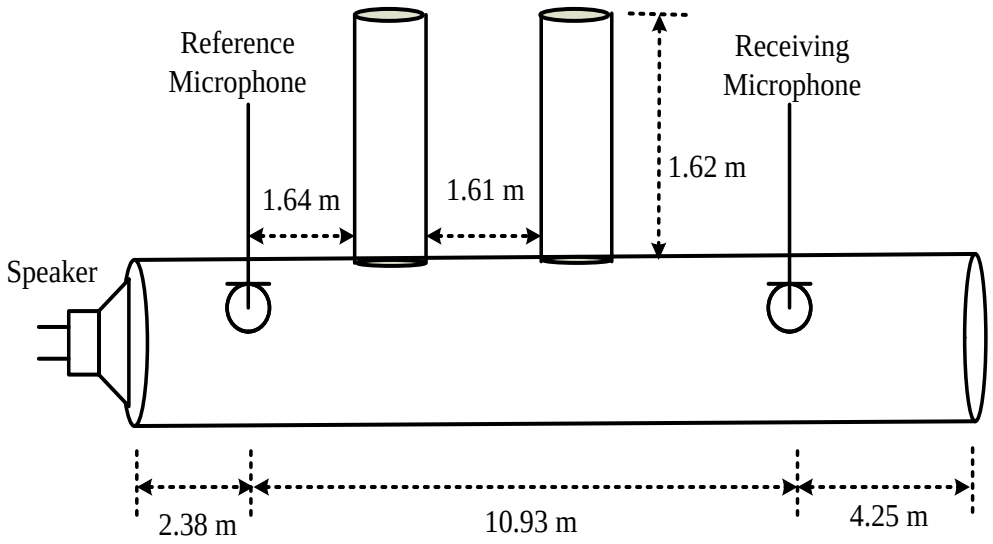

Figure 35: A 17.56 m long conduit with two side branches.

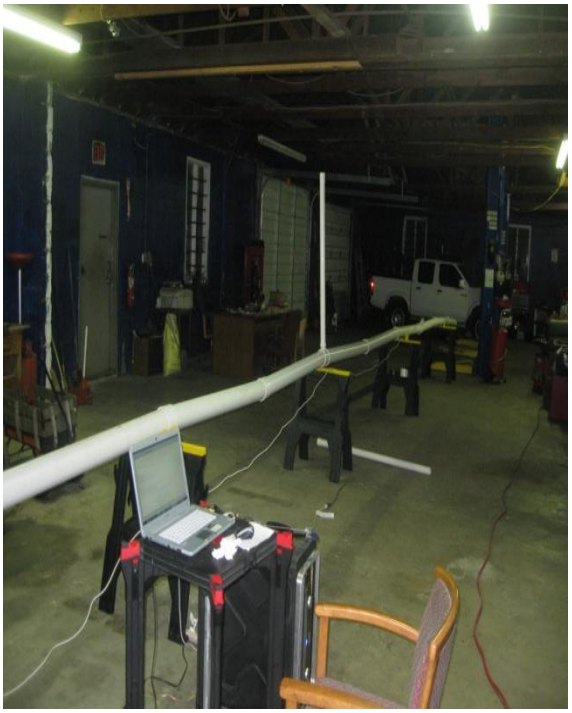

Figure 36: Test set up – 17.56 m long conduit with one side branch.

Figure 37: Test set up – 17.56 m long conduit with three side branches.

6.3 Preprocessing of Empirical Data

The evaluation of transmitted signal pressure variation with distance from the source, using the data measured in the field tests, involved evaluating the mean SPL at each transmitted frequency for each time interval for every measurement through a particular conduit section. The mean SPL of the noise was evaluated from the collected noise data for each test by comparing the noise SPL against a 29 dB lowest offset limit of the PAA3. A spectrogram of the background noise measured at AC_1 manhole is given in Fig. 38. The measured SPL of the signal was measured against the noise threshold that

Table 7: Tested Configurations – 17.56 m long conduit.

Configuration Number	Description	Side branch location from receiving microphone (m)	Side branch lengths (m)
1.	Straight Conduit	-	-
2.	Conduit with one side branch	7.57	1.62 m
3.	Conduit with one side branch	7.57	1.32
4.	Conduit with one side branch	7.57	1.02
5.	Conduit with one side branch	7.57	0.72
6.	Conduit with one side branch	7.57	0.42
7.	Conduit with one side branch	7.57	0.12
8.	Conduit with two side branches	1.64 , 3.25	1.62
9.	Conduit with three side branches	1.64 , 3.25 , 4.89	1.62
10.	Conduit with four side branches	1.64, 3.25, 4.89, 6.53	1.62
11.	Conduit with five side branches	1.64, 3.25, 4.89, 6.53, 8.16	1.62
12.	Conduit with six side branches	1.64, 3.25, 4.89, 6.53, 8.16, 9.81	1.62
13.	Conduit with seven side branches	1.64, 3.25, 4.14, 4.89, 6.53, 8.16, 9.81	1.62

was evaluated through the sum of mean and standard deviation of the noise SPL at each frequency. This SPL data is used to predict the variation of the SPL with range at each transmitted frequency.

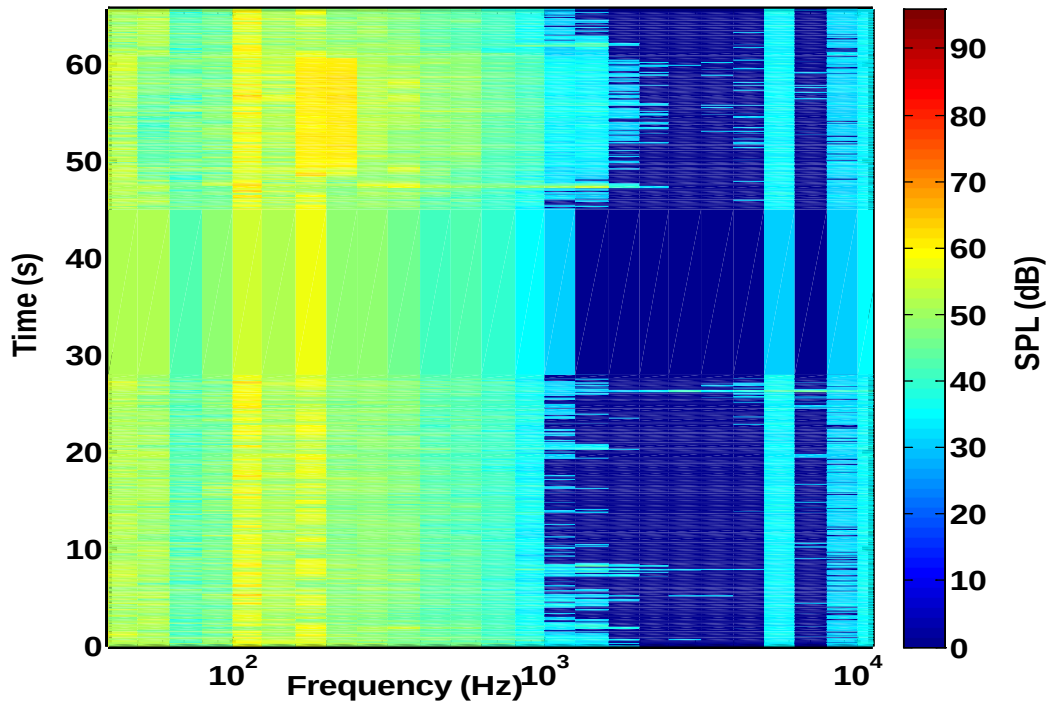

Figure 38: Spectrogram of background noise at the field measurement location (measured at AC_1 manhole.

The data collected in the laboratory tests was converted into dB SPL. To accomplish this, the received signals from reference and receiving microphones was adjusted for the time delay corresponding to 10.93 m distance between two microphones at the speed of sound adjusted for the recorded humidity and temperature readings. This is done by computing the cross-correlation between the data from reference microphone and the receiving microphone. The index of the peak of the cross-correlation is computed. The offset is determined by subtracting the index of the cross-correlation peak from the total number of samples in the data from reference microphone. As an example at the sound speed of 343 m/s, the distance between two microphones corresponds to a time difference of 31.9 ms or 1406 points at the sampling rate of 44,100 samples per second. In order to remove the effects of noise the signal is compared against the sum of mean SPL of noise and its standard deviation. The histograms of the background noise

along with the bell-shaped normal PDF for the tested configurations with 8.22 m and 17.56 m long pipes are given in Figs. 39 and 40. The DC offset is removed from the sampled signals of both microphones by subtracting their mean values and passing the signal through an IIR DC blocking filter with a cut-off frequency of 40 Hz.

The filtered data is divided into bins corresponding to the number of 5 s tones in the test signal. The root mean square value of each bin is computed. The data is converted into pressure in Pascal (Pa) by dividing it with the sensitivity of the microphone ($\approx 40\ mV/Pa$). The pressure in Pascals is then converted into dB referenced to 20 μPa. The SPL in dB is used for finding the variation in attenuation with frequency by changing the side branch parameters.

Having discussed the measurement set up for the field and the laboratory measurements and the preprocessing of data, the next chapter presents the details of the analysis and results.

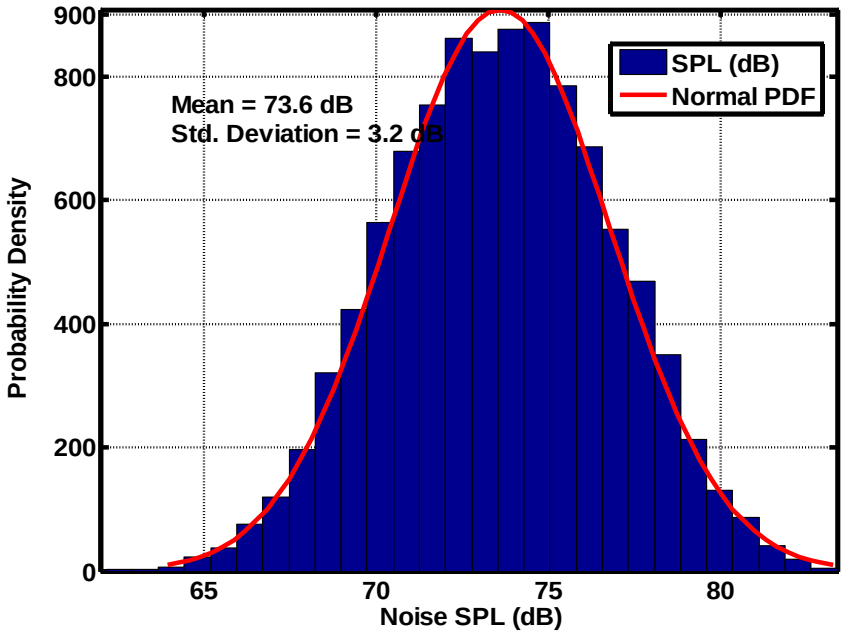

Figure 39: Histogram of background noise in 8.22 m long conduit.

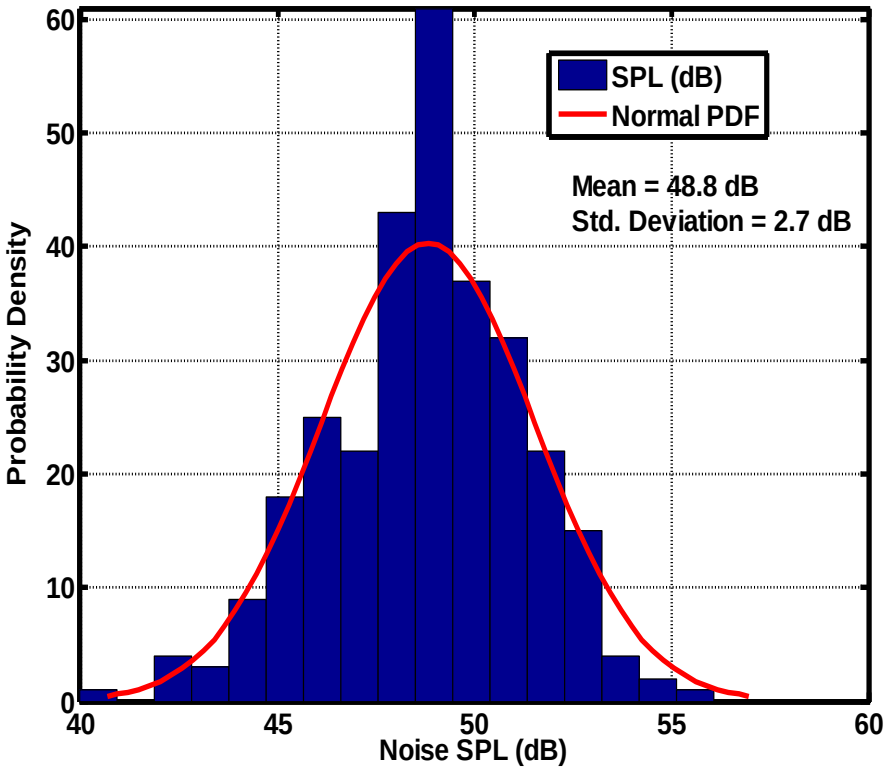

Figure 40: Histogram of background noise in 17.56 m long conduit.

CHAPTER 7: DATA ANALYSIS AND RESULTS

7.1 Introduction

In this chapter, the analysis of collected data from field measurements and laboratory tests is presented. The data analysis is performed in accordance with the approaches presented in section 5.4. The field data is analyzed for evaluating the variation of attenuation with the distance from the source using a linear regression based model. The underlying assumption for a linear regression based model is that the residuals are normally distributed with zero mean and finite variance. Therefore, the residuals are checked for normality using statistical measures and graphical as well as quantitative goodness of fit tests. The analyzed data was collected at the test site shown in Fig. 28. As the field tests spanned many days, very large amount of test data was collected. However, for the purpose of brevity and to illustrate the analysis methodology, only a snapshot of the field data is being analyzed. The analysis and results from the field data are presented in section 7.2.

The laboratory data is used to analyze the variation in acoustic signal attenuation in the conduit with change in frequency, number and lengths of side branches. The analysis and results from laboratory data are presented in sections 7.3, 7.4 and 7.5. For each tested configuration, a representative plot is given for the measured and the predicted attenuation, the side branch input impedance, the measured and predicted SPL, the normal probability plot and the results of the hypothesis testing. The histograms of

residuals from estimates of attenuation in a conduit with and without the correction factor for an open end are also presented along with the probability density function of a normal distribution. The presented results are analyzed and relevant deductions are drawn to validate the proposed modeling approach given in chapter 5.

7.2 Variation of Attenuation with Distance from Source

The data collected during the field measurement campaign is plotted in a scatter plot for each set of trials. Then a first order polynomial is used to check the fitting of the scatter plot data with a straight line. The attenuation is predicted from the slope of the fitted line. Representative scatter plots of measured data fitted with a first order polynomial are given in Figs. 41-44 for 200, 500, 1600 and 6300 Hz.

In order to observe the attenuation of acoustic signal at long ranges some measurements spanned more than one manhole. The statistics of linear regression model $\left(\hat{Y} = g - hz\right)$ are given in Table 8. The bracketed figures of model parameters represent the lower and upper bounds on the predicted data.

The goodness of fit statistics given in Table 8 are explained in detail in (Henke 2007). The goodness of fit is explained in terms of statistical measures. These measures include the sum of squares error (SSE), coefficient of determination (R^2_{reg}), degrees of freedom (DF) and the root mean square error (RMSE). The SSE describes the unexplained variability in the residuals. The DF refers to the number of data points that

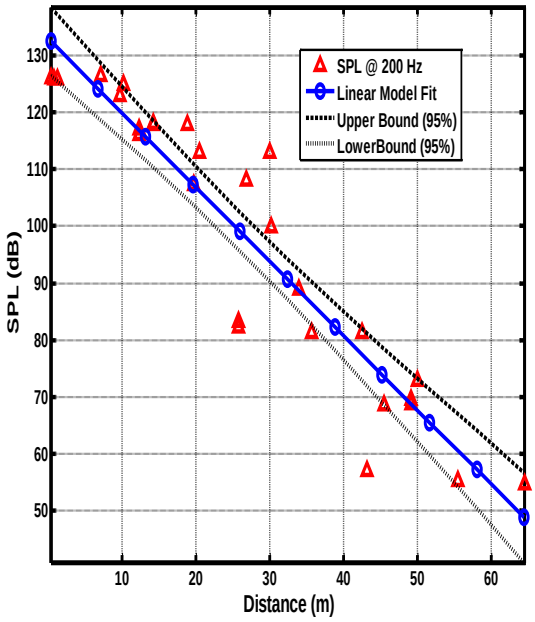

Figure 41: Linear regression through measured data at 200 Hz.

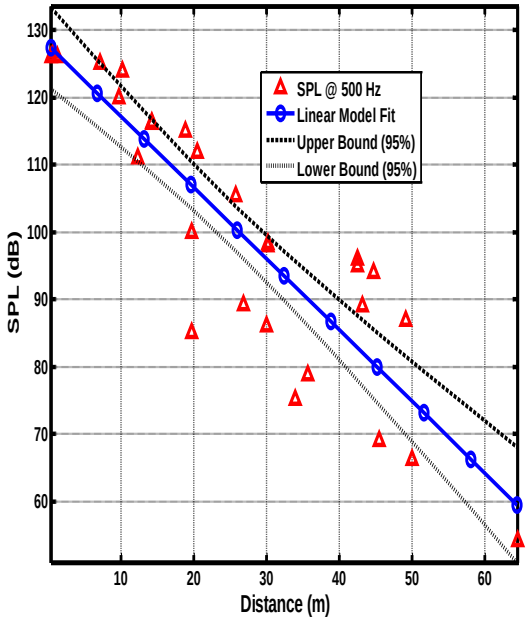

Figure 42: Linear regression through measured data at 500 Hz.

are independent of one another and carry unique information. The standard deviation (σ) of the estimate can be obtained from SSE by dividing it with $DF - 2$ and taking its square root. The parameter R^2_{reg} measures the percentage of variability in the measured data that can be explained through the knowledge of the independent variable (distance). The analysis of the data in Table 8 reveals that as the frequency is increased, the value of R^2_{reg} increases and RMSE and SSE reduce. This indicates the increased strength of regression as the frequency is increased. However, with increase in frequency the data points that carry unique information about variation of received SPL with distance also reduce due to greater attenuation and the regression line fits the data well. The plots also show 95 % confidence bounds on the model prediction. As the frequency increases, there are only few outliers and most of the data lies within the confidence bounds indicating that a linear model is a good fit to the measured data (Henke 2007).

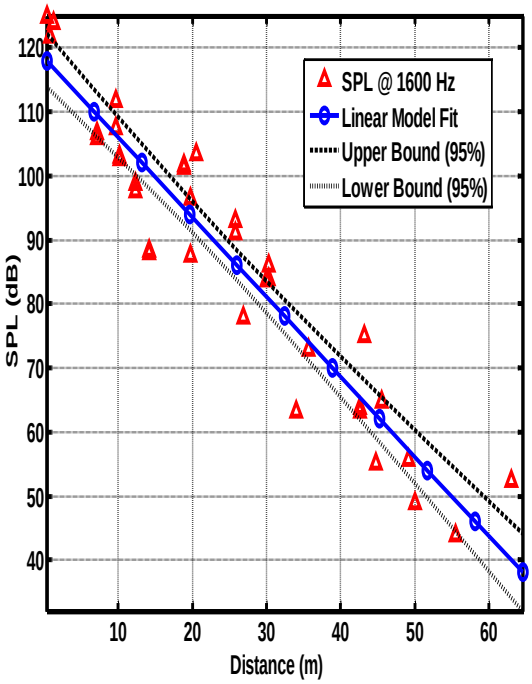

Figure 43: Linear regression through measured data at 1600 Hz.

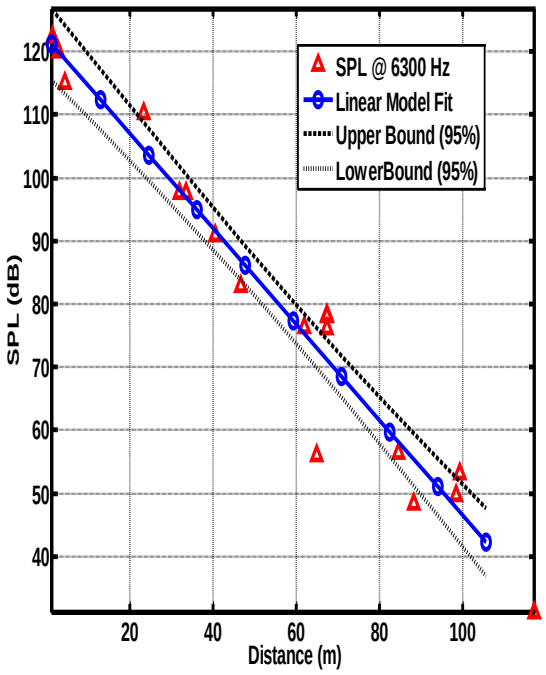

Figure 44: Linear regression through measured data at 6300 Hz.

The use of regression analysis to fit a linear model to the measured data is based on assumption that the residuals are normally distributed with zero mean and finite variance. Therefore the next step is to check the residuals for fitting to a normal distribution. The first step in this process is to scatter plot the residuals to graphically observe their distribution around the zero mean line. For the four representative frequencies, the residuals are plotted with distance in Figs. 45-48. It can be observed that residuals are randomly scattered around the mean and they do not seem to follow any fixed pattern. There are few residuals that belong to outliers but the majority of the residuals are distributed randomly around the zero mean. This is one of the tests that the residuals have to pass so that the assumption of normality for the linear regression model is satisfied.

Table 8: Goodness of Fit Statistics for Linear First Order Polynomial Model.

Measured Frequency	Model Parameters		Goodness of Fit Statistics			
	Y-Intercept (g) [dB]	slope of the estimate (h) (dB/m)	SSE	R^2_{reg}	DF	RMSE [dB]
200 Hz	133 (126.9, 139.1)	1.306 (1.496, 1.116)	1.92 x 10^3	0.884	26	8.60
500 Hz	127.8 (121.7, 133.9)	1.058 (1.26, 0.8554)	2.34 x 10^3	0.797	29	8.98
1600 Hz	118.5 (114.2, 122.8)	1.246 (1.387, 1.105)	1.52 x 10^3	0.907	33	6.80
6300 Hz	122.1 (116.3, 127.9)	0.756 (0.845, 0.668)	579.5	0.953	16	6.01

There are two more tests that the residuals have to pass before it is established that they belong to a normal distribution (Henke 2007).

The normal probability plot is a graphical technique that is used to confirm whether a set of samples belong to a normal probability distribution or not. A straight line on the plot indicates the normal distribution and if the residuals are normally distributed they follow the straight line. The residuals at four representative frequencies are tested for normality using normal probability plots in Figs. 49-52. The plots indicate that the residuals generally follow the straight line indicating that they belong to the normal probability distribution. There are some observations that are outliers and indicate that there was another component to the error in addition to the stochastic component. In

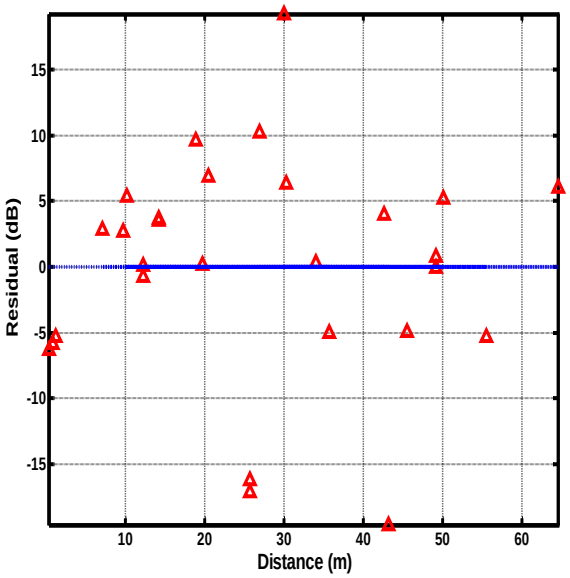

Figure 45: Scatter plot of residuals at 200 Hz.

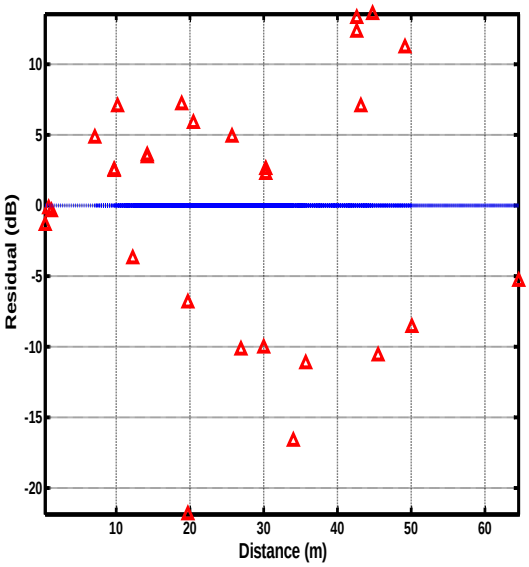

Figure 46: Scatter plot of residuals at 500 Hz.

order to further quantify the normality of residuals, the Andersen Darling (AD) normality test is performed.

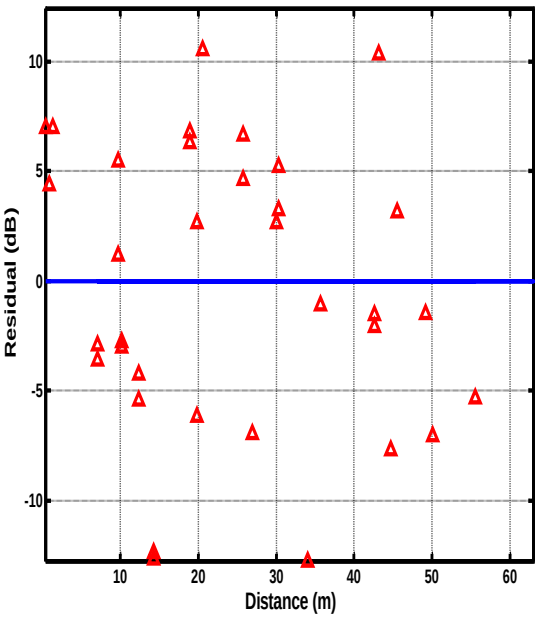

Figure 47: Scatter plot of residuals at 1600 Hz.

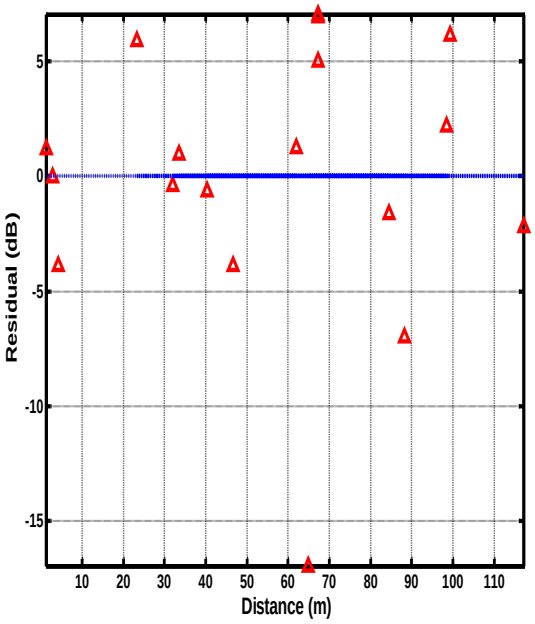

Figure 48: Scatter plot of residuals at 6300 Hz.

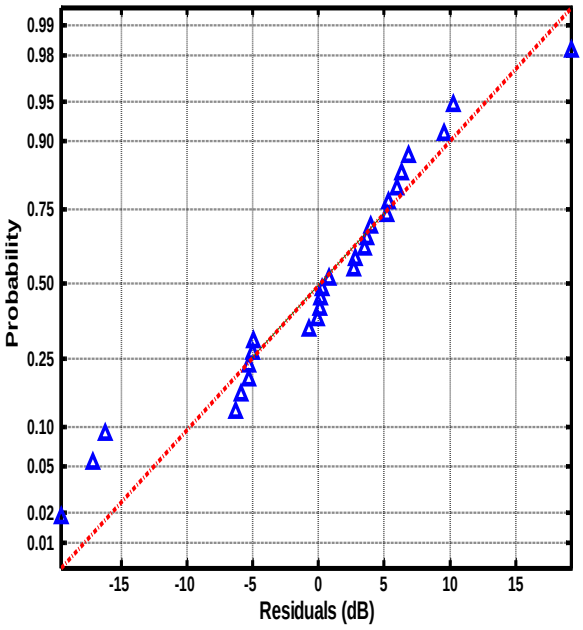

Figure 49: Normal probability plot of residuals at 200 Hz.

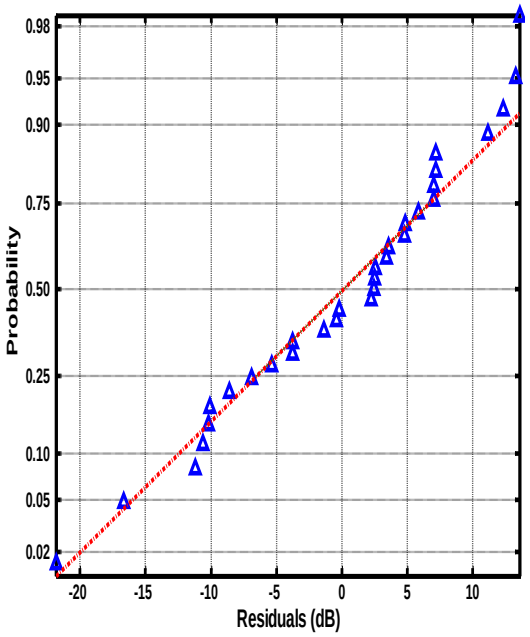

Figure 50: Normal probability plot of residuals at 500 Hz.

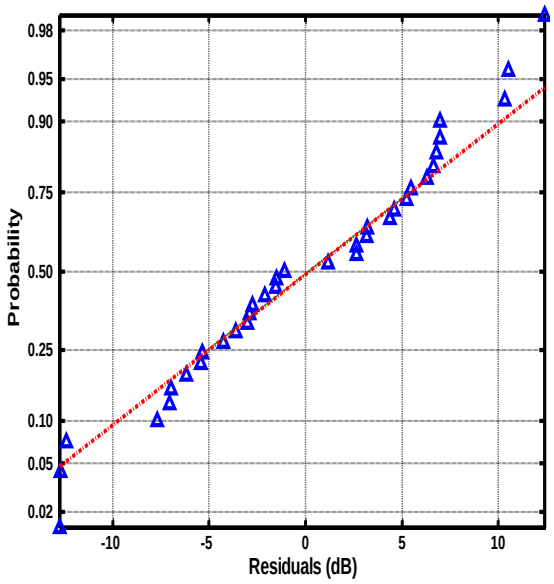

Figure 51: Normal probability plot of residuals at 1600 Hz.

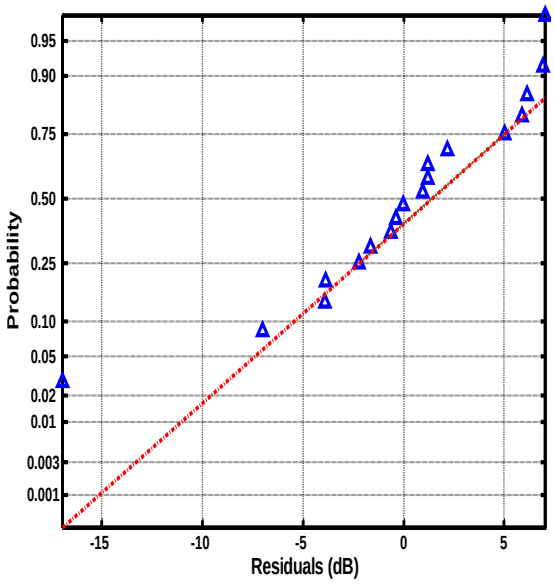

Figure 52: Normal probability plot of residuals at 6300 Hz.

The AD test is used for the data, where the number of observations is not large. The advantage of using this test is that it is one of the more sensitive tests based on computing the cumulative distribution function (CDF). It belongs to a class of tests that compare the distance between the theoretical CDF of the normal distribution with that of the CDF of residuals. The functional form of AD test statistic is given by (Romeu 2003):

$$AD = \sum_{i=1}^{M} \frac{1-2i}{M} \{\ln(F_0[Z_{(i)}]) + \ln(1 - F_0[Z_{(M+1-i)}]) +\} - M. \qquad (77)$$

Where F_0 is the assumed normal distribution with assumed or sample estimated parameters (μ, σ), $Z_{(i)}$ is the sorted, standardized sample value, M is the sample size, ln is the natural logarithm and subscript *i* runs from 1 to M.

The null hypothesis (H_0) is that the data belongs to the normal distribution. This hypothesis is rejected when the probability associated to AD test statistic is less than the specified significance level (0.05). In that case, the alternate hypothesis stands and the data does not belong to the normal distribution. The AD test results for the representative plots in Figs. 49-52 are given in Table 9.

Using the above procedure of fitting the linear model to the measured data at each frequency and then computing the residuals between the measured data and fitted model, the residuals were computed for all the measured data. The histogram of the residuals with the probability density function (PDF) of normal distribution is given in Fig. 53. The histogram indicates that the data fits a normal probability distribution of zero mean and a variance of 73.1. It also shows that the assumption of normality of residuals is valid at 95% significance level. Normally distributed residuals also show that the linear regression model adequately describes the variation of SPL with the distance in a conduit

Table 9: Andersen Darling goodness of fit test results – Linear Regression Model.

Frequency (Hz)	AD Test Statistic	Probability of AD statistic	Normal Distribution Mean and Variance	Results
200	0.676	0.069	Mean = 0.0, Variance = 80.00	H_0 is true.
500	0.446	0.2817	Mean = 0.0, Variance = 86.66	H_0 is true.
1600	0.365	0.4165	Mean = 0.0, Variance = 49.03	H_0 is true.
6300	0.559	0.1263	Mean = 0.0, Variance = 41.39	H_0 is true.

network. The normal probability plot of the residuals is given in Fig. 54. The residuals mostly follow the straight line indicating that they belong to a normal distribution. The tails of the data are, however, longer and residuals at the tails depart from normality. This is caused by outliers in the regression analysis that can be attributed to the inaccuracies of

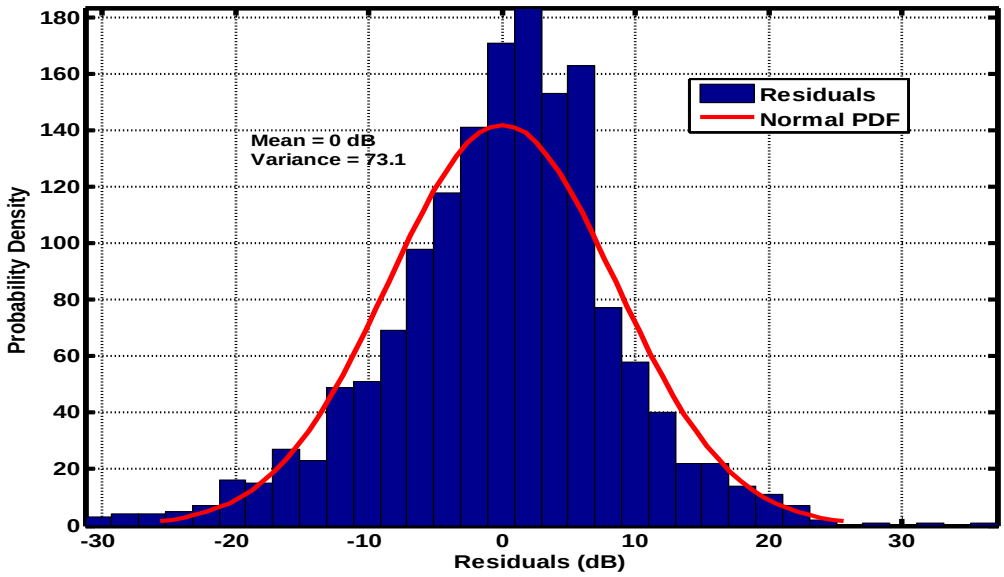

Figure 53: Histogram of residuals from all measurements and probability density function of normal probability distribution.

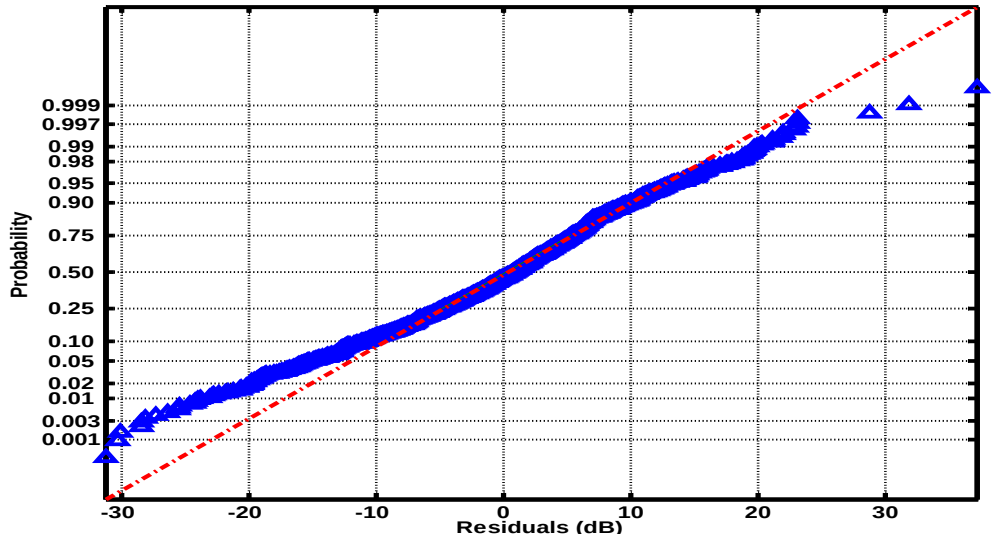

Figure 54: Normal probability plot of the residuals from all measurements.

the measurements which resulted in systematic rather than random error in the measured data.

As the analysis indicates the residuals generally follow a normal distribution and therefore, a linear fit through the measured data is a valid model. The slope of the measured data signifies the predicted attenuation coefficient of the model. Based on all the field measurements in 0.2 m diameter conduits, the attenuation coefficient is predicted using the linear model for the case of conduit between OL_6 and OL_5 manholes (distance 40.28 m, four side branches). The theoretical attenuation coefficient is obtained from (39) and (64). The attenuation coefficient is also measured from the difference between reference and received pressures. The plot is given in Fig. 55. It can be observed that the predicted attenuation from the linear model gives a much closer estimate of the measured attenuation coefficient compared to that from a purely theoretical computation for frequencies less than 2.0 kHz.

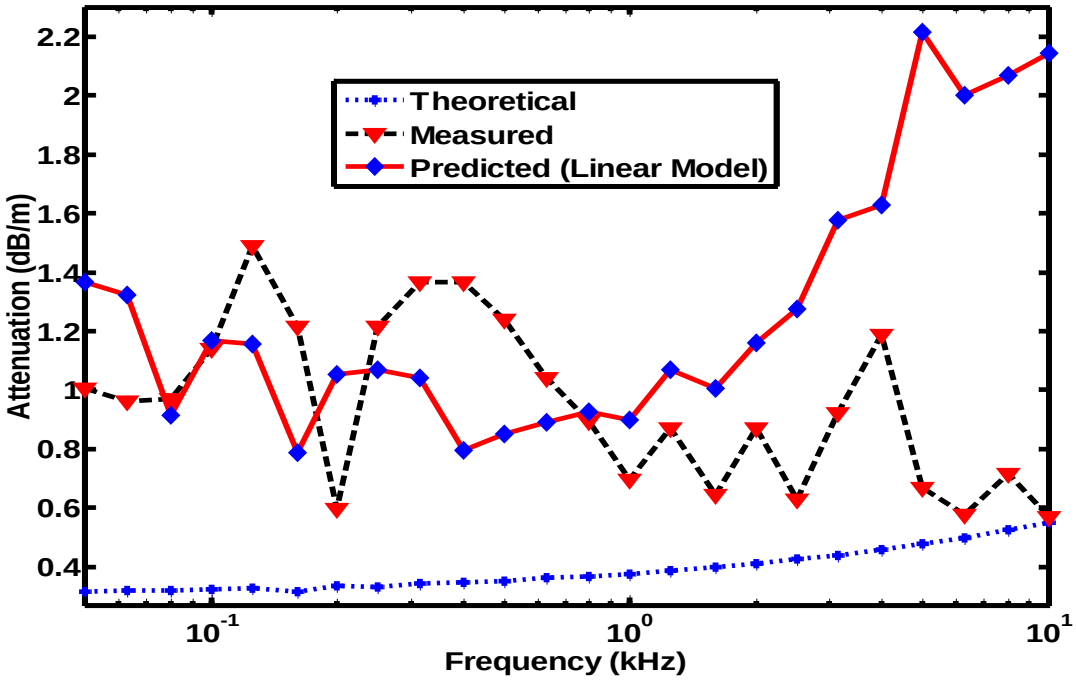

Figure 55: Measured, predicted and theoretically evaluated attenuation coefficient.

7.3 Variation of Attenuation with Frequency

In this section, the data collected from laboratory tests is analyzed to observe the variation of attenuation with frequency of the transmitted signal. For each tested configuration, the predicted attenuation coefficient from (39) is compared with that measured in the laboratory tests. The initial comparison is made for an 8.22 m long and a 17.56 m long conduit with no side branches. The plots of measured attenuation and that predicted from theory for both cases are given in Figs. 56 and 57.

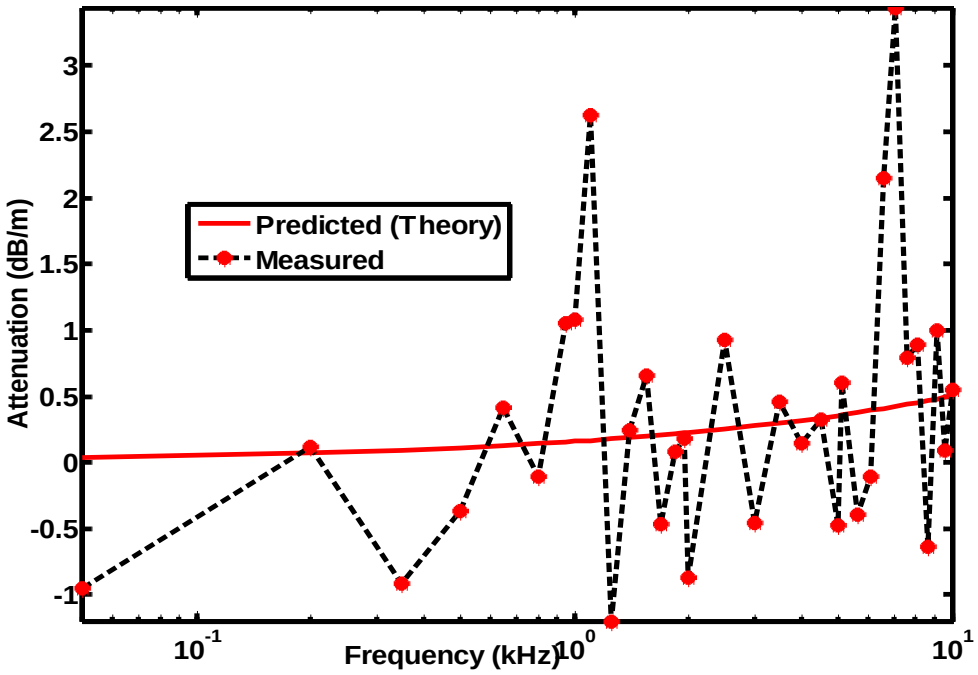

Figure 56: Predicted and measured attenuation in 8.22 m long 0.1m diameter conduit.

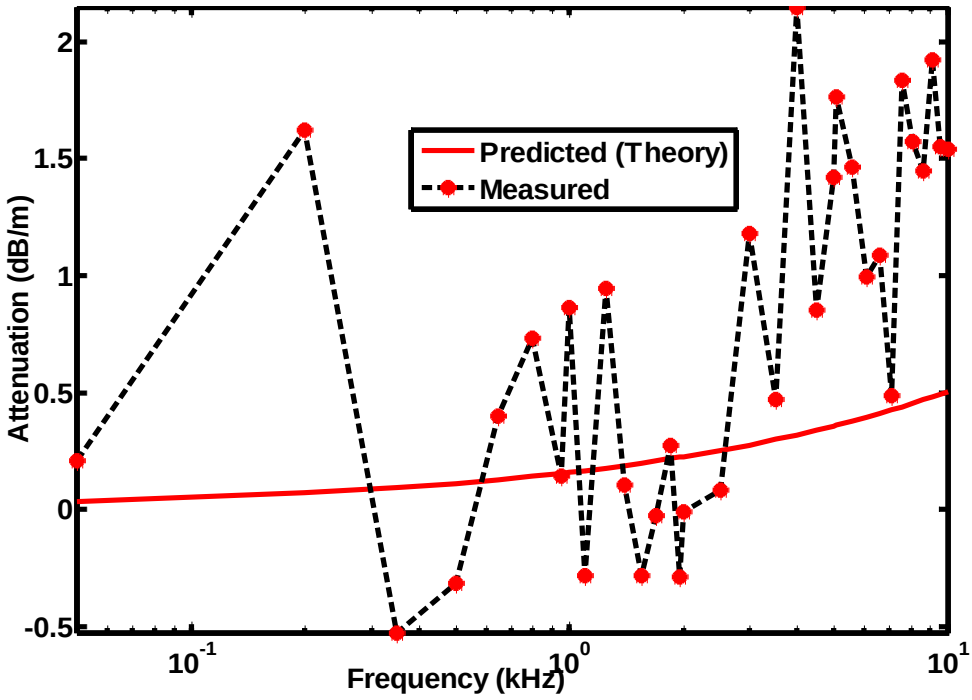

Figure 57: Predicted and measured attenuation in 17.56 m long 0.1 m diameter conduit.

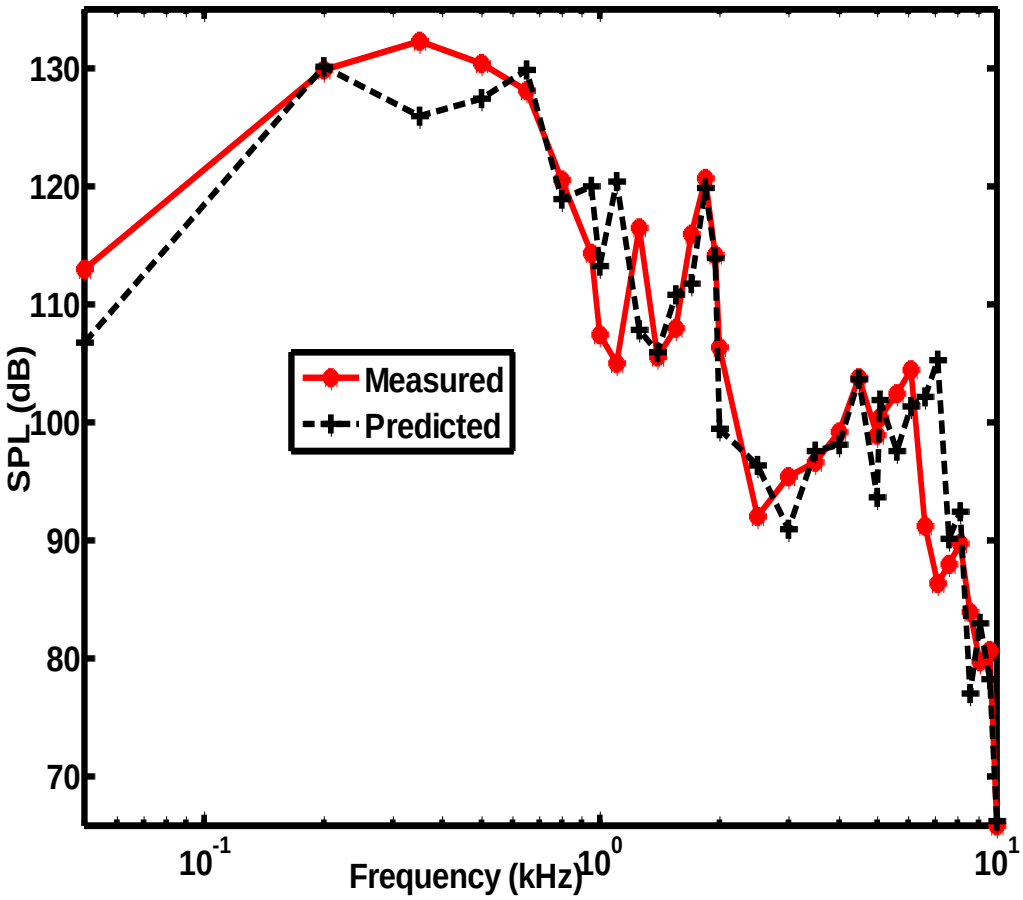

Figure 58: Predicted and measured SPL in 8.22 m long 0.1m diameter conduit.

The effect of pipe resonances is visible especially at frequencies between 350 Hz to 3.0 kHz for 17.56 m long conduit. In Figs. 58 and 59, the measured SPL at the receiving microphone and that predicted from (71) are plotted. The model predicted SPL compares well with that measured during the laboratory tests especially at frequencies less than 3.0 kHz for 17.56 m long conduit.

In order to determine the stochastic component of the attenuation, the residuals are computed between the measured and predicted attenuation. The normal probability plots of the residuals for both cases are given in Figs. 60 and 61. The plot for 8.22 m

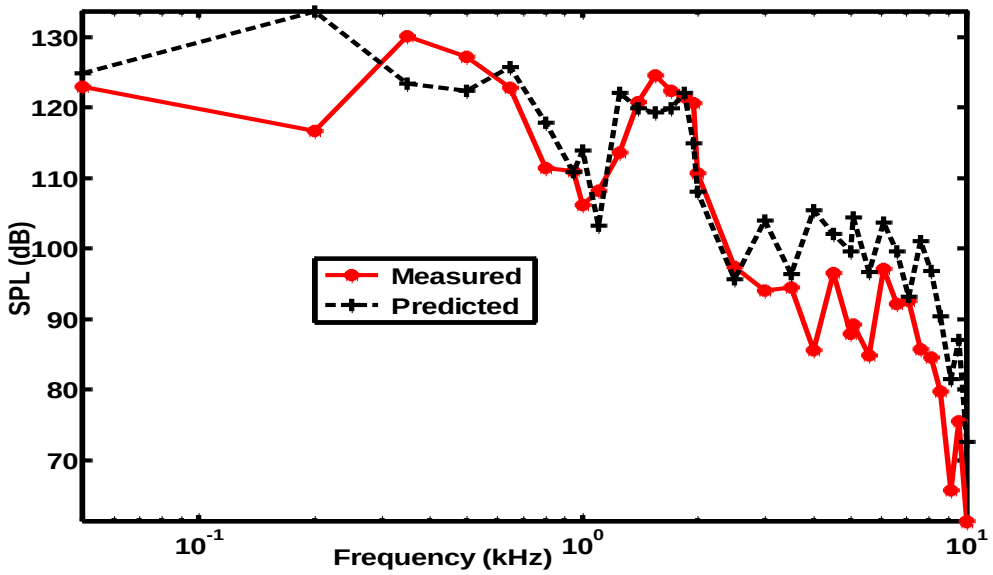

Figure 59: Predicted and measured SPL in 17.56 m long 0.1m diameter conduit.

conduit shows a slight right skew and a long tail. This can be attributed to the outliers in the attenuation coefficient as a result of the effect of conduit resonances. The plot for a 17.56 m long conduit has a long tail at both ends with a slight bend in the middle. This indicates that due to the effect of outliers a higher degree of variability is visible in the residuals compared to that in a normal distribution. On the whole, though, as the results of AD tests given in Table 10 indicate the residuals belong to normal distribution validating the assumption that the error between the measured and predicted attenuation is a random variable belonging to a normal probability distribution with a zero mean and finite variance.

The variation of attenuation coefficient with frequency has also been analyzed due to the change in number and length of side branches. This is given in the next sections.

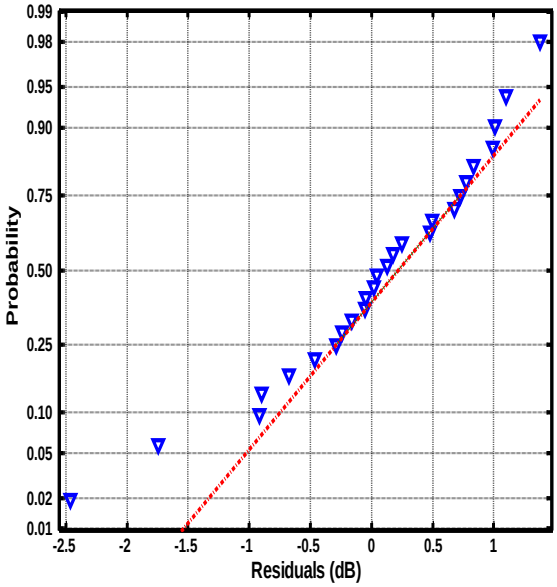

Figure 60: Normal probability plot of residuals for 8.22 m long 0.1 m diameter conduit.

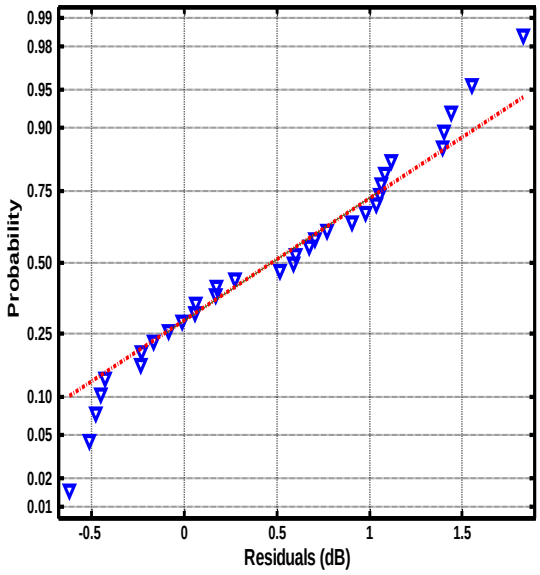

Figure 61: Normal probability plot of residuals for 17.56 m long 0.1 m diameter conduit.

7.4 Variation of Attenuation with Number of Side Branches

Variation in attenuation due to change in number of side branches is observed by initially introducing one side branch in a straight 17.56 m long conduit of 0.1 m diameter. The length of the side branch is 1.62 m with a diameter of 0.05 m. Attenuation due to the side branch is measured by subtracting the received SPL from the reference SPL.

The measured attenuation is compared with that obtained from theory and corrected

Table 10: Goodness of Fit test results - 8.22 m and 17.56 m long conduits.

Conduit Length (m)	AD Test Statistic	Probability of AD statistic	Normal Distribution Mean and Variance	Results
8.22	0.485	0.207	Mean = 0.04, Variance = 0.78	H_0 is true.
17.56	0.470	0.230	Mean = 0.491, Variance = 0.479	H_0 is true.

for the losses due to reflections from impedance mismatches in the straight conduit. The measured, corrected and theoretically evaluated attenuations are obtained for all tested configurations. The results are plotted in Figs. 62-68 for conduits with one through seven side branches. The theoretically evaluated attenuation reduces for frequencies greater than 2.0 kHz as the side branch impedance increases. However, as the theoretically evaluated attenuation only considers the signal attenuating effects of reflections from the junction point with the main conduit, therefore, it does not match up well with the measured attenuation especially at frequencies greater than around 2.0 kHz. The measured attenuation indicates sharp increase beyond 2.5 kHz. This could be attributed to the increased attenuation at the junction point with the side branch at frequencies greater than 2.5 kHz.

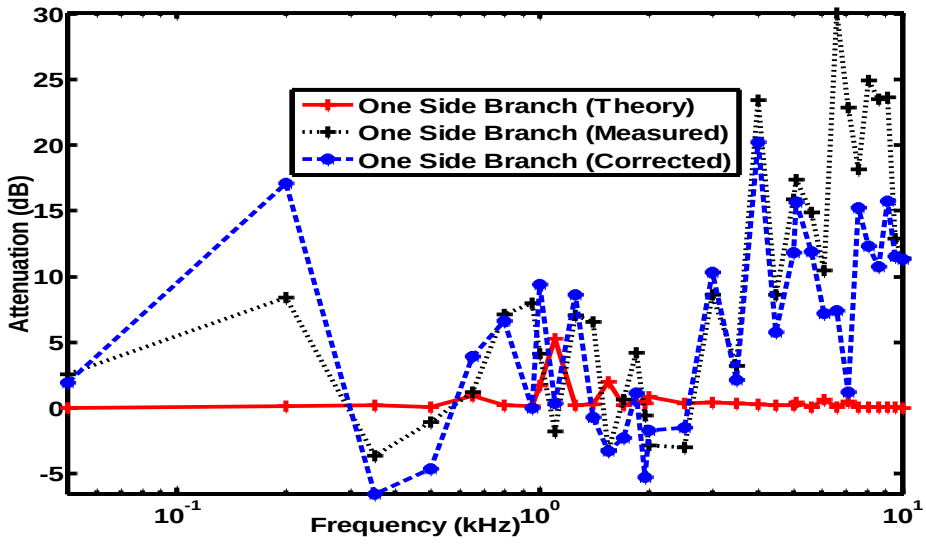

Figure 62: Measured and theoretical attenuation for a 17.56 m long conduit with one 1.62 m side branch.

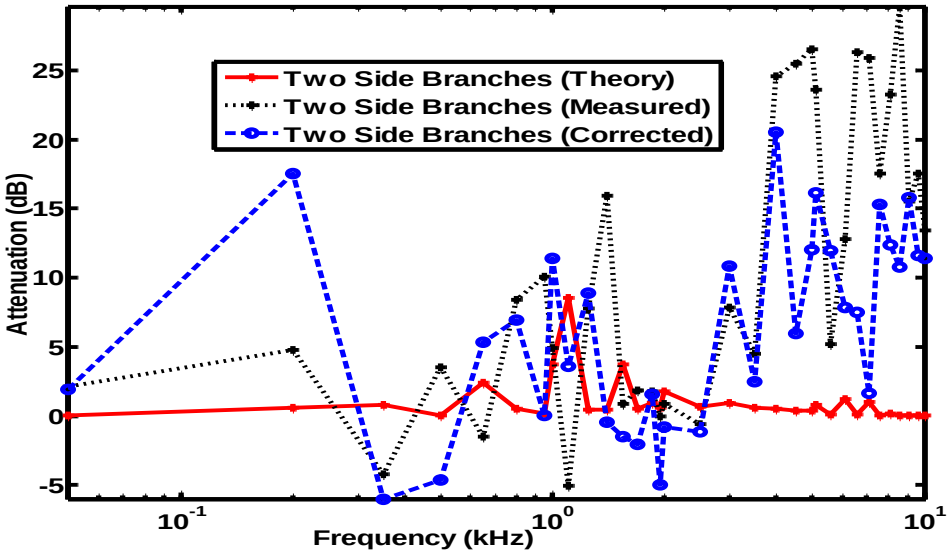

Figure 63: Measured and theoretical attenuation for a 17.56 m long conduit with two side branches.

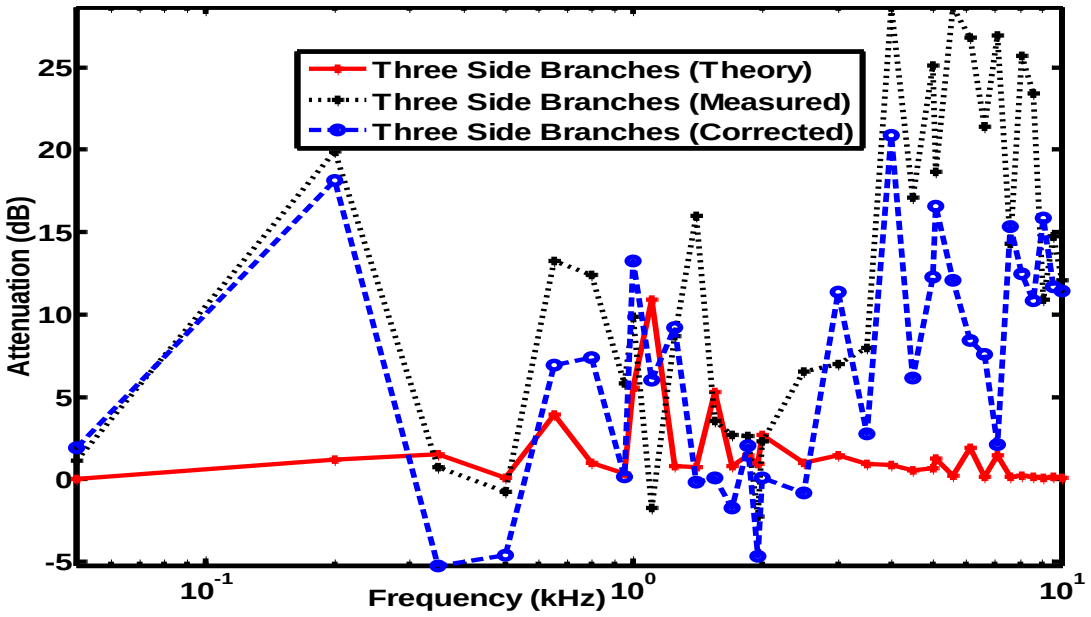

Figure 64: Measured and theoretical attenuation for a 17.56 m long conduit with three side branches.

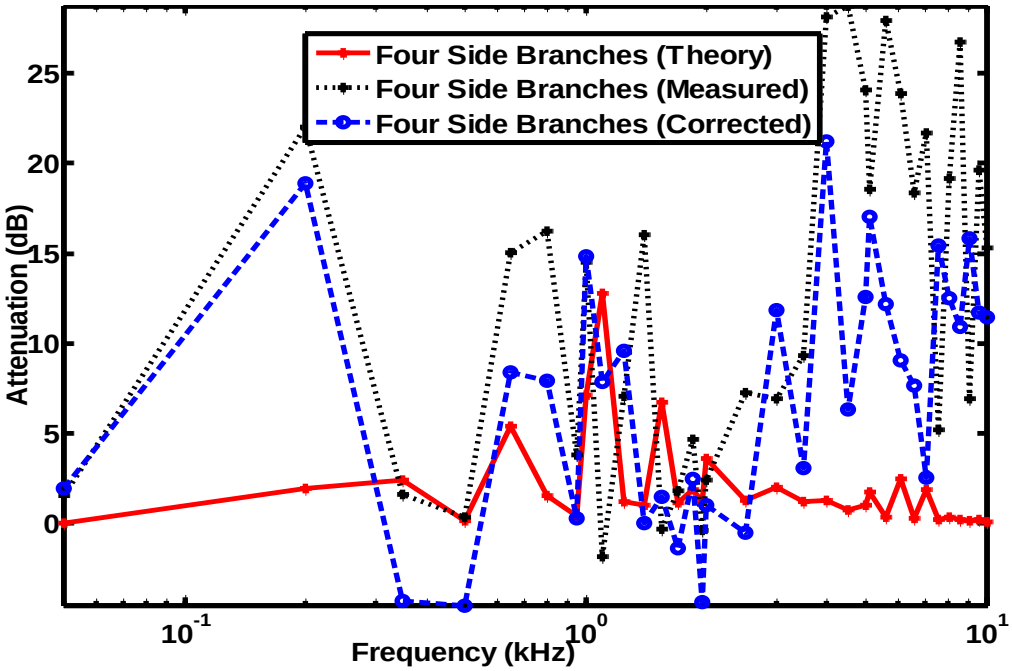

Figure 65: Measured and theoretical attenuation for a 17.56 m long conduit with four 1.62 m side branches.

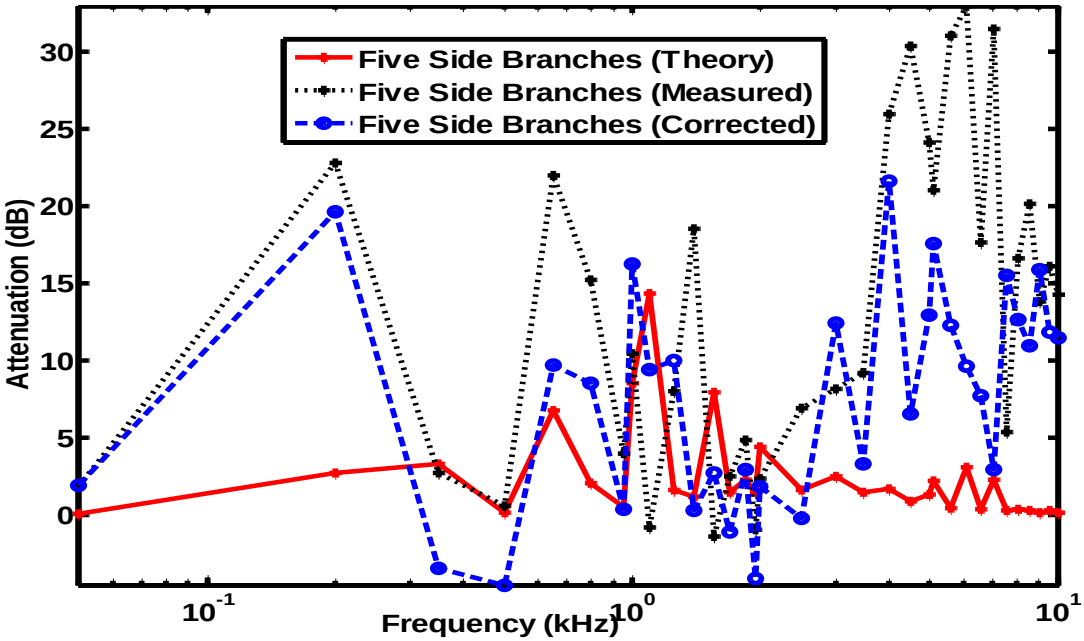

Figure 66: Measured and theoretical attenuation for a 17.56 m long conduit with five 1.62 m side branches.

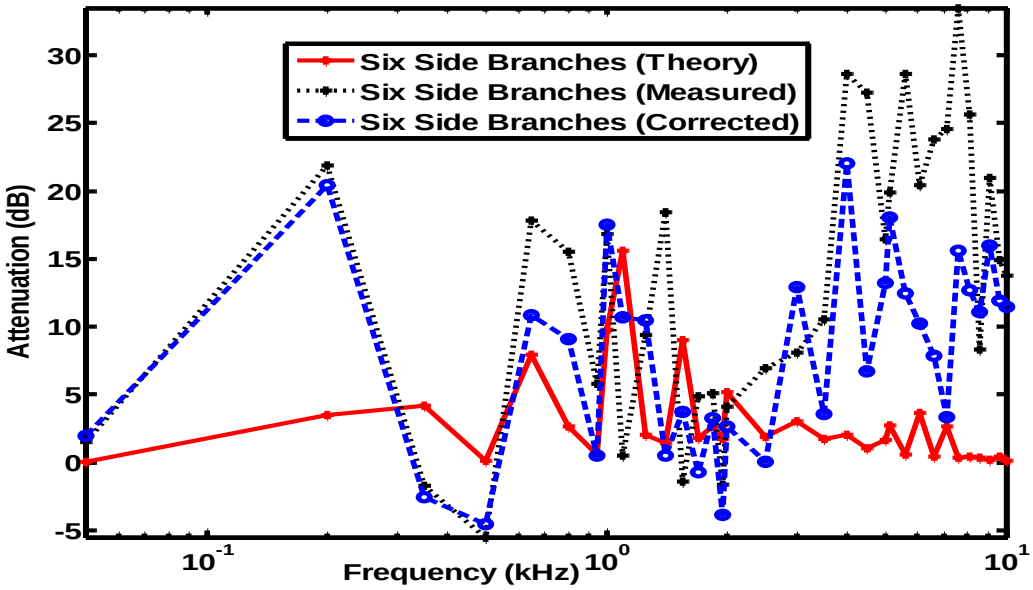

Figure 67: Measured and theoretical attenuation for a 17.56 m long conduit with six 1.62 m side branches.

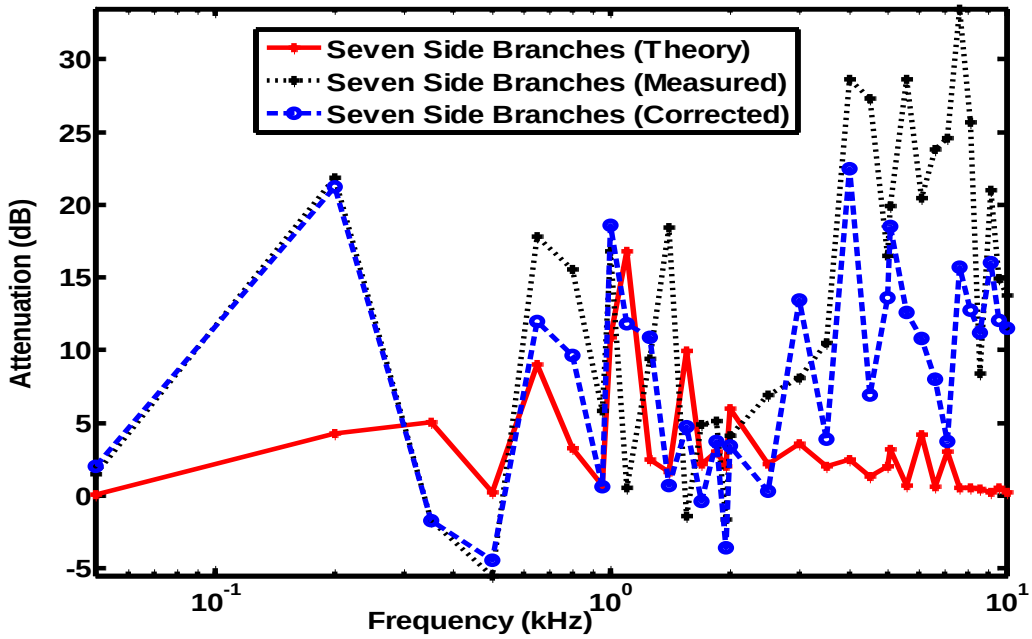

Figure 68: Measured and theoretical attenuation for a 17.56 m long conduit with seven 1.62 m side branches.

The plots also indicate that the signal attenuation increases with the increase in number of side branches. The effect of side branch resonances is also visible which causes large variations in the measured attenuation. As the attenuation computed from theory does not take into account the radiation loss from the side branches, therefore, it does not indicate appreciable variation at higher frequencies except for in a band between 5 kHz to 7.0 kHz.

The empirical correction factor, when added to the theoretically evaluated attenuation, results in a close agreement between the measured and the predicted attenuation except for a frequency band between 6.0 kHz to 9.0 kHz. At these frequencies

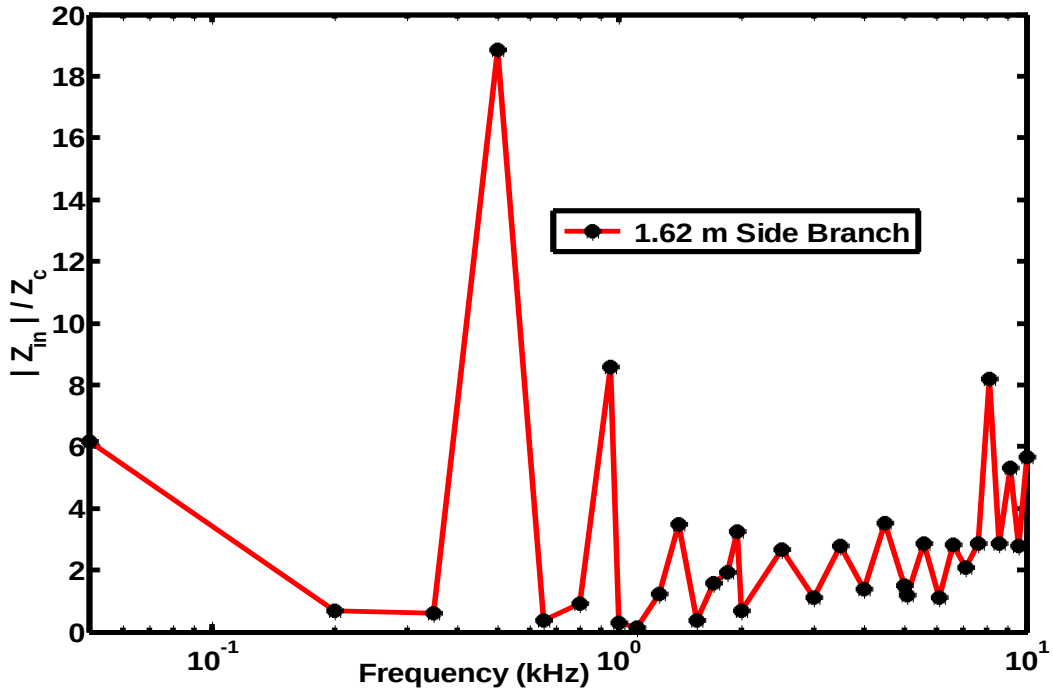

Figure 69: Side branch input impedance vs. frequency.

the additional attenuation can be attributed to the radiation of acoustic energy through the side branches. At frequencies less than 6.0 kHz, the corrected attenuation compares well

with the measured attenuation. The minima of theoretically evaluated attenuation correspond with the maxima of side branch input impedance as shown in Fig. 69.

The input impedance has strong peaks and troughs at relatively lower frequencies. The deep minima of side branch input impedance causes reflections back into the main conduit and buildup of standing wave which attenuates the propagating signal. At higher frequencies the side branch impedance increases with increase in frequency and the minima of impedance are not as deep as is the case with relatively lower frequencies. Therefore, the theoretically evaluated transmission loss due to the side branch reduces at higher frequencies. However, the total attenuation of the signal in the main conduit increases due to the buildup of standing wave and increased transmission of the signal through the side branches. As the number of side branches is increased, the total attenuation of the propagating signal in the main conduit increases with the increase in frequency.

In order to compare the measured SPL with that predicted from the proposed model, the transmission loss is computed from (64) for the case of one through seven side branches. A comparison between the model predicted SPL and that measured at the receiving microphone for one through seven side branches is given in Figs. 70-76. As expected the theoretical model does not sufficiently cater for the reflected signal from the open ended conduits and radiation of the signal at higher frequencies through the side branches. Therefore, there is large error between the predicted and measured SPL especially at higher frequencies. The predicted SPL with empirical correction factor shows better agreement with the measured SPL than that predicted from theory only.

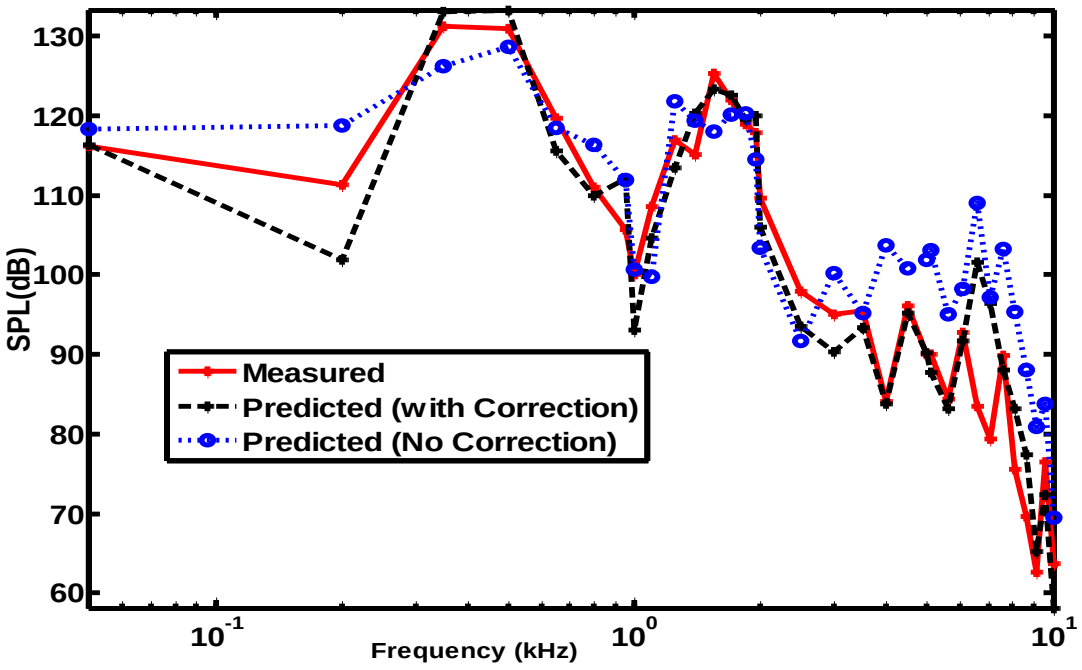

Figure 70: Predicted and received SPL for a 17.56 m long conduit with one 1.62 m side branches.

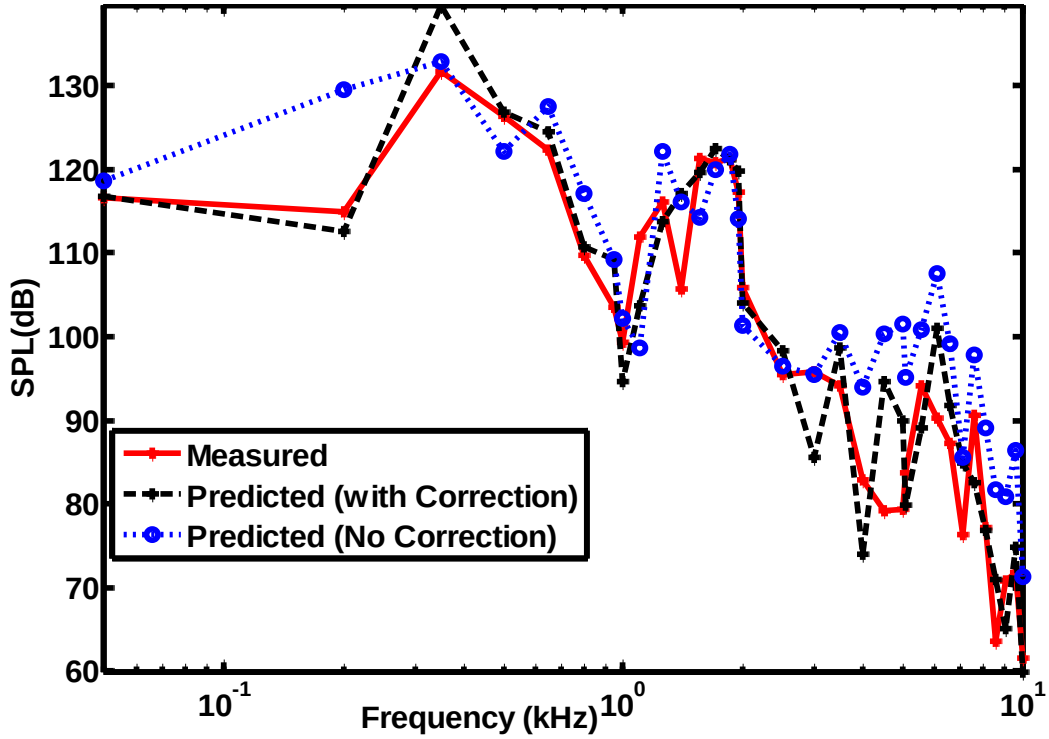

Figure 71: Predicted and received SPL for a 17.56 m long conduit with two 1.62 m side branches.

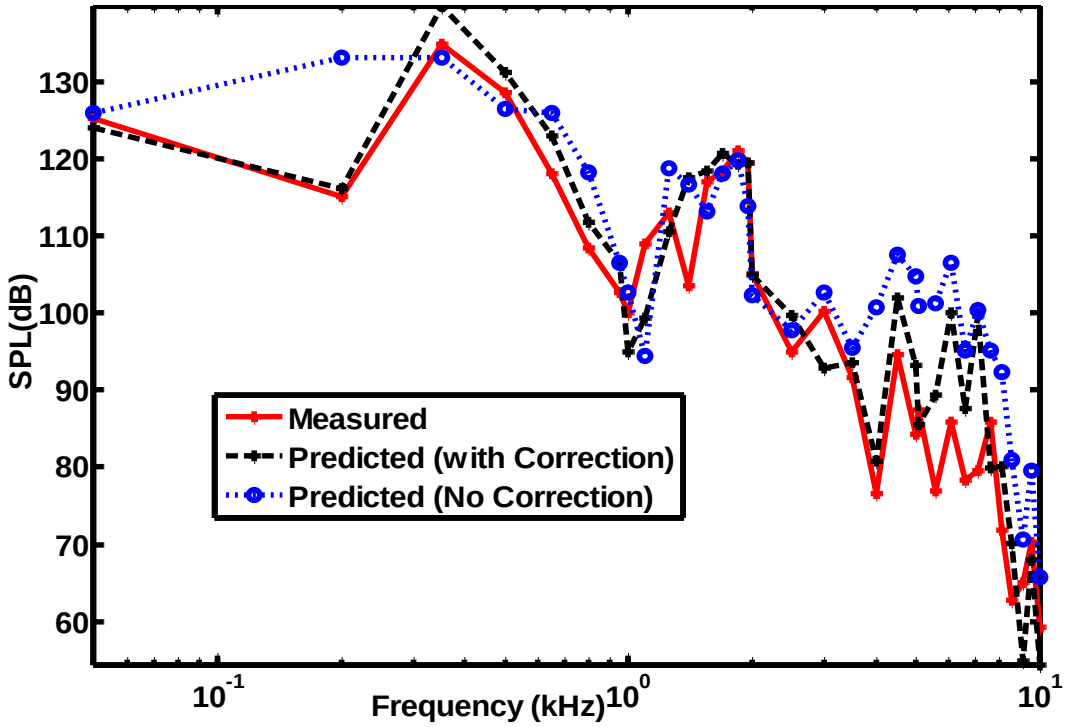

Figure 72: Predicted and received SPL for a 17.56 m long conduit with three 1.62 m side branches.

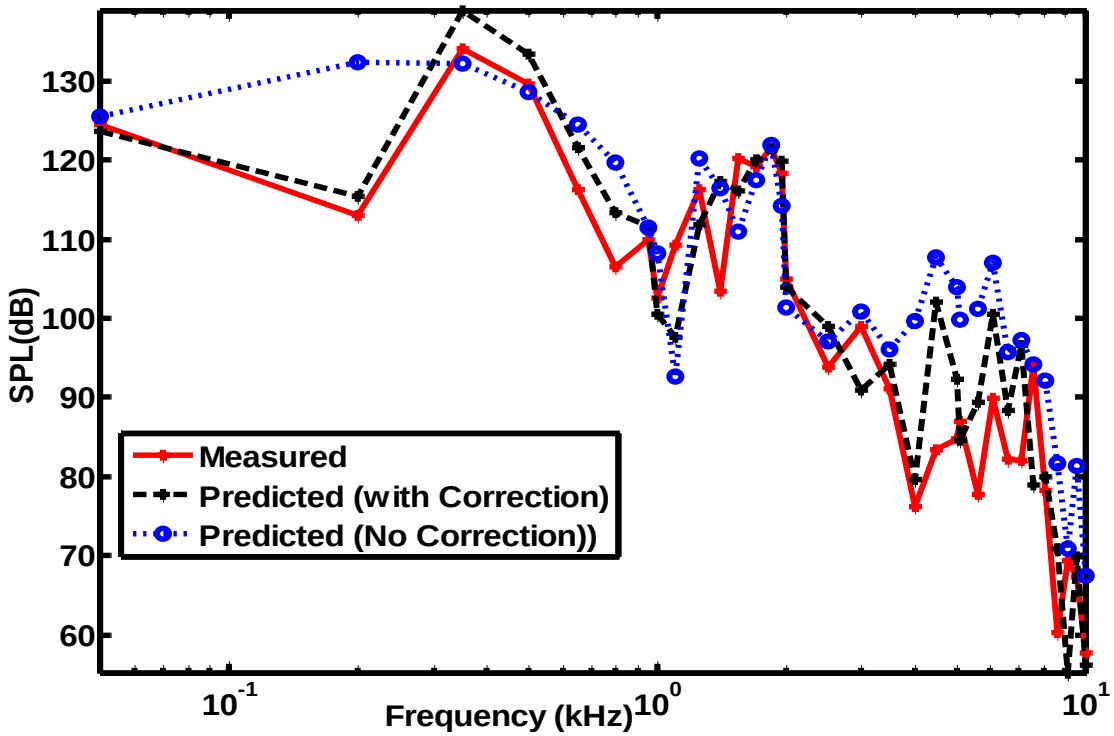

Figure 73: Predicted and received SPL for a 17.56 m long conduit with four 1.62 m side branches.

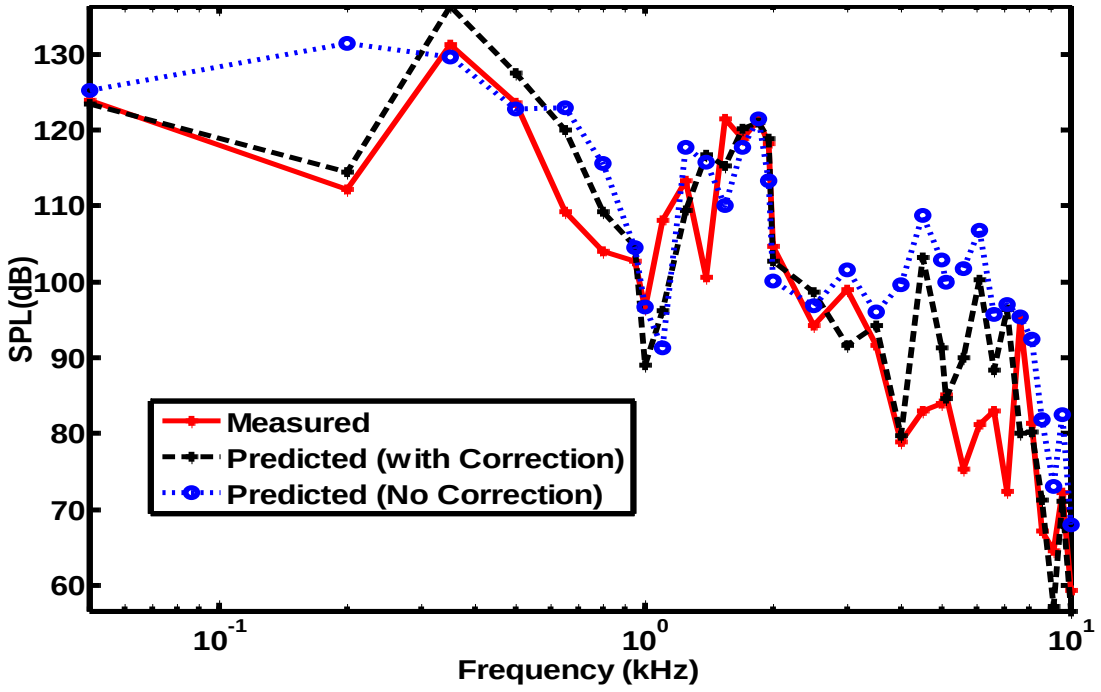

Figure 74: Predicted and measured SPL for a 17.56 m long conduit with five 1.62 m side branches.

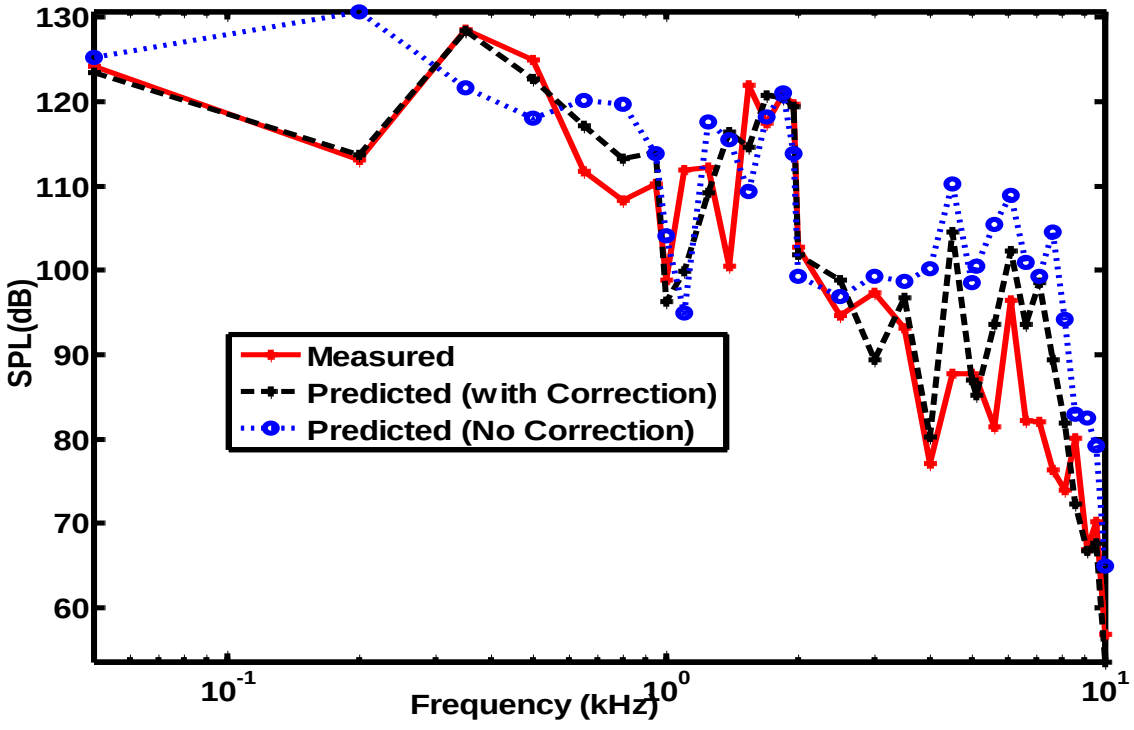

Figure 75: Predicted and received SPL for a 17.56 m long conduit with six 1.62 m side branches.

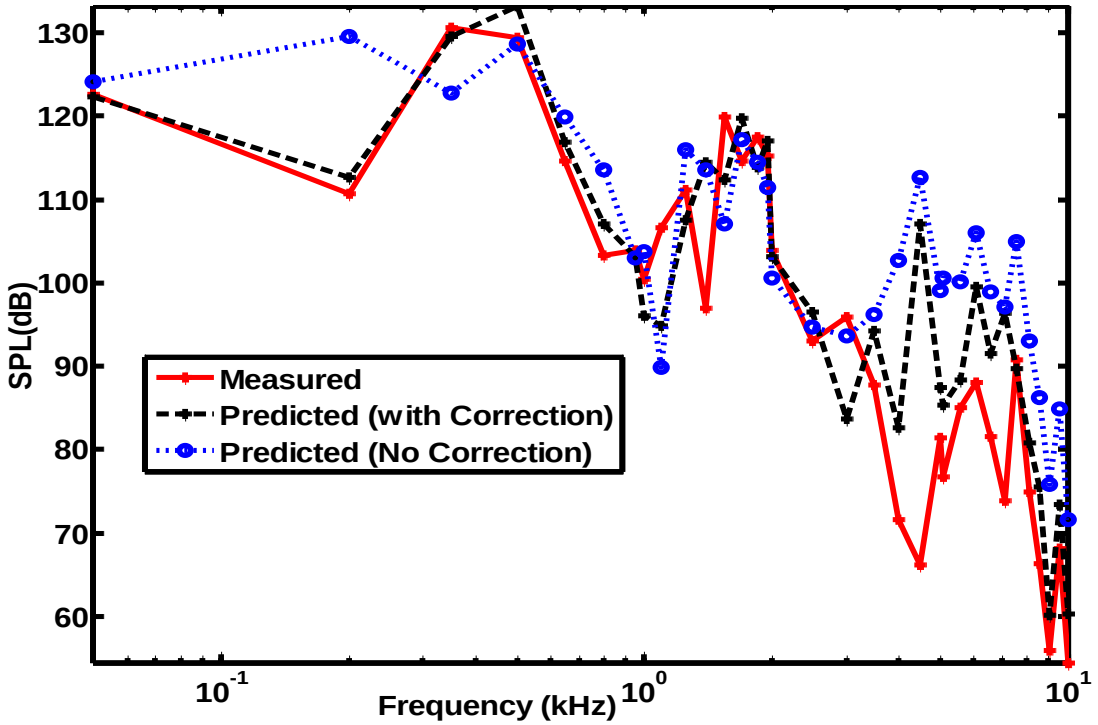

Figure 76: Predicted and received SPL for a 17.56 m long conduit with seven 1.62 m side branches.

The residuals between the predicted SPL with the correction factor and the measured SPL are computed from (72) and statistically analyzed. The model's assumption is that the residuals belong to a normal distribution with finite mean and variance. In order to graphically check the residuals for normality, normal probability plots of the residuals are generated. The plots are given in Figs. 77-83 for the case of one through seven side branches.

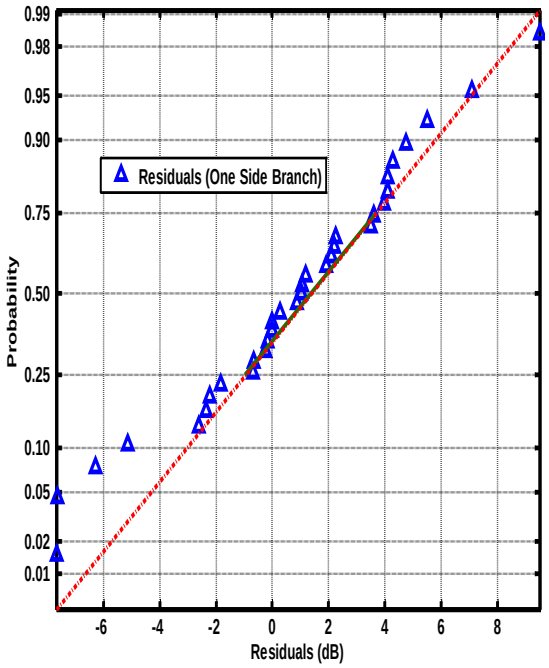

Figure 77: Normal probability plot for a 17.56 m long conduit with one 1.62 m side branch.

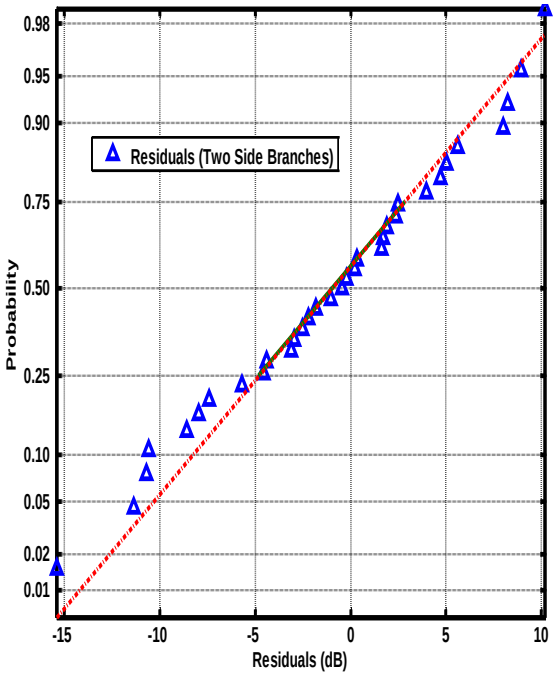

Figure 78: Normal probability plot for a 17.56 m long conduit with two 1.62 m side branches.

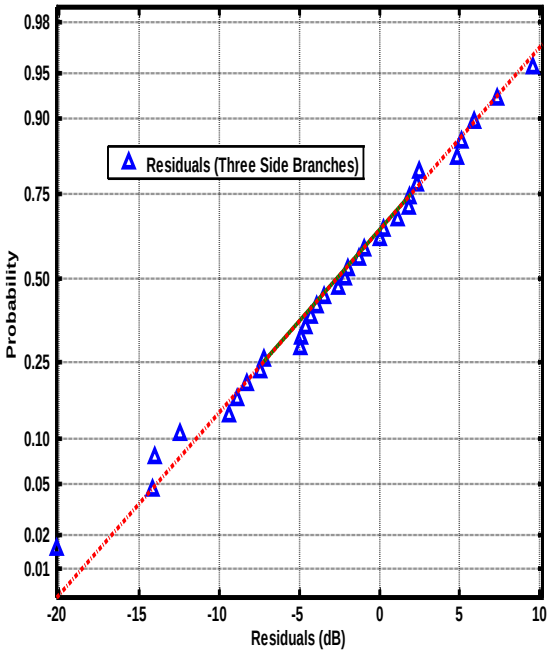

Figure 79: Normal probability plot for a 17.56 m long conduit with three 1.62 m side branches.

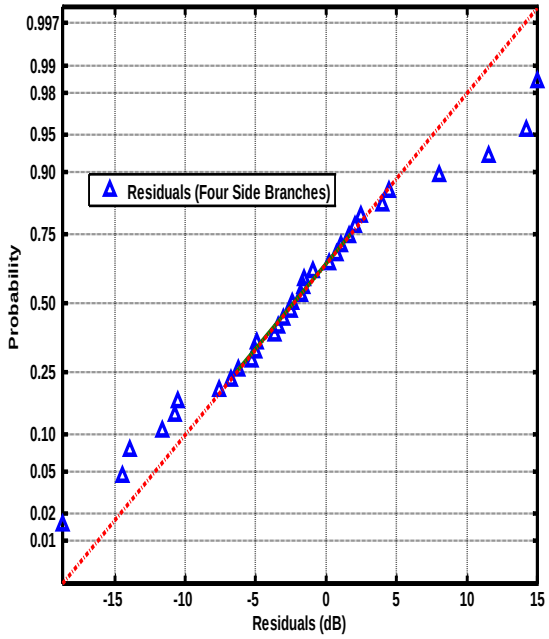

Figure 80: Normal probability plot for a 17.56 m long conduit with four 1.62 m side branches.

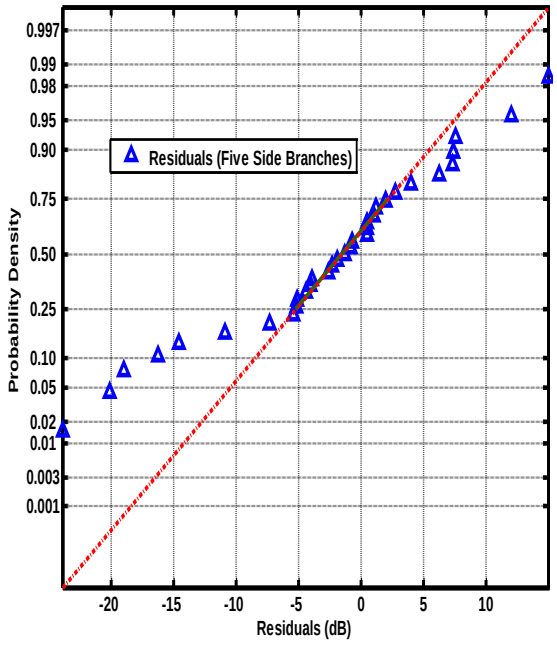

Figure 81: Normal probability plot for a 17.56 m long conduit with five 1.62 m side branches.

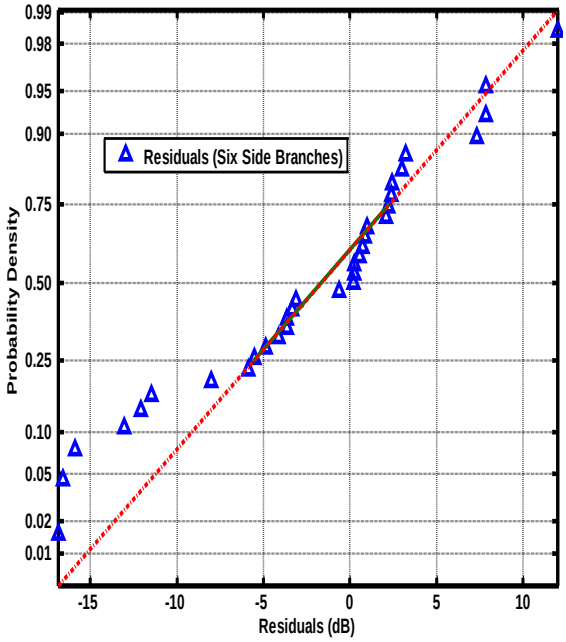

Figure 82: Normal probability plot for a 17.56 m long conduit with six 1.62 m side branches.

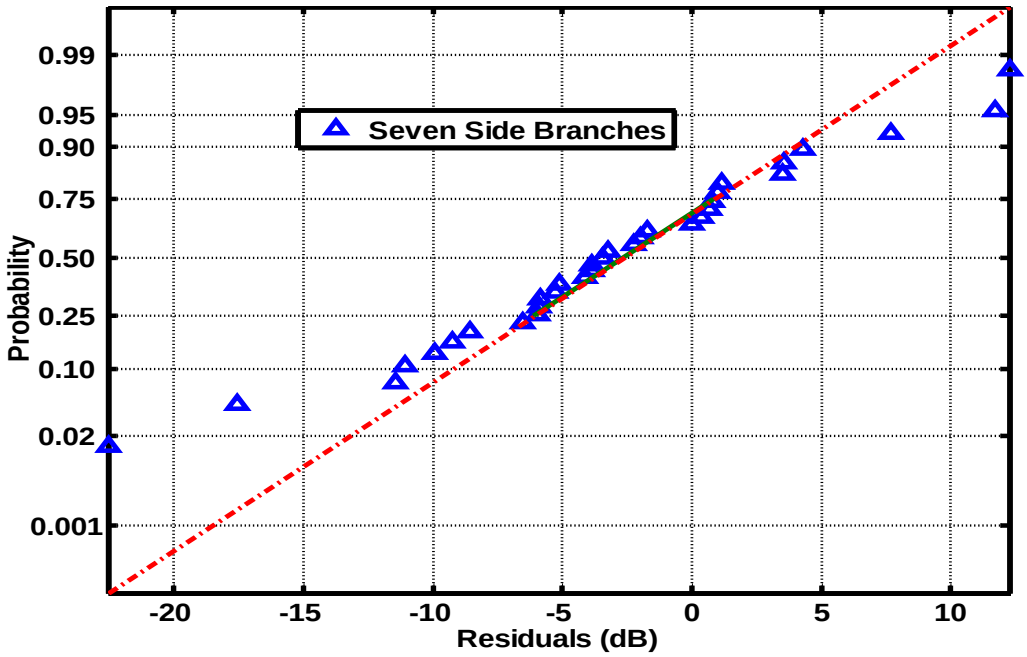

Figure 83: Normal probability plot for a 17.56 m long conduit with seven 1.62 m side branches.

The plots indicate that the residuals mostly follow the straight line of normal distribution. There are deviations from normality at the tails for the case of four, five, six and seven side branches. These deviations are caused by large residuals at high frequencies between the predicted and the measured data. The AD test results are given in Table 11. It can be seen that the null hypothesis is true in all tested cases indicating that the residuals belong to normal distribution with a finite mean and variance as given for each case in Table 11.

The histogram of residuals obtained from SPL data corrected for the standing wave effects in the straight conduit is plotted in Fig. 84. Histogram of residuals without the correction factor is also given in Fig 85. It can be observed from the histograms that the residuals with the correction factor applied follow the normal distribution more closely than the residuals without the correction factor. The mean and variance of the

Table 11: Goodness of Fit test results – Change in number of side branches.

Number of side branches	AD Test Statistic	Probability of AD statistic	Normal Distribution Mean (dB) and Variance	Results
One	0.376	0.390	Mean = 0.78, Variance = 15.44	H_0 is true.
Two	0.170	0.924	Mean = -1.07, Variance = 40.12	H_0 is true.
Three	0.158	0.945	Mean = -2.54, Variance = 49.20	H_0 is true.
Four	0.332	0.497	Mean = -2.16, Variance = 59.79	H_0 is true.
Five	0.671	0.072	Mean = -2.48, Variance = 79.16	H_0 is true.
Six	0.682	0.068	Mean = -2.25, Variance = 52.19	H_0 is true.
Seven	0.376	0.392	Mean = -3.10, Variance = 52.68	H_0 is true.

corrected residuals is significantly lower than the case of residuals with no correction. In order to further check the residuals for normality, the normal probability plots of the residuals for both cases are given in Figs. 86 and 87. Both the plots indicate that the residuals mostly belong to the normal probability distribution. There is more deviation from normality around the lower tail of the normal probability plots due to the effect of outliers in the measured data.

In the next section the variation in attenuation with change in the length of side branches is analyzed and the evaluated residuals are tested for normality.

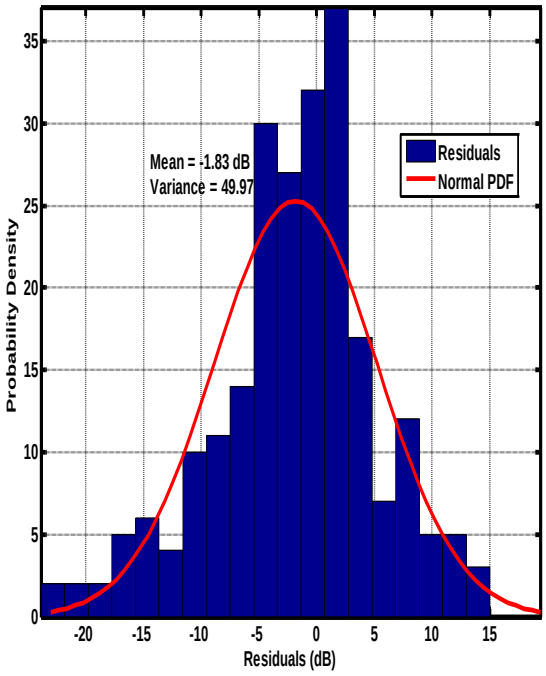

Figure 84: Histogram of residuals (with correction included) from all measurements (Change in number of side branches).

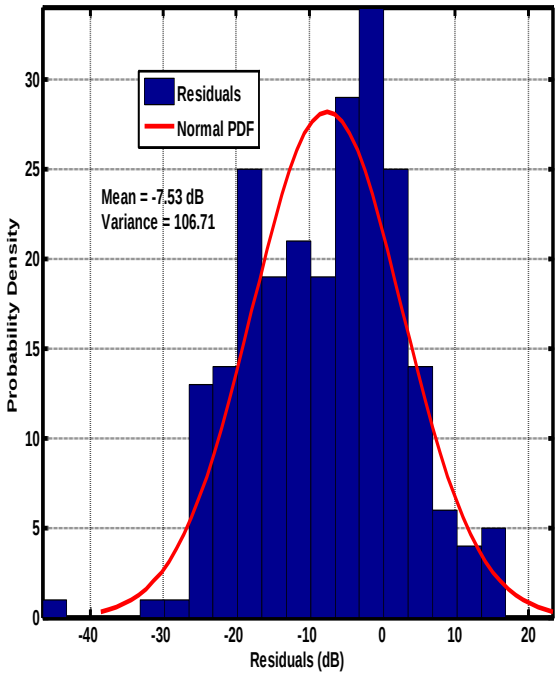

Figure 85: Histogram of residuals (without correction) from all measurements (Change in number of side branches).

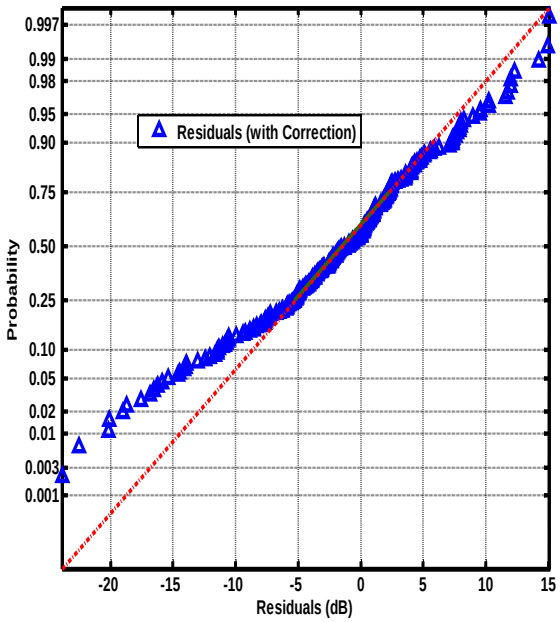

Figure 86: Normal probability plot of residuals (with correction) from all measurements (due to change in number of side branches).

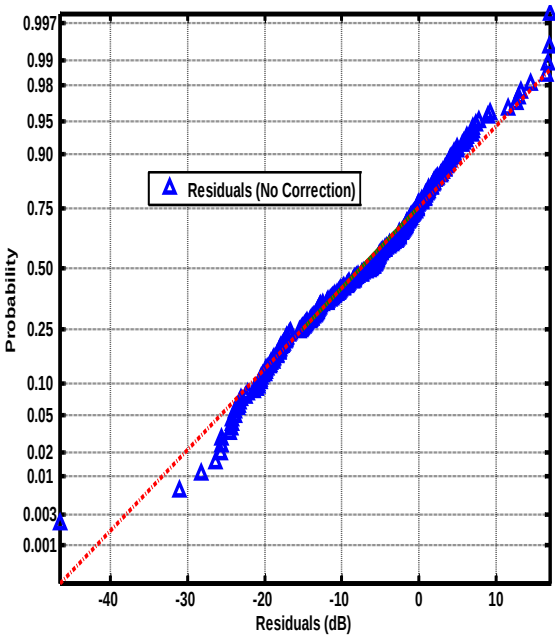

Figure 87: Normal probability plot of residuals (with no correction) from all measurements (due to change in number of side branches)

7.5 Variation of Attenuation with Length of a Side Branch

The change in attenuation coefficient of the propagating signal with the change in length of side branch was tested for six cases. The side branch length was varied from 1.62 m to 0.12 m in 0.3 m steps. In each case the reference SPL and the received SPL were recorded. The main effect of the change in the length of side branch is a change in its input impedance. This change can cause either a transmission or a reflection condition at the junction point with the main conduit. The input impedances and the corresponding attenuation due to change in the length of side branch are plotted in Fig. 88-97.

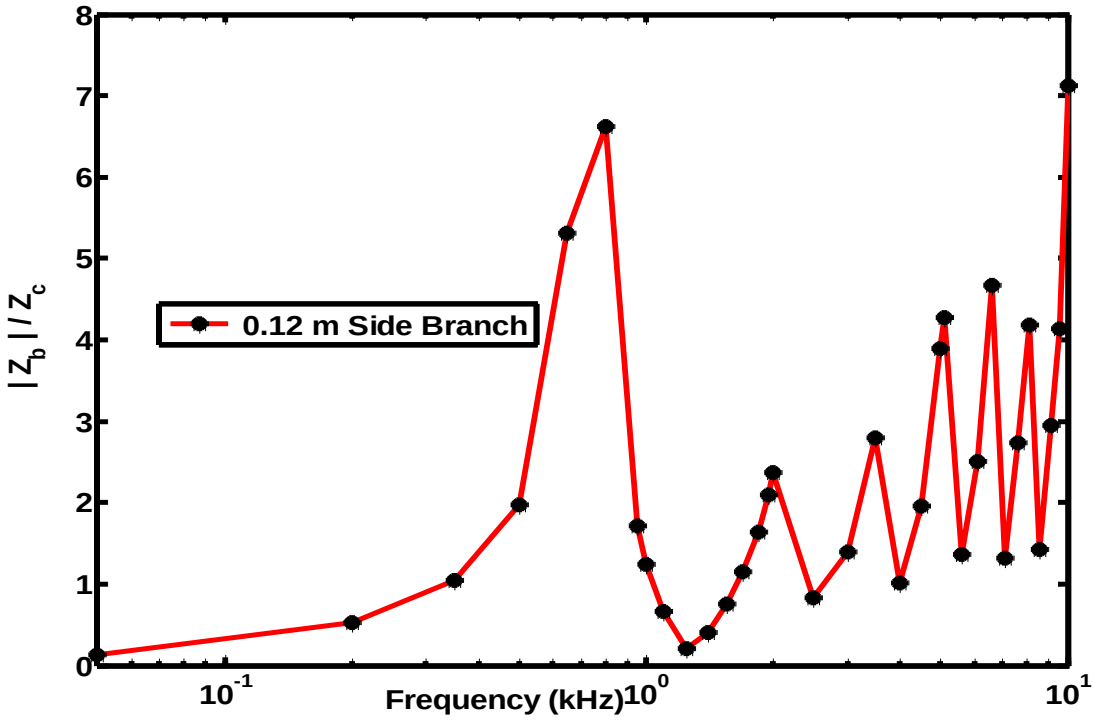

Figure 88: Normalized input impedance for a 0.12 m long side branch.

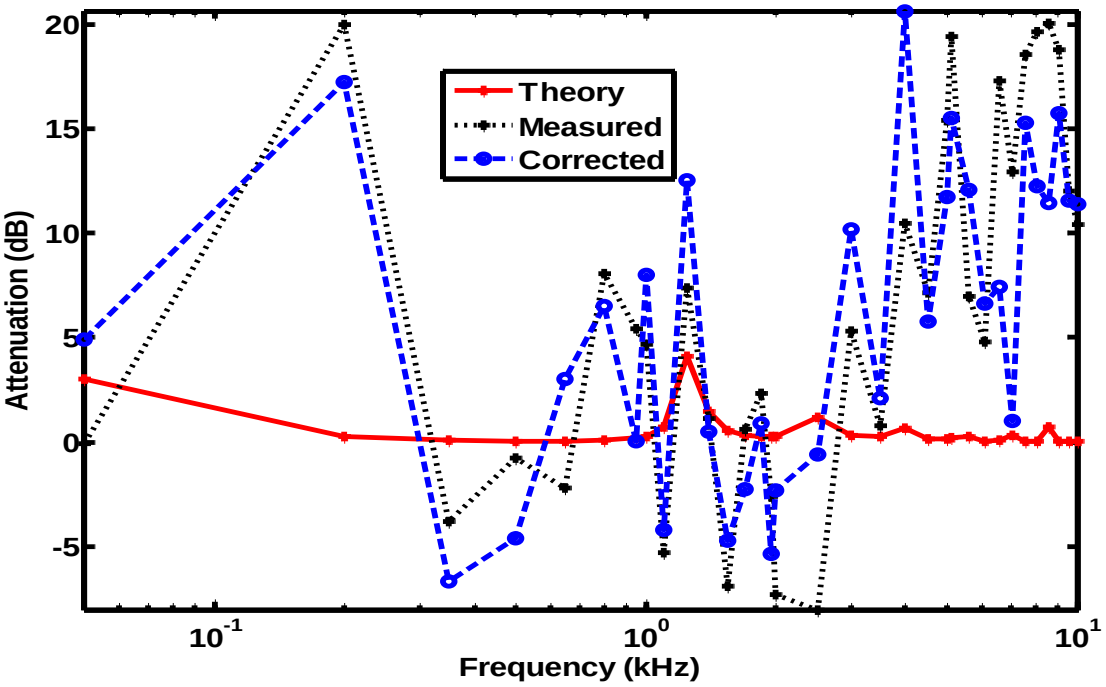

Figure 89: Attenuation due to a 0.12 m long side branch.

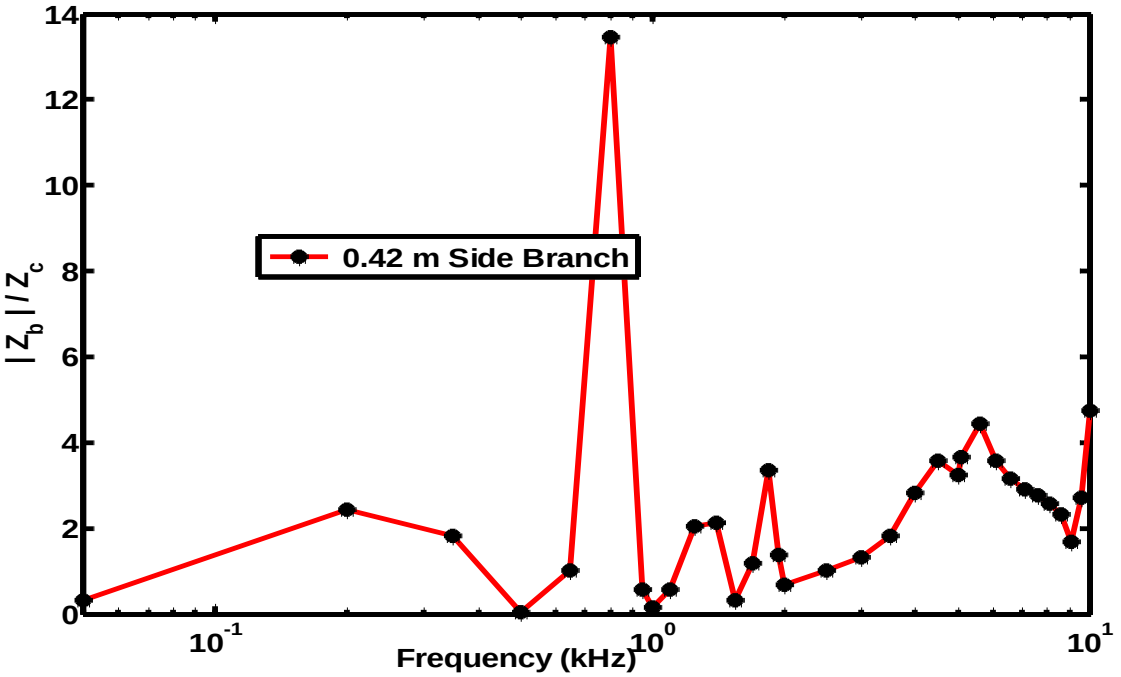

Figure 90: Normalized input impedance for a 0.42 m long side branch.

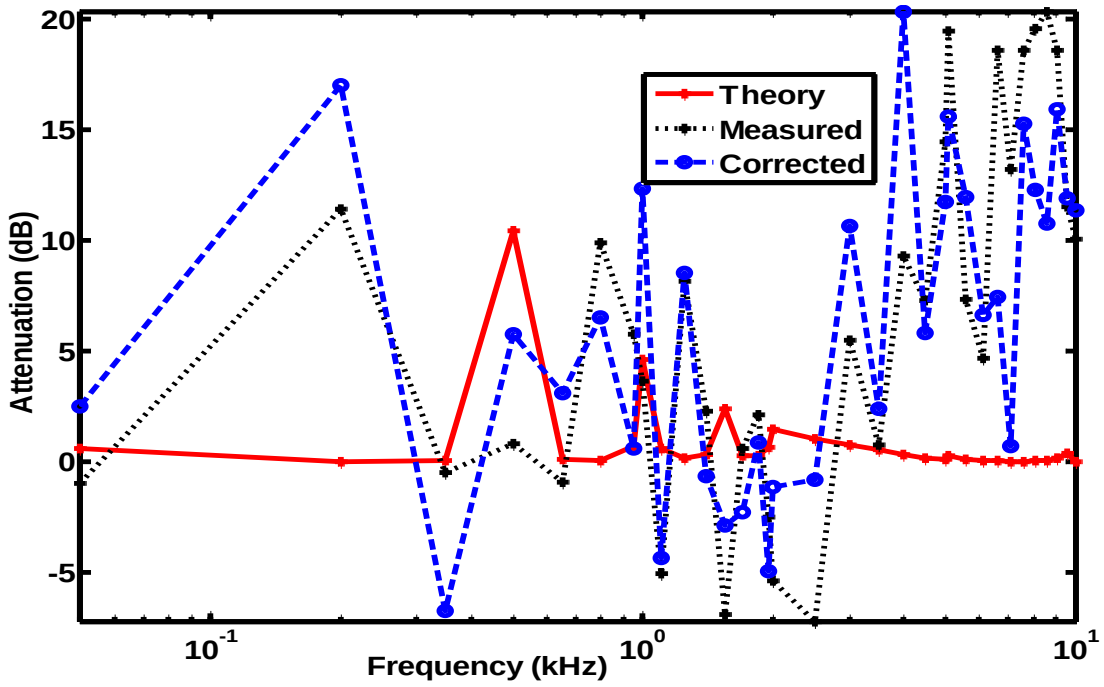

Figure 91: Attenuation due to a 0.42 m long side branch.

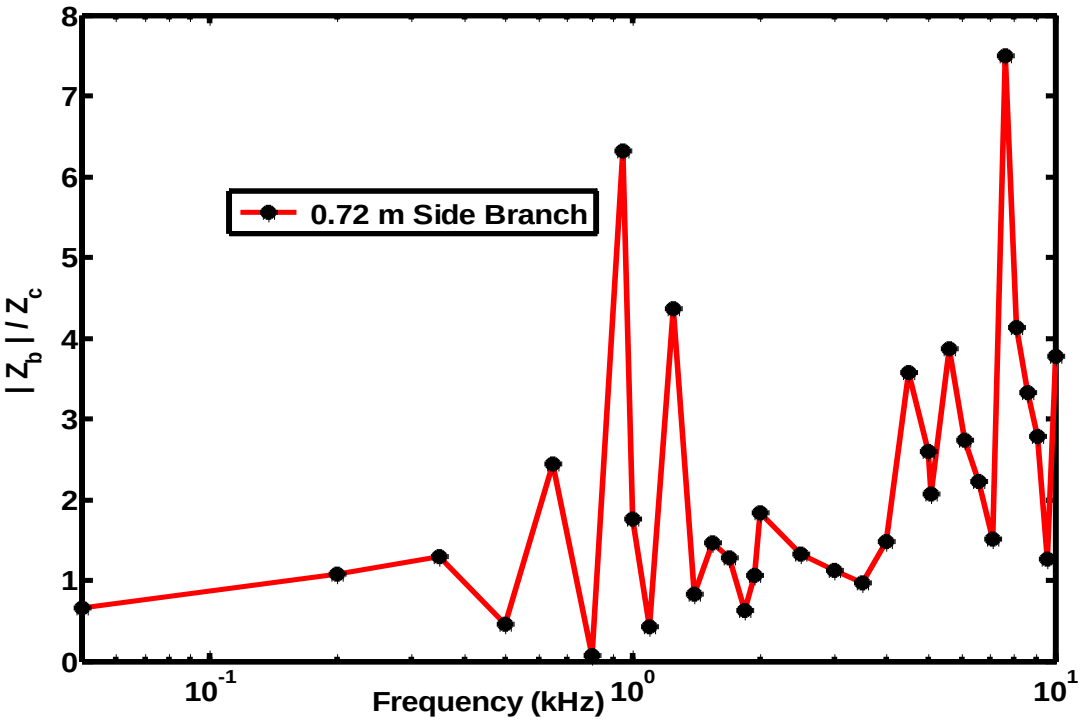

Figure 92: Normalized input impedance for a 0.72 m long side branch.

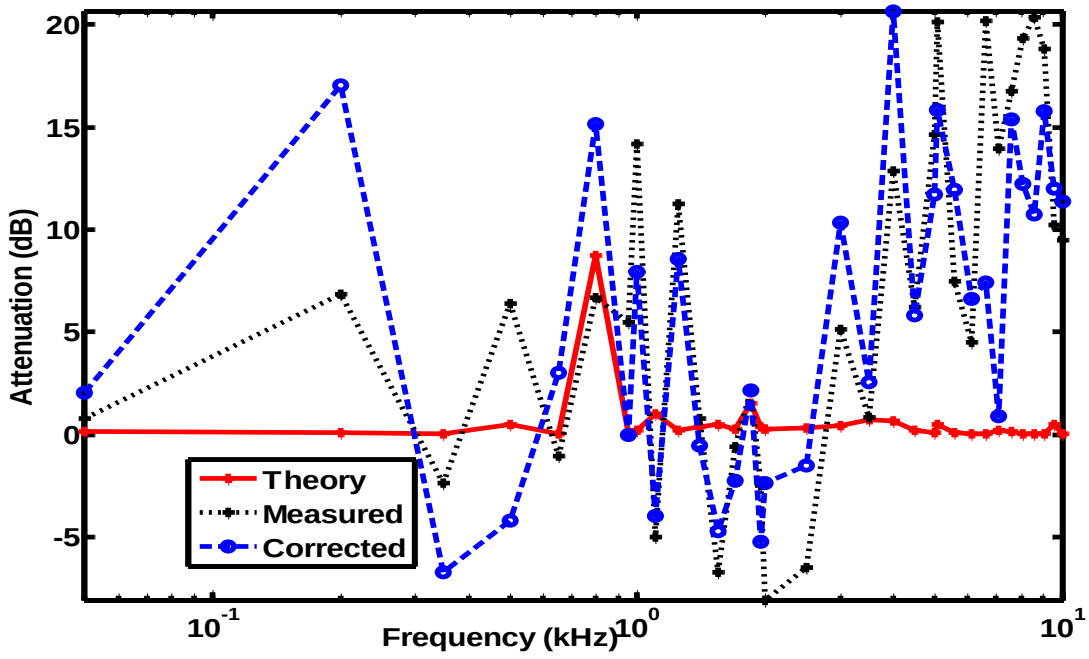

Figure 93: Attenuation due to a 0.72 m long side branch.

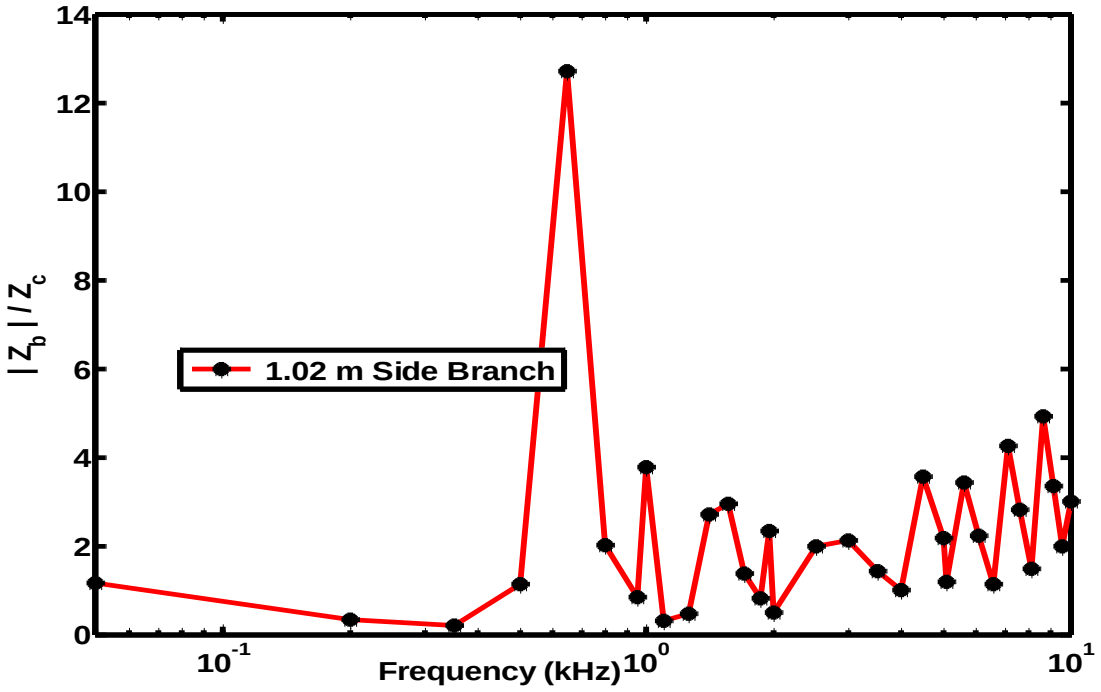

Figure 94: Normalized input impedance for a 1.02 m long side branch.

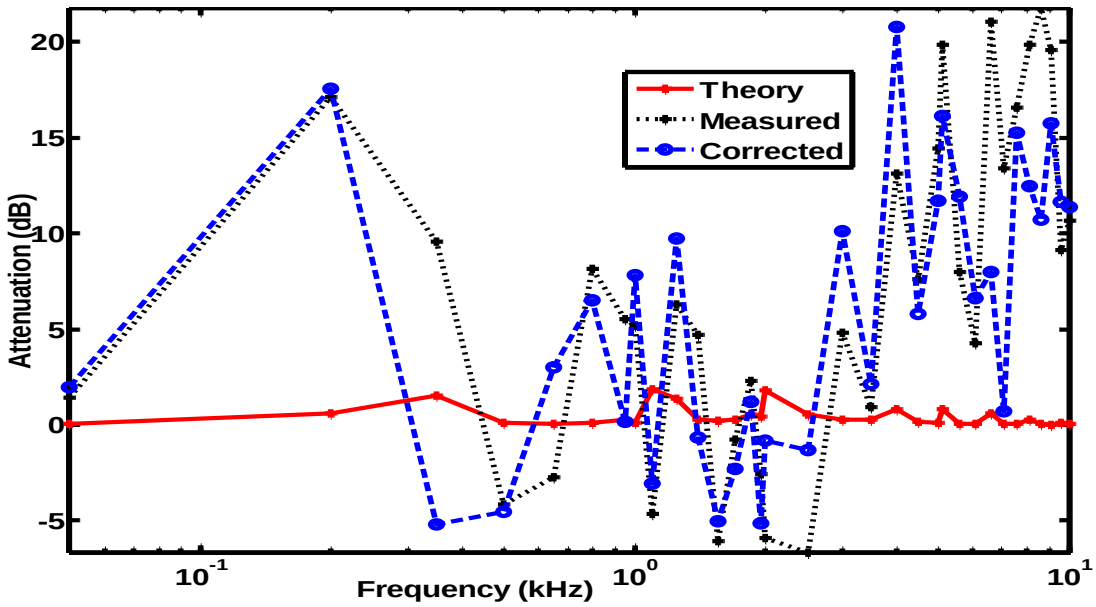

Figure 95: Attenuation due to a 1.02 m long side branch.

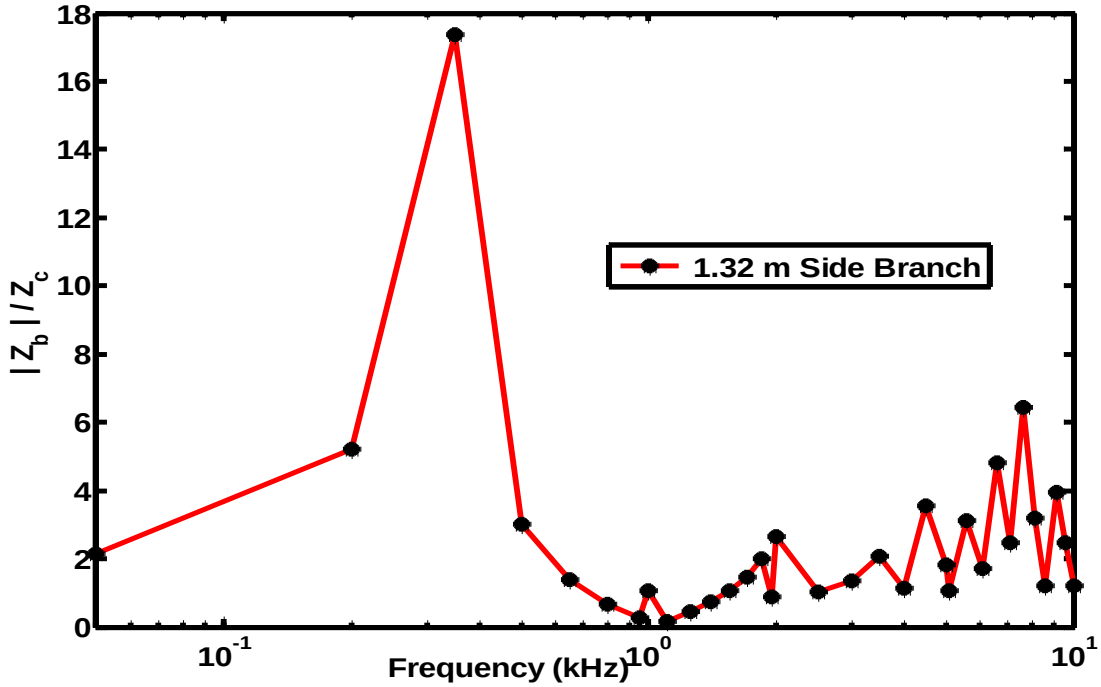

Figure 96: Normalized input impedance for a 1.32 m long side branch.

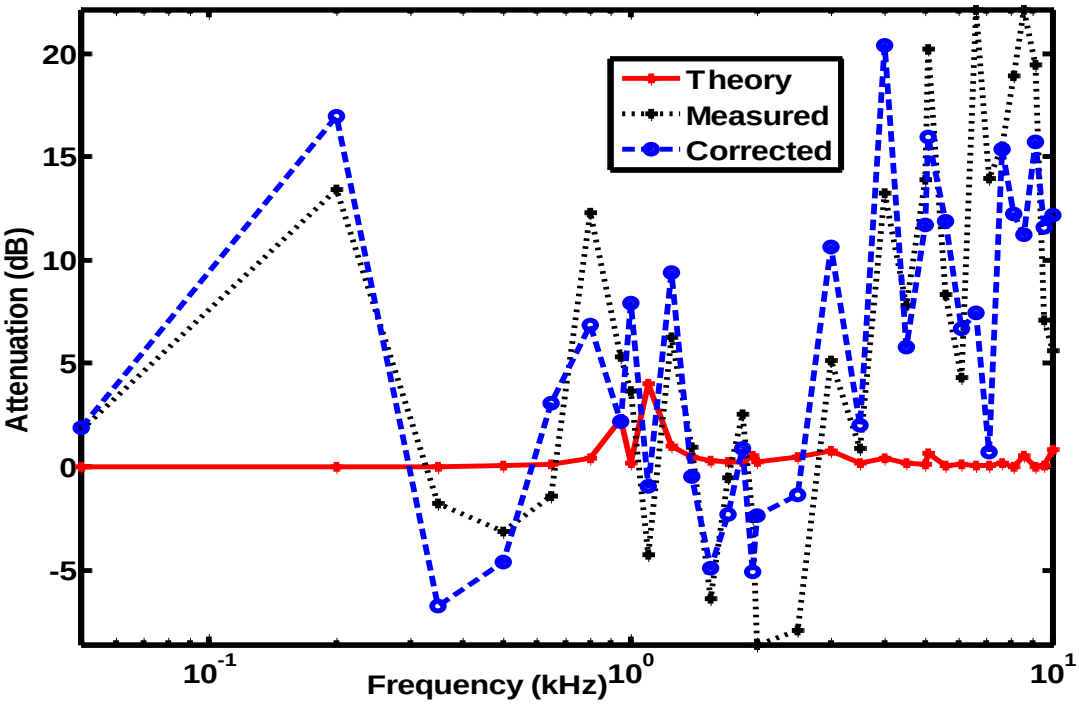

Figure 97: Attenuation due to a 1.32 m long side branch.

It is noticeable from the plots that at higher frequencies as the length of side branch is reduced the input impedance increases. The increase in input impedance causes radiation of the signal conduit through the side branch. The shorter side branch acts as a high pass filter for the signal propagating in the main conduit. The transmission loss is computed from (64) and is used in (71) for each case of change in the length of side branch to predict the received SPL. The predicted and measured SPL are plotted for each change of side branch length in Figs. 98-103. The predicted SPL, corrected for the losses due to standing waves in the main conduit, provides a better fit to the measured data compared to the theoretically predicted SPL. As the frequency is increased beyond 2.0 kHz, there is rapid rise in attenuation of the measured SPL. This can be attributed to the radiation through the open ended side branches causing transmission loss of the signal in main conduit.

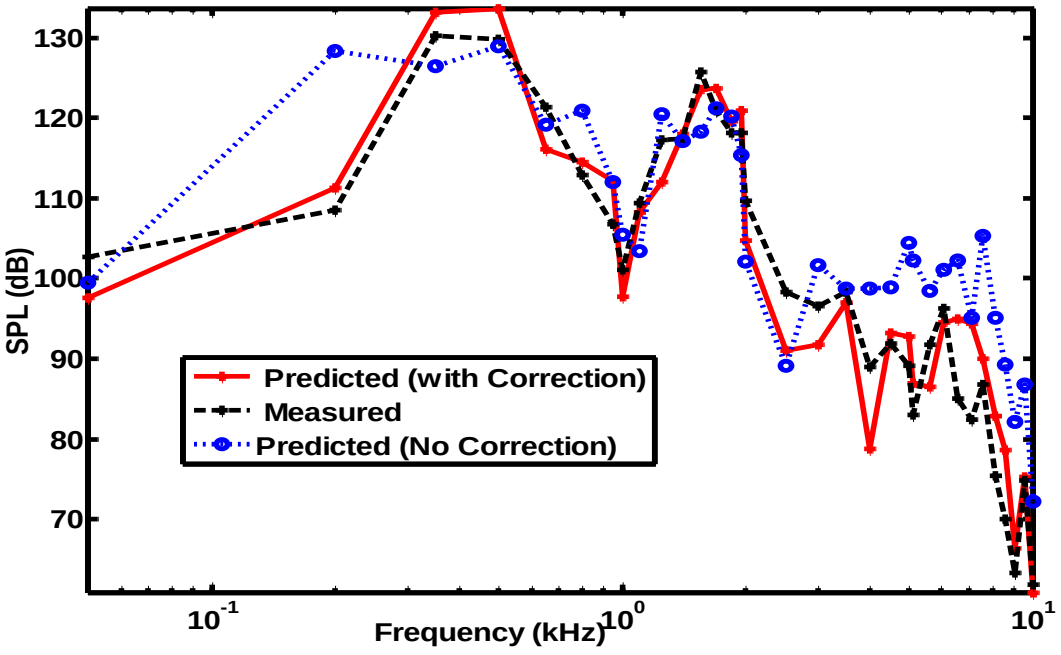

Figure 98: Measured and Predicted SPL in a conduit with 0.12 m long side branch.

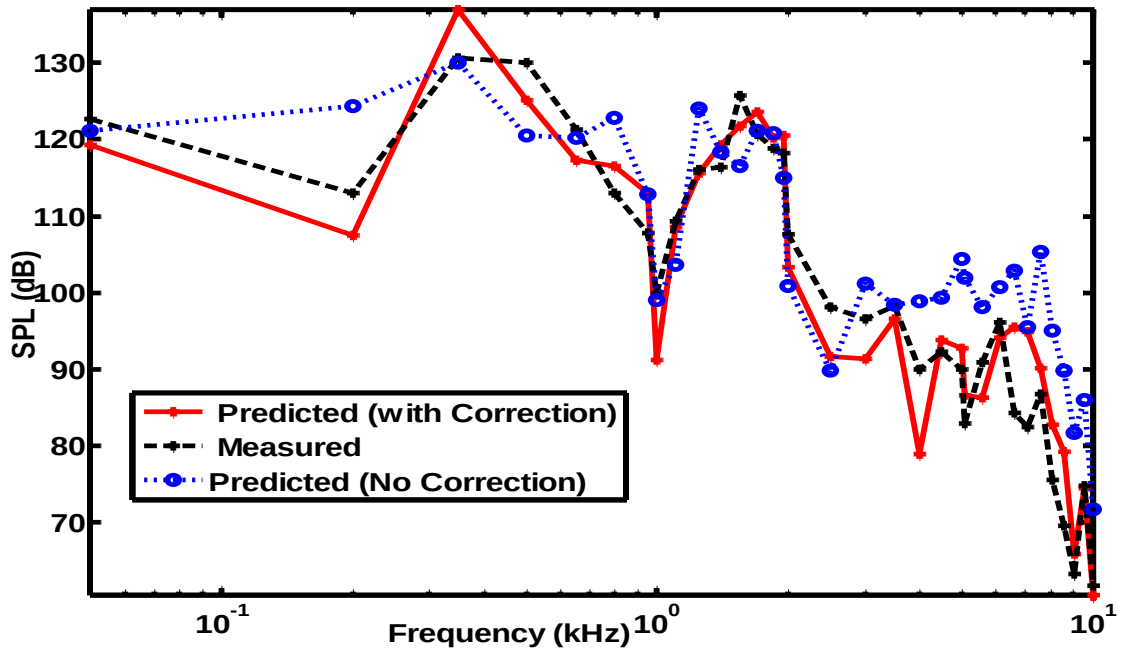

Figure 99: Measured and Predicted SPL in a conduit with 0.42 m long side branch.

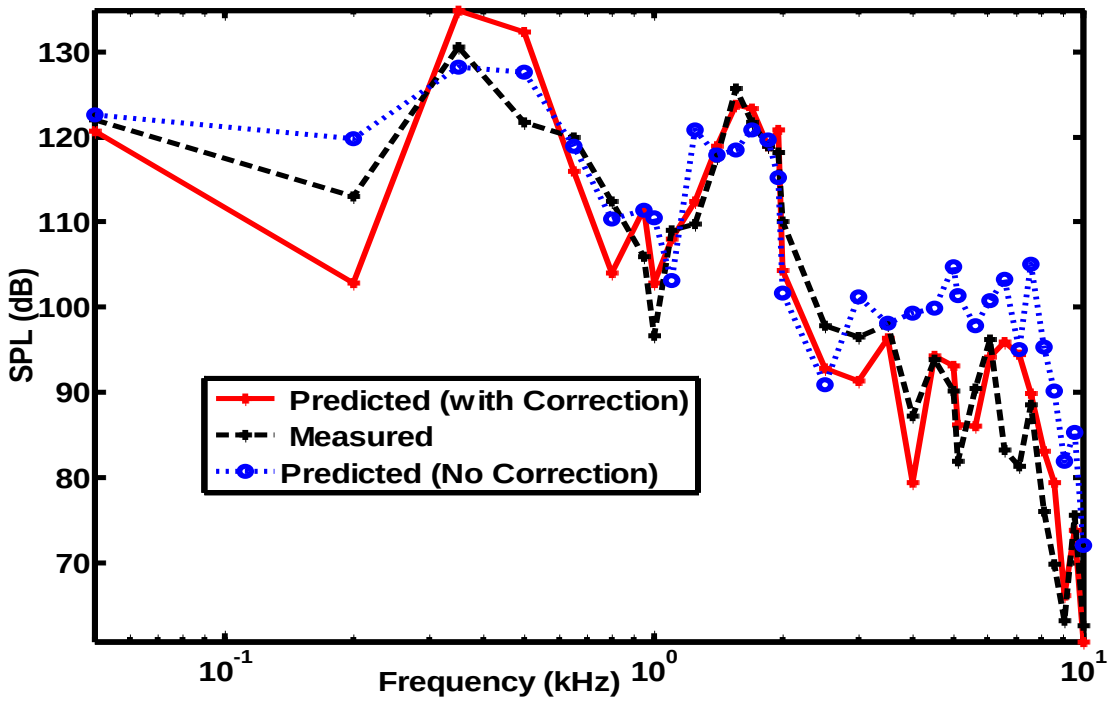

Figure 100: Measured and Predicted SPL in a conduit with 0.72 m long side branch.

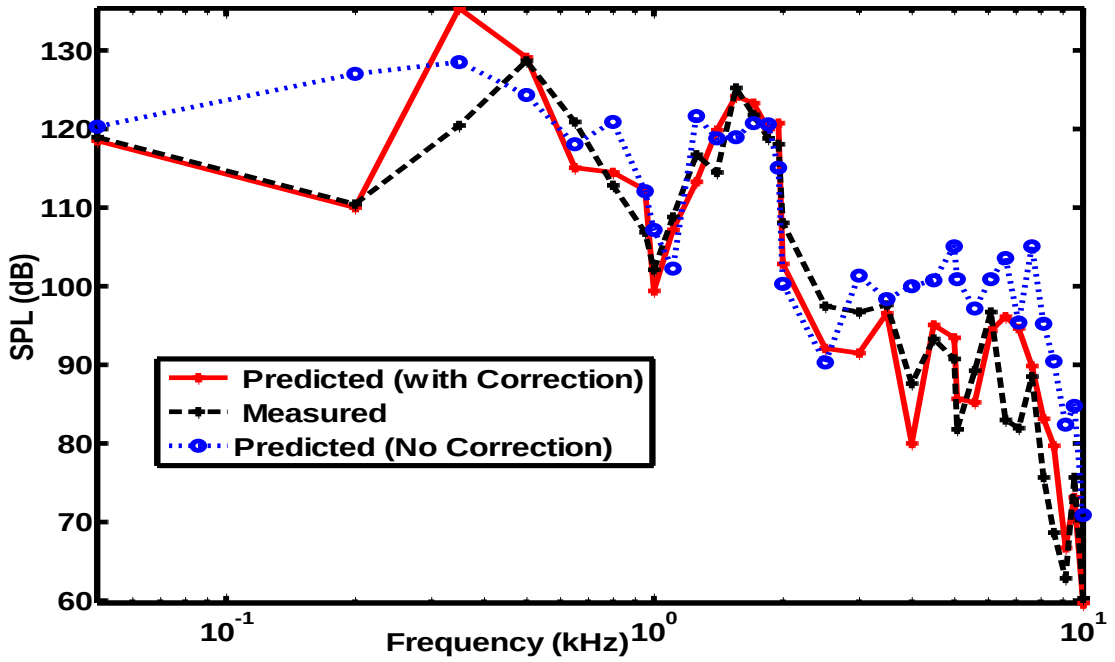

Figure 101: Measured and Predicted SPL in a conduit with 1.02 m long side branch.

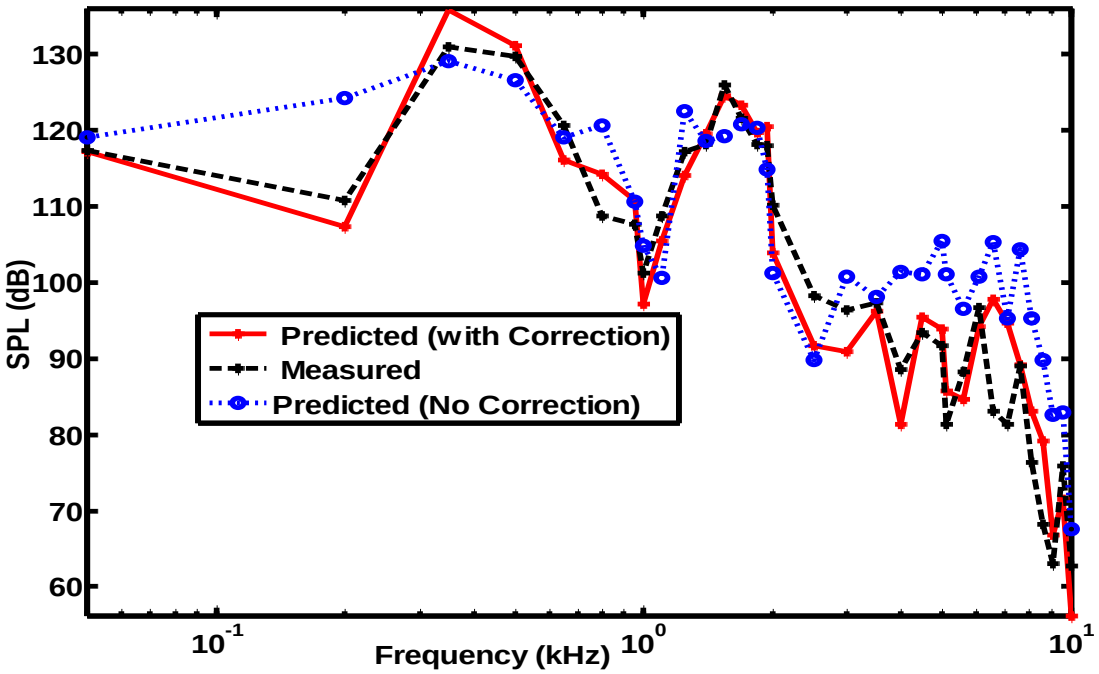

Figure 102: Measured and Predicted SPL in a conduit with 1.32 m long side branch.

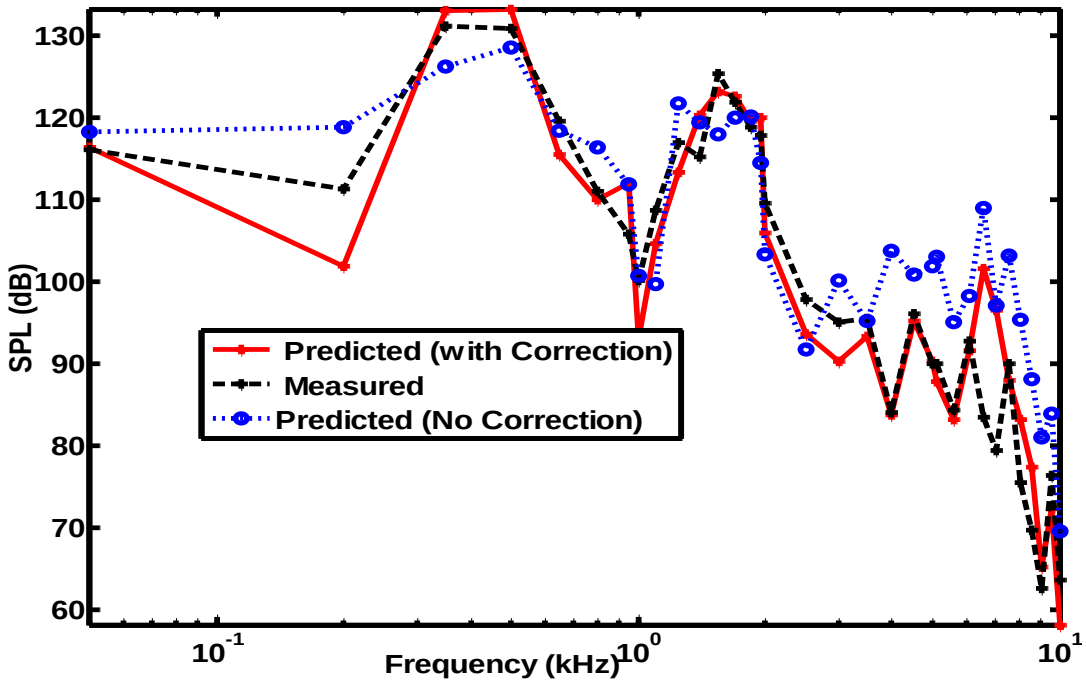

Figure 103: Measured and Predicted SPL in a conduit with 1.62 m long side branch.

In order to statistically characterize the nature of error between the predicted results from (71) and the measured SPL, the residuals are computed for each tested configuration. The normal probability plots are given in Figs. 104-109 for the six side branch lengths tested during the laboratory tests. The residuals generally follow the straight line of normal distribution except at the tails where the deviations from normality exist due to outliers in the residuals.

In order to quantify the effect of deviations from normality, the AD test is performed. The results are given in Table 12. The probability of AD test statistic is checked against the specified significance level of (0.05). The results of AD test show that the null hypothesis holds in all cases, therefore, the residuals belong to the normal

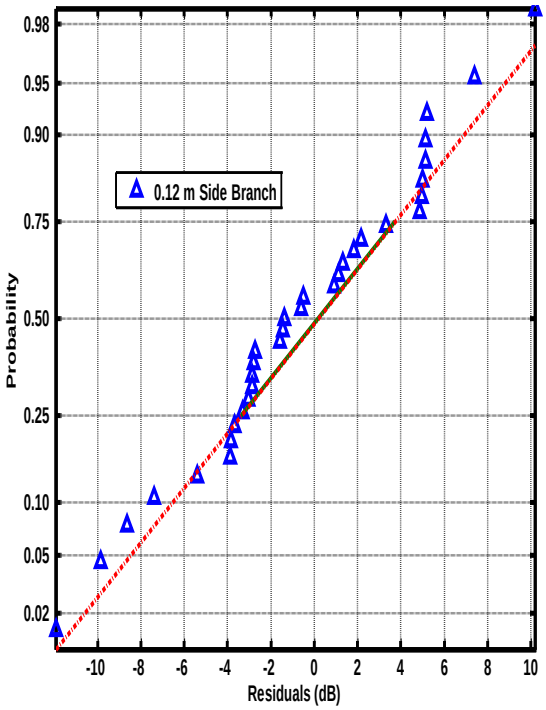

Figure 104: Normal probability plot of residuals for a 0.12 m long side branch.

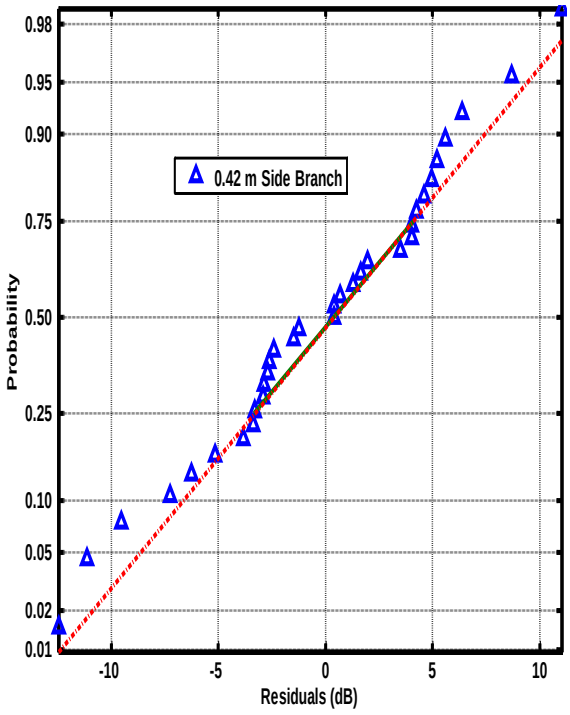

Figure 105: Normal probability plot of residuals for a 0.42 m long side branch.

probability distribution. The AD test also gives the mean and variance of the fitted distribution. The residuals from all tests are computed for corrected data as well as data without correction. The histograms of residuals for both cases are given in Figs. 110 and 111 along with the probability density function of the normal distribution. It can be graphically observed that the residuals from the corrected SPL data provide better fit to the normal probability distribution than residuals from SPL data with no correction. The normal probability plots of the residuals for both cases are also given in Figs. 112 and 113. The plots indicate that the residuals generally follow the straight line of normal probability distribution. Some residuals at the tails, however, deviate from normality corresponding to the outliers in the measured data.

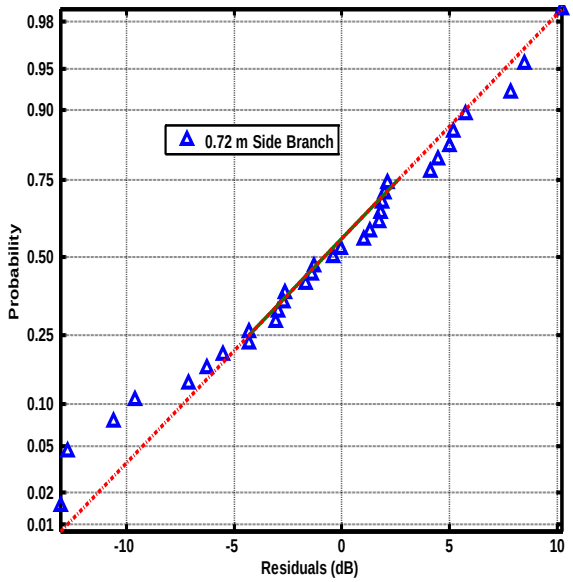

Figure 106: Normal probability plot of residuals for a 0.72 m long side branch.

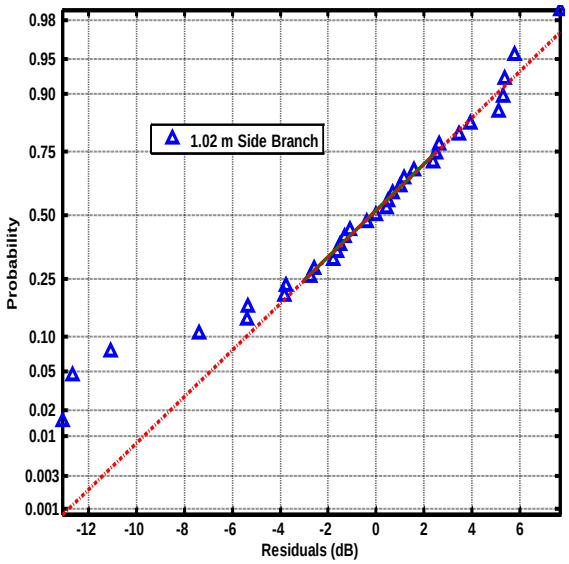

Figure 107: Normal probability plot of residuals for a 1.02 m long side branch.

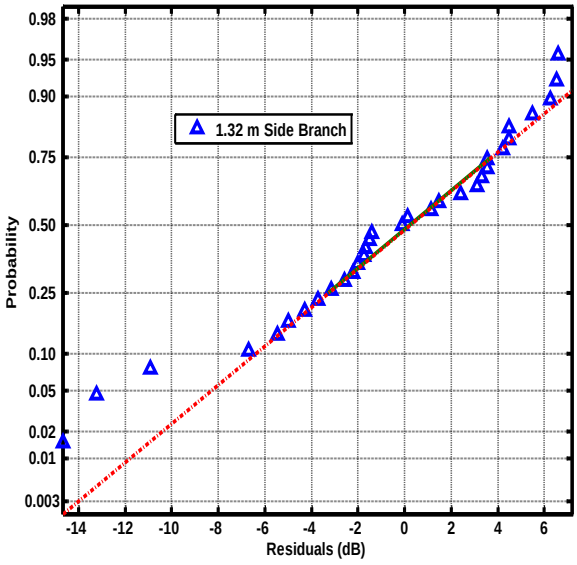

Figure 108: Normal probability plot of residuals for a 1.32 m long side branch.

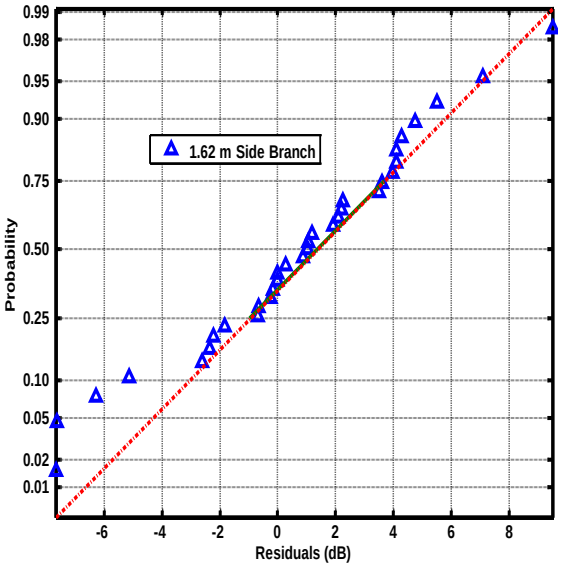

Figure 109: Normal probability plot of residuals for a 1.62 m long side branch.

Table 12: AD goodness of fit test results – Change in length of side branch.

Side branch lengths	AD Test Statistic	Probability of AD statistic	Normal Distribution Mean and Variance	Results
1.62	0.376	0.390	Mean = 0.78, Variance = 15.4	H_0 is true.
1.32	0.578	0.122	Mean = -0.49, Variance = 30.8	H_0 is true.
1.02	0.580	0.120	Mean = -0.78, Variance = 25.9	H_0 is true.
0.72	0.225	0.804	Mean = -0.81, Variance = 34.0	H_0 is true.
0.42	0.265	0.670	Mean = -0.30, Variance = 30.5	H_0 is true.
0.12	0.351	0.447	Mean = -0.57, Variance = 25.7	H_0 is true.

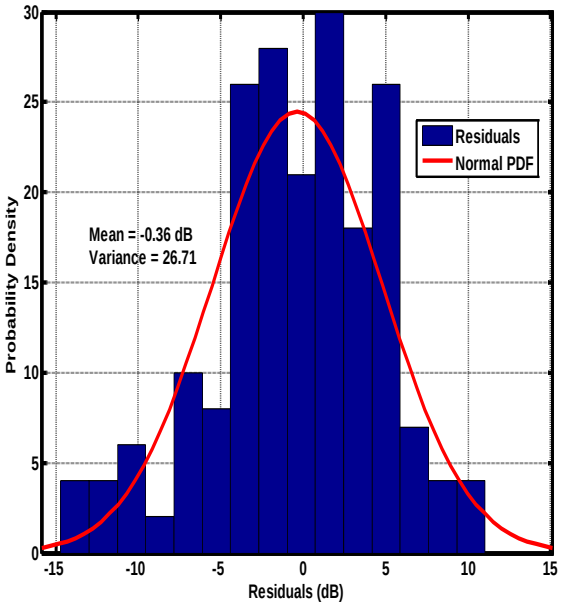

Figure 110: Histogram of residuals (with correction included) from all measurements (Change in length of side branches).

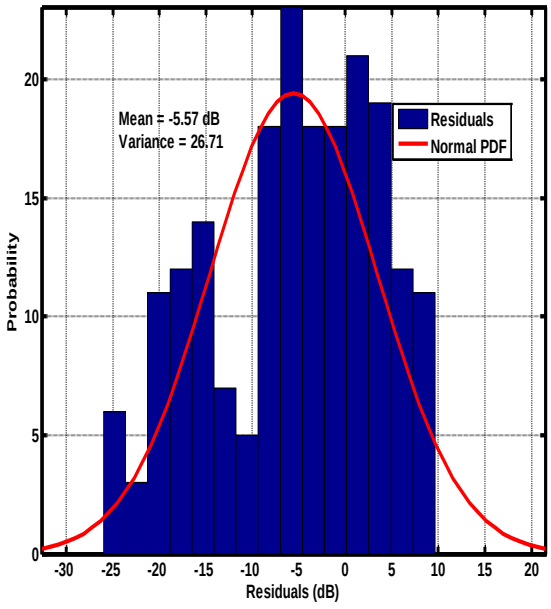

Figure 111: Histogram of residuals (with no correction) from all measurements (Change in number of side branches).

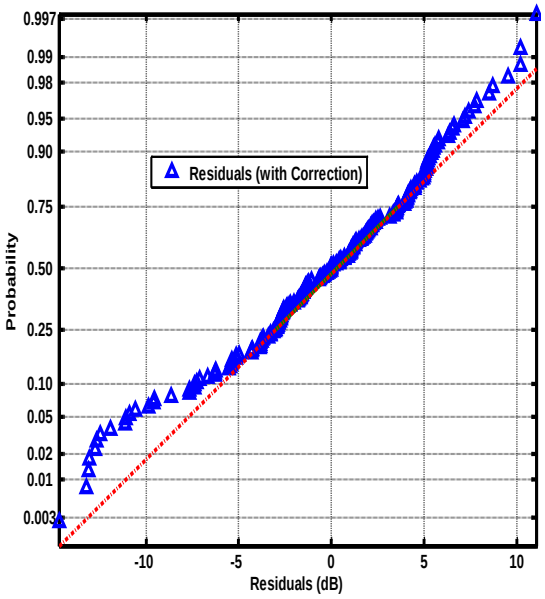

Figure 112: Normal probability plot of residuals (with correction) from all tests of side branch length changes.

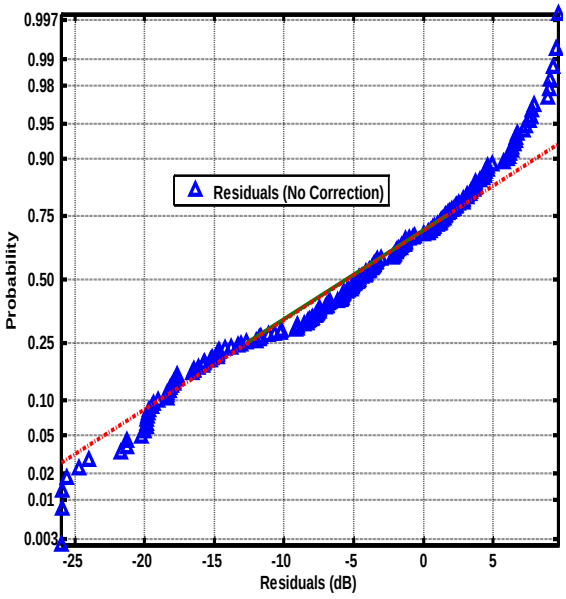

Figure 113: Normal probability plot of residuals (no correction) from all tests of side branch length changes.

In the previous sections, the variation in attenuation with distance along the length of conduit, frequency of transmitted signal, the number and length of side branches have been analyzed. In the next section, relevant deductions are drawn from the analysis and results presented in the previous sections.

7.6 Deductions from Analysis

Having analyzed the residuals in all cases of change in the number and lengths of side branches, it is evident that the residuals generally follow normal probability distribution. The histograms and corresponding normal probability plots of the residuals (with and without the correction) from all tested configurations of change in numbers and lengths of side branches are given in Figs. 114-117. The histogram of residuals with

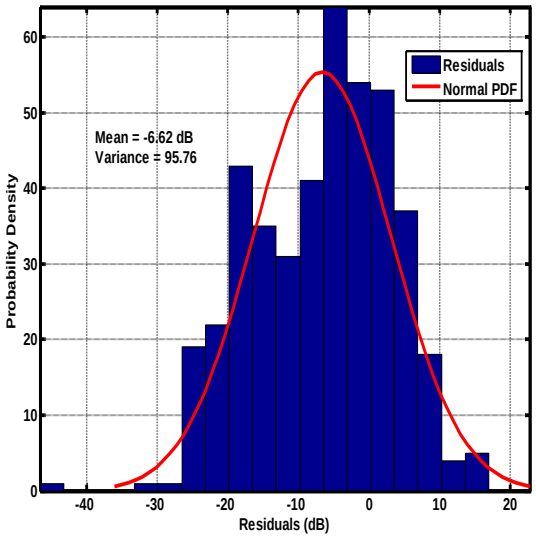

Figure 114: Histogram of residuals from all tests with no correction.

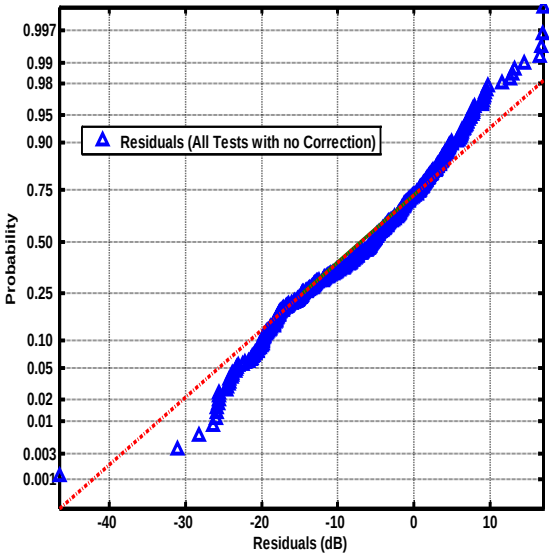

Figure 115: Normal probability plot of residuals from all tests with no correction.

correction has a mean of -1.15 dB and variance of 39.68. The residuals with no correction have a mean of -6.62 dB and a variance of 95.76.

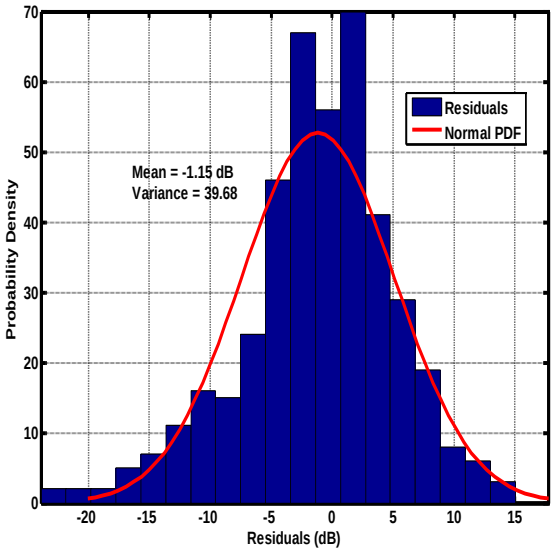

Figure 116: Histogram of residuals from all tests with correction.

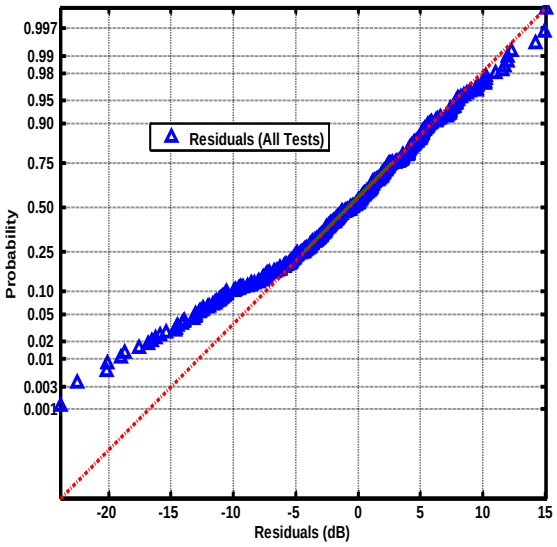

Figure 117: Normal probability plot of residuals from all tests with correction.

The probability plots indicate that the corrected residuals have a probability of between 10% to 98% that they belong to a normal distribution with a finite mean and variance before the deviations start. In case of residuals with no correction, their probability of following a normal distribution lies between 12% to around 80% before they start to deviate from normality. This indicates that adding a correction factor in the theoretical model of side branch transmission loss provides more accurate prediction of received SPL compared to the side branch transmission loss with no correction. Also, the corrected residuals more closely follow normal probability distribution compared to the residuals with no correction.

Through the analysis of data from the field and laboratory tests, variability in attenuation of propagating signal has been analyzed due to change in the distance from the source, the frequency, the number and length of the side branches. The following overall deductions are made based on the presented results:

1) The first order polynomial linear regression model fits the measured SPL versus distance data well. The representative samples of received SPL at 200 Hz, 500 Hz, 1600 Hz and 6300 Hz analyzed through a linear regression model have strong (closer to 1) coefficients of determination (R^2_{reg}). This indicates that most of the variation in the received SPL can be explained by a first order polynomial relationship between distance from the source and the SPL. The variability in the linear relationship that cannot be explained by linear regression model has been analyzed through statistical analysis of residuals between the measured data and the fitted model. The analysis indicates that the residuals are random variables belonging to a normal probability distribution with zero mean and finite variance.

2) The analysis of variation in attenuation with frequency, for a conduit with no side branches, indicates that the residuals between measured and predicted attenuation belong to a normal probability distribution with finite mean and variance. The statistical analysis of residuals indicates that they have a variability that can be best explained by a normally distributed stochastic component of finite mean and variance.
3) Variation in signal attenuation with the change in number of side branches also introduces a random variable error in the measured attenuation that can be best modeled as a normally distributed random variable with a finite mean and variance. The mean error between the prediction from the model and the measured data can be reduced to a marginal level if a correction factor is included in the theoretically computed attenuation to take into account the standing wave effects of an open ended conduit.
4) Change in the length of side branch has significant effect on the signal attenuation in a conduit as the input impedance of side branch varies with length. As the side branch length decreases, the transmission loss increases and the maxima of the transmission loss correspond to the minima of the side branch input impedance. The variation in the length of side branch also introduces a random variable error in the measured attenuation that is normally distributed with a finite mean and variance.

The proposed propagation model as the sum of analytical deterministic part and a stochastic part from (74) is reproduced below:

$$\bar{P}(z, f, N, l, a, b) = \bar{P}_0 - \alpha_c(z, f, N, l, a, b) + \psi(\mu, \sigma^2). \qquad (78)$$

Based on the deductions from analysis of empirical data, it can be concluded that the proposed model to characterize the acoustic signal propagation in conduit networks with variations in distance from the source, frequency, number and lengths of side branches is a valid model as it describes not only the deterministic component of the signal attenuation but also the stochastic component contributed by random variable sources. It has also been validated that the stochastic component of the model $\psi(\mu, \sigma^2)$ can be most accurately described by a normal distribution with a finite mean and variance. Therefore, the model in (78) can be used to more accurately predict the signal attenuation in conduit networks than the existing analytical models.

In the next chapter the conclusions drawn from the present study and some recommendations for future work are presented.

CHAPTER 8: CONCLUSION AND FUTURE WORK

8.1 Conclusion

Development of models to characterize acoustic propagation in conduits has historically been an important subject for scientific investigators especially due to applications in the design of musical instruments, sound absorbing liner material for muffling applications, acoustic based delay lines, noise analysis in HVAC ducts and pipeline condition monitoring systems. The motivation for the present study stems from the need to characterize the propagation of an acoustic signal in a conduit in the presence of random sources that introduce an uncertainty in the signal attenuation measurements. Some of these random variable sources of error include the presence of temperature and humidity gradients, blockages of variable sizes and types, defects due to aging and ambient noise variations. Characterizing the random variable error due to random variable sources using analytical approaches can be intractable to model due to increased complexity. This study proposes a stochastic based approach to model the random variable error in the attenuation of the propagating signal with the change in the distance from the source, the frequency, the number and lengths of side branches. An empirical based model is proposed that can describe the propagation in a conduit network in presence of random variable error sources with better accuracy compared to the theoretical based approaches only.

Extensive field and laboratory measurements have been made to collect the data for validating the proposed model. The predicted results from the model show good agreement with those from the theoretical model calibrated for the effects of standing waves in an open conduit. Graphical and statistical approaches are used to analyze the residuals between measured and predicted data. The analysis of residuals indicates that they belong to a normal distribution with a finite mean and variance. The addition of a stochastic part in the propagation model to describe random variable error in signal attenuation is validated by close agreement between the predicted and measured SPL for all tested conduit configurations. The proposed propagation model can be used for predicting signal attenuation in conduit networks more accurately compared to theoretical models only.

8.2 Future Work

In order to improve the accuracy of the model for use in field applications following aspects can be studied:

1) During field measurements some tests involved measuring the pressure response of the conduit with one or more manholes between the source and the receiver. The effect of manholes on the propagating signal in terms of transmission loss on the propagating signal, reflection back into the source conduit and coupling to the next conduit section needs to be analyzed. There is also a need to analyze the effect of placing the source as well as receiver in the manhole cavity rather than at the open ends of the conduit.
2) Routinely, conduit networks in the field have a thin layer of water along with variable level of blockage. The depth of layer of water can momentarily vary

depending on the use of the conduit. Therefore, there is a need to analyze its effect on the signal attenuation. The effect of variable sizes and types of blockages in conduits can also be studied and their effects included in the propagation model.

3) The sources of noise in the conduit in the field are random variables and their effect on ambient noise inside the conduit need to be analyzed. A probability distribution to best model the ambient noise affecting the propagating signal inside the conduit environment may be investigated.

REFERENCES

Andersen, J. B., T. S. Rappaport, et al. (1995). "Propagation measurements and models for wireless communications channels." IEEE Communications Magazine **33**(1): 42-49.

Andersen, S. H., Ostensen, F. C. (1928). "Effect of frequency on the end correction of pipes." Physical Review **31**: 267-274.

Anderson, T. W., and Darling, D.A. (1954). "A test of goodness-of-fit." Journal of the American Statistical Association**.49**: 765-769.

ANSI/ASTM (1977). Standard test method for impedance and absorption of acoustical materials by the tube method. C384-77.

Bait, A. E. (1937). "The end correction of an unflanged pipe." Philosophical Magazine Series 7 **Series 7**: 453-458.

Beatty Jr, R. E. (1950). "Boundary layer attenuation of higher order modes in rectangular and circular tubes." The Journal of the Acoustical Society of America **22**(6): 850-854.

Benade, A. H. (1968). "On the Propagation of Sound Waves in a Cylindrical Conduit." The Journal of The Acoustical Society of America **44**(2): 616-623.

Beranek, L. L., J. L. Reynolds, et al. (1953). "Apparatus and procedures for predicting ventilation system noise." The Journal of The Acoustical Society of America **25**(2): 313-321.

Blackstock, D. T. (2000). Fundamentals of Physical Acoustics. New York, John Wiley and Sons, Inc.

Blaikley, D. J. (1879). "Experiments for determining the correction to be added to the length of a cylindrical resonant tube." Phil. Mag. (V) **VII**: 339.

Boden, H. and M. Abom (1986). "Influence of errors on the two-microphone method for measuring acoustic properties in ducts." The Journal of The Acoustical Society of America **79**(2): 541-549.

Boehm, W. M. (1910). "A determination of the correction for the open end of a cylindrical resonator." Philosophical Magazine **Vol. XXXI** 332-341.

Bohn, D. A. (1987). Environmental effects on speed of sound. 83rd Convocation of the Audio Engineering Society. New York.

Brown, F. T. (1962). "The transient response of fluid lines." Trans. ASME **84**: 547-553.

Bruneaua, A. M., M. Bruneaua, et al. (1987). "Boundary layer attenuation of higher order modes in waveguides." The Journal of Sound and Vibration **119**(1): 15-27.

BSWA (2013). "Prepolarized Free-field Microphone Capsule-MP215." from http://www.bswa-tech.com/products-microphone%20capsules-mp215.htm

Chen, K. T., Y. H. Chen, et al. (1998). "The improvement on the transmission loss of a duct by adding Helmholtz resonators." Applied Acoustics **54**(1): 71-82.

Chu, W. T. (1986). "Extension of the two-microphone transfer function method for impedance tube measurements." The Journal of The Acoustical Society of America **80**(1): 347-348.

Chu, W. T. (1986). "Transfer function technique for impedance and absorption measurements in an impedance tube using a single microphone." The Journal of The Acoustical Society of America **80**(2): 555-560.

Chung, J. Y. and D. A. Blaser (1980). "Transfer function method of measuring acoustic intensity in a duct system with flow." The Journal of The Acoustical Society of America **68**(6): 1570-1577.

Chung, J. Y. and D. A. Blaser (1980). "Transfer function method of measuring in-duct acoustic properties. I. Theory." The Journal of The Acoustical Society of America **68**(3): 907-913.

Chung, J. Y. and D. A. Blaser (1980). "Transfer function method of measuring in-duct acoustic properties. II. Experiment." The Journal of The Acoustical Society of America **68**(3): 914-921.

Dalmont, J. P. (2001). "Radiation impedance of tubes with different flanges: Numerical and experimental investigations." Journal of Sound and Vibration **244**(3): 505-534.

Daniels, F. B. (1950). "On the propagation of sound waves in a cylindrical conduit." The Journal of The Acoustical Society of America **22**(5): 563-564.

Dyer, I. (1958). "Measurement of noise sources in ducts." The Journal of The Acoustical Society of America **30**(9): 833-841.

Enescu, N., and Magheti, I., (1999). Acoustical characteristics of tubes with lateral Derivations. IIAV 6 Congress. Copenhagen, Denmark.

Feng, Z., K. Horoshenkov, et al. (2012). An acoustic method for condition classification in live sewer networks. 18th World Conference on Non-destructive Testing. Durban, South Africa.

Fishburne, J. and I. Howitt (2010). An acoustical approach for detecting sewer line obstructions. NC-AWWA Spring Fling Conference.

Fletcher, N. H. and T. D. Rossing (1998). The Physics of Musical Instruments. New York, Springer-Verlag.

Franken, H., J. Clement, et al. (1981). "Oscillating flow of a viscous compressible fluid through a rigid tube: A theoretical model." IEEE Transactions of Biomedical Engineering **28**: 416-420.

Helmholtz, H. (1885). On the Sensations of Tone as a Physiological Basis for the Theory of Music. London, Longmans, Green and Co. .

Henke, J. E. (2007). Business Forecasting. New Delhi, Prentice-Hall India.

Horoshenkov, K. V., Ashley, R. M., and Blanksby, J (2003). "Determination of sewer roughness and sediment properties using acoustic techniques." Water Science and Technology **47**(2): 87-93.

Howitt, I. (2012). Monitoring systems and methods for sewer and other conduit systems. USPTO. USA, University of North Carolina at Charlotte.

Howitt, I., S. Khan, et al. (2008). "A mode based model for radio wave propagation in storm drain pipes." PIERS Online **4**(6): 635-640.

Hull, A. J. (1992). A comparison of acoustic impedance measurement techniques. New London, Connecticutt, Naval Undersea Warfare Center Detachment.

Irons, E. J. (1931). "A simple theory of acoustical filters." Journal of Scientific Instruments **8**(3): 89-93.

Johnston, J. P. and W. E. Schmidt (1978). "Measurement of acoustic reflection from an obstruction in a pipe with flow." The Journal of The Acoustical Society of America **63**(5): 1455-1460.

Kang, Y. J. and I. H. Jung (2001). "Sound propagation in circular ducts lined with noise control foams." Journal of Sound and Vibration **239**(2): 255-273.

Keefe, D. H. (1982). "Theory of the sigle woodwind tone hole." The Journal of the Acoustical Society of America **72**(3): 676-687.

Keefe, D. H. (1984). "Acoustical wave propagation in cylindrical ducts: Transmission line parameter approximations for isothermal and nonisothermal boundary conditions." The Journal of Acoustical Society of America **75**(1): 58-62.

Kinsler, L. E., A. R. Frey, et al. (2000). Fundamentals of Acoustics. New York, John Wiley and Sons.

Kirchhoff, G. (1883). "Toward a theory of light rays." Ann. Phys. Chem **18**: 663-695.
Levine, H. and J. Schwinger (1948). "On the radiation of sound from an unflanged circular pipe." Phys. Rev. **73**(4): 383-406.

Lindsay, R. B. (1929). "Note on the theory of acoustic wave filters." Physical Review **34**(4): 652-655.

Long, T. H. (1947). "The performance of cup-mouthpiece instruments." The Journal of The Acoustical Society of America **19**(5): 892-901.

Mason, W. P. (1927). "A study of regular combinations of acoustic elements, with applications to recurrent acoustic filters, tapered acoustic filters, and horns." Bell Systems Technical Journal **6**: 258-294.

Mason, W. P. (1928). "The Propagation characteristics of sound tubes and acoustic filters." Physical Review **31**(2): 283-295.

Mason, W. P. (1930). "The approximate networks of acoustic filters." The Journal of The Acoustical Society of America **1**(2A): 263-272.

McSkimin, H. J. (1948). "Theoretical analysis of the mercury delay line." The Journal of The Acoustical Society of America **20**(4): 418-424.

Morse, P. M. and H. Feshbach (1953). Methods of Theoretical Physics, McGraw Hill.

Morse, P. M. and K. U. Ingard (1968). Theoretical Acoustics. Princeton, New Jersey, Princeton University Press.

Munjal, M. L. (1987). Acoustics of Ducts and Mufflers. New York, John Wiley and Sons, Inc.

Nederveen, C. J., J. K. Jansen, et al. (1998). "Corrections for woodwind tonehole calculations." Acustica **84**: 957-966.

Noble, B. (1988). Methods Based on the Wiener-Hopf Technique for the Solution of Partial Differential Equations. New York, American Mathematical Society.

Norris, A. N. and I. C. Sheng (1989). "Acoustic radiation from a circular pipe with an infinite flange." **135**(1): 85-93.

Okamoto, Y., H. Boden, et al. (1994). "Active noise control in ducts via side branch resonators." The Journal of the Acoustical Society of America **96**(3): 1533-1538.

Olson, H. F. (1947). Elements of acoustical engineering. Princeton, New Jersey, D. Van Nostrand Co. .

Rayleigh, L. (1896). Theory of Sound London, Macmillan and Company.

Romano, E. L. L. J. P. (2005). Testing Statistical Hypotheses, Springer.

Romeu, J. L. (2003) Andersen-Darling: A Goodness of Fit Test for Small Samples Assumptions. Selected Topics in Assurance Related Technologies **10**, 1-6

Ross, D. F. and A. F. Seybert (1977). "Experimental determination of acoustic properties using a two-microphone random-excitation technique." The Journal of The Acoustical Society of America **62**(S1): S57-S57.

Schroeder, M. R. (1967). "Determination of the geometry of the human vocal tract by acoustic measurements." The Journal of The Acoustical Society of America **41**(4B): 1002-1010.

Seybert, A. F. and D. F. Ross (1977). "Experimental determination of acoustic properties using a two-microphone random-excitation technique." The Journal of The Acoustical Society of America **61**(5): 1362-1370.

Seybert, A. F. and B. Soenarko (1980). "In-duct measurement of acoustic properties using a two-microphone technique with random and pure tone excitation." The Journal of The Acoustical Society of America **67**(S1): S73-S73.

Shi, Y. (2009). Comparing Theory and Measurements of Woodwind-Like Instrument Acoustic Radiation. Montreal Canada, MS Thesis, McGill University

Shields, F. D., K. P. Lee, et al. (1965). "Numerical solution for sound velocity and absorption in cylindrical tubes." The Journal of The Acoustical Society of America **37**(4): 724-729.

Silva, F., P. Guillemain, et al. (2009). "Approximation formulae for the acoustic radiation impedance of a cylindrical pipe." Journal of Sound and Vibration **322**(1-2): 255-263.

Stewart, G. W. (1922). "Acoustic wave filters." Physical Review **20**(6): 528-551.

Stewart, G. W. (1924). "Acoustic aave filters: attenuation and phase factors." Physical Review **23**(4): 520-524.

Stewart, G. W. (1925). "Acoustic wave filters; An extension of the theory." Physical Review **25**: 90-98.

Stewart, G. W. (1925). "Influence of a branch line upon acoustic transmission of a conduit." Physical Review **26**: 688-690.

Stewart, G. W. (1926). "Direct absolute measurement of acoustic impedance." Physical Review **28**: 1038-1047.

Stewart, G. W. (1926). "The tube as a branch of an acoustic conduit: the special case of the Quincke tube." Phys. Rev. **27**: 494-498.

Stewart, G. W. and C. W. Sharp (1929). "Experimental and Theoretical mid-series characteristic impedance of acoustic wave filters." Journal of Optical Society of America **19**: 17-28.

Stokes, G. G. (1845). "On the theories of internal friction of fluids in motion and of the equilibrium and motion of elastic solids." Trans. Cambridge Philos. Soc **8**: 75-102.

Tang, S. K. (2004). "Sound transmission characteristics of Tee-junctions and the associated length corrections." The Journal of The Acoustical Society of America **115**(1): 218-227.

Tijdeman, H. (1975). "On the propagation of sound waves in cylindrical tubes." Journal of Sound and Vibration **39**(1): 1-33.

Tolstoy, A., K. V. Horoshenkov, et al. (2009). "Detecting pipe changes via acoustic matched field processing." Applied Acoustics **70**(5): 695-702.

USEPA (2012). Wastewater Collection Systems. U. EPA. **2012**.

Wyerman, B. R. (1976). A theoretical and experimental study of acoustic propagation in multi-sectioned ducts, Pennsylvania State University. **PhD Dissertation**.

Yin, Y. and K. V. Horoshenkov (2005). "The attenuation of the higher-order cross-section modes in a duct with a thin porous layer." The Journal of The Acoustical Society of America **117**(2): 528-535.

Zorumski, W. E. (1973). "Generalized radiation impedance and reflection coefficients of circular and annular ducts." The Journal of the Acoustical Society of America **54**(6): 1667-1673.

APPENDIX A: EFFECT OF TEMPERATURE AND HUMIDITY VARIATIONS ON SPEED OF SOUND

The speed of sound in air has strong dependence on the variations in temperature and humidity. The temperature changes cause change in the density of the medium that change the speed of sound. The variation of sound with changes in relative humidity and temperature are given in (Bohn 1987). Here the variation in speed of sound is analyzed through expressions given in (Bohn 1987) at variation in relative humidity conditions encountered during the field tests. The speed of sound (c) in air with temperature (T) in degree Celsius is given by:

$$c = 20\sqrt{T + 273}\,. \tag{79}$$

The moisture in air affects the density of air and hence the speed of sound in air. Moist air is less dense than the dry air and hence speed of sound in dry air is less than the moist air. The presence of water vapors in the air cause its specific heats ratio to change. The variation in speed of sound due to temperature (T) and humidity (h) changes is given by:

$$c = 1.5 \times 10^5 \sqrt{\frac{\gamma_{moist}(273 + T)}{(7917 - 3003h)}}, \tag{80}$$

where h is the water molecule fraction that can be converted to the percent relative humidity (RH) and γ_{moist} is the ratio of specific heats for moist air. The change in speed of sound with temperature and relative humidity is plotted in Fig. 115 for a temperature range from 0 to 30°C and for relative humidity range of 10 to 90% with 10% step.

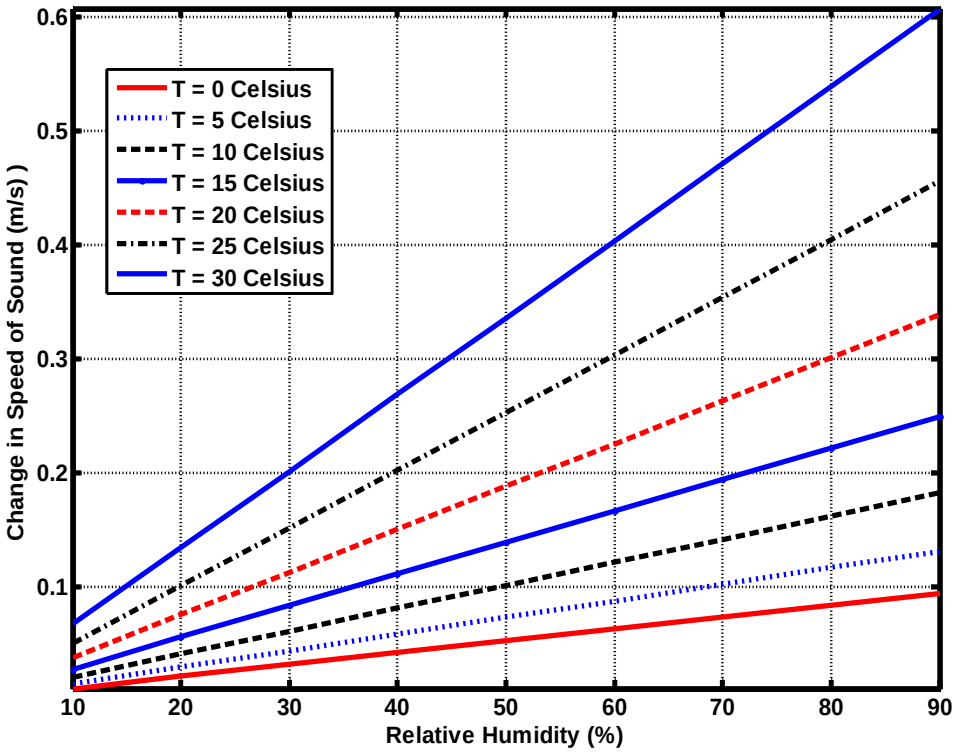

Figure 118: Change in speed of sound vs. relative humidity and temperature.

The plot indicates that with the change in humidity the speed of sound slightly varies. The variation becomes more pronounced with the increase in temperatures. For the purpose of this study the temperatures and humidity readings during the field and laboratory tests have been recorded and are used to analyze the speed of sound in conduit networks.

APPENDIX B: THERMODYNAMIC PROPERTIES OF AIR

The variation in thermodynamic properties of air with temperature is given in the following table. Those properties are included that are relevant to this study:

Thermodynamic constants of air: All constants are evaluated at $T = 26.85°C\ (300°K)$ and are accurate to within $\pm 10°C$ of that temperature. The temperature difference relative to $26.85°C$ is ΔT.	
Equilibrium density of air (ρ_0)	$\rho_0 = 1.1769(1 - 0.00335\ \Delta T)\ \frac{kg}{m^3}$
Coefficient of shear viscosity (η)	$\eta = 1.846 \times\ 10^{-5}(1 + 0.0025\ \Delta T)\ \frac{kg}{m\ s}$
$\gamma = \frac{C_p}{C_v}$	$\gamma = 1.4017(1 - 0.00002\ \Delta T)$
Prandtl number, $P_r = \frac{\eta C_p}{\kappa}$	$\sqrt{P_r} = 0.8410(1 - 0.0002\ \Delta T)$
Characteristic impedance of air	$\rho_0 c = 408.65(1 - 0.0017\ \Delta T)\ \frac{kg}{m^2 s}$